Spin-orbit Interaction of Light in Graded-index Medium

Pradeep Chakravarthy. T

School of Physics
University of Hyderabad

Spin-orbit Interaction of Light in Graded-index Medium

A thesis submitted during 2021-22 to the University of Hyderabad in partial fulfillment of the award of a Ph.D. degree in School of Physics

by

Pradeep Chakravarthy . T



School of Physics

University of Hyderabad
(P.O) Central University, Gachibowli,
Hyderabad - 500046

Telangana

India



CERTIFICATE

This is to certify that the thesis entitled "Spin-orbit Interaction of Light in Graded-index Medium" submitted by T. Pradeep Chakravarthy bearing Registration Number 14PHPH02 in partial fulfilment of the requirements for award of Doctor of Philosophy in the School of Physics is a bonafide work carried out by him under my supervision and guidance.

This thesis is free from Plagiarism and has not been submitted previously in part or in full to this or any other University or Institution for award of any degree or diploma.

Further, the student has the following publications before submission of the thesis for adjudication and has produced evidence for the same in the form of acceptance letter or the reprint in the relevant area of his research:

- 1. Direct and reciprocal spin-orbit interaction effects in a graded-index medium (ISSN Number 2578-7519), Chapters of dissertation where this publication appears are 2, 3 and 4,
- 2. Geometric phase due to orbit-orbit interaction: rotating LP_{11} modes in a two-mode fiber (ISSN Number 2040-8986), Chapter of dissertation where this publication appears is 6,

and

has made presentations in the following conferences:

- 1. Complex Light and Optical Forces XI Vol 10120 International Society for Optics and Photonics, 2017 (International)
- 2. OSI International Symposium on Optics (OSI-ISO 2018), Indian Institute of Technology Kanpur (International)

Further, the student has passed the following courses towards fulfilment of coursework requirement for Ph.D. / was exempted from doing coursework (recommended by Doctoral Committee) on the basis of the following courses passed during his M.Phil. Program and the M.Phil. Degree was awarded:

Course Co	de Name	Credits	Pass/Fail
1. PY80	Advanced Quantum Mechanics	4	Pass
2. PY80	Advanced Statistical Mechanics	4	Pass
3. PY80	4 Advanced Electromagnetic Theory	4	Pass
4. PY82	Research Methodology	4	Pass

Supervisor Nirmal K. Viswanathan School of Physics

School of Physics
University of Hyderabad
HYDERABAD-500 046 (1997)

Head of the Department

DECLARATION

I T. Pradeep Chakravarthy hereby Declare that this thesis entitled "Spin-orbit Interaction of Light in Graded-index Medium" Submitted by me under the guidance and supervision of Professor Nirmal K. Viswanathan is a bonafide research work. I also declare that it has not been submitted previously in part or in full to this University or any other University or Institution for the award of any degree or diploma.

Date: 05 | 11 | 21

Name: T. Pradeep Chakravarthy

Signature of the Student:

Regd. No. 14PHPH02

ACKNOWLEDGEMENT

Throughout the Doctoral Journey, I have received a great deal of support and love from my family.

I would like to thank my supervisor, Prof. Nirmal K. Viswanathan, whose guidance, support, and patience enabled me to complete the thesis without which it would not have been possible.

I would like to acknowledge my colleagues Dr. Dinesh, Dr. Samlan, Sujai, Rashmi (late), Dr. Chandravathi, Dr. Rakhi, Anagha, and Anirban for their inquisitive discussions and memories.

I am grateful to A.G.Bandagi Teja for the help I received in writing my thesis.

Likewise, I would also like to thank my doctoral committee members Prof. Anantha Lakshmi and Prof. Asoka Vudayagiri, and other teaching and non-teaching staff of School of Physics for their guidance and support.

I could not have completed this dissertation without the support of my friends who provided stimulating discussions as well as happy distractions to rest my mind outside my research.

Furthermore, I use this opportunity to thank the Department of Science and Technology (DST-INDIA) for providing INSPIRE Fellowship during my Ph.D.

Finally, the university ecosystem and biodiversity provided muchneeded relaxation during my stay.

ABSTRACT

The angular momenta of light associated with polarization, phase singular helical wavefronts, and shifted trajectory of a beam are referred to as spin angular momentum (SAM), intrinsic orbital angular momentum (IOAM) and extrinsic orbital angular momentum (EOAM) respectivley. The mutual interaction and influence of SAM, IOAM, and EOAM of light in a variety of physical configurations such as reflection, refraction, or propagation through an inhomogeneous or an anisotropic or a bi-axial media leads to spin-orbit (SO) and orbit-orbit (OO) interaction (I) of light. In this thesis, we investigate the spin-orbit and orbit-orbit interaction of light in an inhomogeneous and weakly anisotropic (GRIN rod) medium under on-axis and off-axis symmetry considerations with Rytov-Vladimirskii-Berry (RVB) phase as an underlying mechanism.

Initially, the SOI and OOI due to on-axis (symmetric) propagation of circularly polarized (CP) Gaussian and linearly polarized optical vortex (OV) beam, resulting in spin to orbit AM conversion (SOC) and reciprocal SOC are investigated. Further, the off-axis (asymmetric) propagation of vertically polarized Gaussian beam leads to different phase gradients for right and left CP resulting in spin-Hall effect (SHE) and Rytov-Vladimirskii-Berry phase accumulation, which exhibits a non-linear behaviour due to weak anisotropy of GRIN rod. Likewise, the off-axis propagation of linearly polarized optical vortex and zero OAM HG beams are studied, which resulted in orbital-Hall effect (OHE) and orbital-Berry phase (OBP) accumulation respectively.

Additionally, mutual interactions of three AM of light are studied for different input launch positions through the GRIN rod system. The on-axis and off-axis propagation of CP optical vortex (OV) resulted in addition and subtraction of net topological charge in orthogonal CP projection. The SHE under the influence of OV beam is investigated which exhibits an asymmetric behaviour as a function of input launch position due to contributions from the OHE of light. Even the polarization content due to OV beam revealed an asymmetric behaviour as a function of input lauch position. The asymmetric behaviour can also be attributed to the curvature of the trajectory taken by the beams through the GRIN rod. The SHE is measured and amplified through weak measurement technique. Weak stokes parameters are used to measure the

small polarization changes in the output optical field. The optical phases of the output optical fields are measured through an interference.

Moreover, the OOI of light is also studied in a two-mode optical fiber (TMF) for all the input positions. The rotation of HG-like output optical field due to azimuthal off-axis excitation of TMF with a Gaussian beam is understood as the orbital-Berry phase accumulation of constituent LG beams of +1 and -1 topological charges respectively due to OOI of light. The rotation values of HG-like modes are extracted using an auto-correlation technique. The overall rotation characteristics of HG-like mode revealed a topological character when mapped onto an input position dependent grid.

Finally, we outline the future prospects of the SOI and OOI's of light to be explored in polarization singularities, Airy-beams, and Elliptical optical vortex beams, which may provide additional degrees of freedom for investigation and efficient manipulation of light at nanoscale level.

CONTENT

1	Introduction	1
	1.1 Brief History of light	3
	1.2 GRIN rod	4
	1.3 Angular momentum of light	6
	1.3.1 Spin angular momentum of light	6
	1.3.2 Orbital angular momentum of light	7
	1.4 Geometric phase	9
	1.4.1 Rytov-Vladimirskii-Berry phase	10
	1.4.2 Pancharatnam-Berrt phase	10
	1.5 Spin-orbit interactions (SOI) of light	11
	1.5.1 SOI due to RVB phase	12
	1.5.2 SOI due to PB phase	13
	1.6 Thesis outline	14
	References	16
2	Spin-to-orbital and orbital-to-spin angular onversion of light in inhomogeneous media	momentum 23
	2.1Introduction	25
	2.2 SOI of light in an inhomogeneous media	27
	2.3 Theoretical formalism	28
	2.3.1 Spin-to-orbital AM conversion	28
	2.3.2 Reciprocal Spin-orbit Coupling	31
	2.4 Experimental details	33
	2.5 Results and discussion	34
	2.5.1 Spin-to-orbital AM conversion	34
	2.5.2 Orbital-to-spin AM conversion	36
	2.6 Summary	37
	References	39

3 Reciprocity of spin-Hall effect of light in GRIN rod	4
3.1 Introduction	
3.2 SHE in inhomogeneous media	
3.3 Theoretical formalism	
3.3.1 Spin-Hall effect of light	
3.3.2 Reciprocal spin-Hall effect of light	
3.4 Experimental details	
3.5 Results and discussion	
3.5.1 Spin-Hall effect of light	
3.5.2 Reciprocal spin-Hall effect of light	
3.6 Summary	
References	
4 Orbital-Hall effect of light in GRIN rod	
4 Orbital-Hall effect of light in GRIN rod 4.1 Introduction	
4.1 Introduction	
4.1 Introduction 4.2 Orbital-Hall effect of light	
4.1 Introduction4.2 Orbital-Hall effect of light4.3 Theoretical formalism	
4.1 Introduction 4.2 Orbital-Hall effect of light 4.3 Theoretical formalism 4.3.1 Orbital-Hall effect of light	
 4.1 Introduction 4.2 Orbital-Hall effect of light 4.3 Theoretical formalism 4.3.1 Orbital-Hall effect of light 4.3.2 Reciprocal orbital-Hall effect of light 	
 4.1 Introduction 4.2 Orbital-Hall effect of light 4.3 Theoretical formalism 4.3.1 Orbital-Hall effect of light 4.3.2 Reciprocal orbital-Hall effect of light 4.4 Experimental details 	
4.1 Introduction 4.2 Orbital-Hall effect of light 4.3 Theoretical formalism 4.3.1 Orbital-Hall effect of light 4.3.2 Reciprocal orbital-Hall effect of light 4.4 Experimental details 4.5 Results and discussion	
4.1 Introduction 4.2 Orbital-Hall effect of light 4.3 Theoretical formalism 4.3.1 Orbital-Hall effect of light 4.3.2 Reciprocal orbital-Hall effect of light 4.4 Experimental details 4.5 Results and discussion 4.5.1 Orbital-Hall effect of light	

5 Mutual influence of SAM, IOAM and EOAM of lig GRIN rod	ht in 75
5.1 Introduction	77
5.2 Spin-induced effects on OAM of light	78
5.2.1 Experimental results and discussion	81
5.3 Spin-mediated orbital-Hall effect of light	82
5.3.1 Experimental results and discussion	84
5.4 Influence of IOAM on SHE	86
5.4.1 Experimental results and discussion	88
5.5 Polarization changes due to IOAM beams	93
5.5.1 Experimental results and discussion	94
5.6 Summary	98
References	99
6 Orbit-orbit interaction of light in two-mode optical fiber	101
6.1 Introduction	103
6.2 Theoretical formalism	103
6.3 Experimental details	110
6.4 Results and discussion	111
6.5 Summary	114
References	115
7 Summary, Concluding remarks and Future prospects	117
7.1 Summary	119
7.2 Concluding remarks	122
7.3 Future prospects	123
References	124
List of Publications	125

1

INTRODUCTION

This chapter gives a brief historical account of some essential milestones that brought out several note-worthy aspects of light which are relevant to the thesis. The spin angular momentum, intrinsic orbital angular momentum, and extrinsic orbital angular momentum concepts associated with polarization, helical phase structure, and shifted trajectory of the beam are discussed. Origin of the geometric phase is also discussed and categorized into two phases Rytov-Vladimirskii-Berry (RVB) phase related to the propagation direction and Pancharatnam-Berry (PB) phase associated with polarization manipulation of light. The spin-orbit interaction based on the RVB and PB phase is also introduced with examples.

1.1 Brief History of light

The advances in the study of of light and its properties provided humanity with excellent tools to probe the fundamentals of nature. It was the ancient Greek philosophers Socrates (469-399 B.C), Plato (427-347 B.C), and Aristotle (384-322 B.C) who laid the foundation for modern optics [1]. The optical effects such as diffusion, reflection, and vision were summarized by Euclid (330- 275 B.C) into a concise book titled "Optics" [1]. After Euclid, the research concerning the optics remained untouched for more than 1300 years. Around 1000 A.D, an Islamic Scholar and philosopher named Ibn al-Haytham (965-1040) compiled his works on reflection and refraction of light through the mirrors and lenses into a book called "Book of optics" [1,2]. Around 16th-century, Bartholinus observed double refraction of light in Iceland Spar which brought out the polarization aspect of light [3]. The speed of light has been a contention of debate regarding whether it is finite or infinite. Galileo attempted to measure the speed of light by using lamps to observe delay at a distance. In 1679, Rømer was the first one to experimentally measure speed of light, and the value was closer to contemporary measurement. The speed of light is one of the fundamental aspects of nature, and it is constant in free space.

Newton described the light as a collection of particles and proposed the corpuscular theory of light. He also experimentally demonstrated the white light as a mix of various colours in his famous prism experiment [4]. Around the same time, Christiaan Huygens opposed the particle theory of light and suggested that light is a wave [5]. In 1801, Thomas Young experimentally demonstrated the wave nature of light in the remarkable Double-slit experiment [6]. The formulation of Maxwell's Equations by James Clerk Maxwell in 1864 established light as an electromagnetic (EM) wave with finite energy and momentum [7]. The electric and magnetic field oscillations of light are perpendicular to each other and to the direction of propagation, valid for the free-space propagation of EM field.

At the start of 19^{th} Century, there was a paradigm shift in the understanding the fundamental nature of light. Max Planck explained the black body radiation's emission or absorption by considering light as discrete energy packets - Quanta. He introduced Planck's constant \hbar in the mathematical formalism to explain the black-body radiation in 1900 [8]. Albert Einstein in his famous paper [9] used the quantum aspect of light to describe the photoelectric effect which fetched him Nobel Prize in 1921 [9]. The dual behaviour of light for the photoelectric effect, Interference, and Diffraction questioned the very nature of light. The Young's

Double-slit experiment outcome with and without observer added to the existing complexity. Later, it was resolved that light is both particle and wave establishing particle-wave duality.

The applications of light are plenty abound, being used in optical fiber communication, gravitational wave research, and trapping particles to slow down and cool to ultra-low (sub kelvin) temperatures. The Laser cooling mechanism provides the reference optical frequencies to improve atomic clock precision [10]. Data transfer is done using the semiconductor Laser sources, through optical fiber for millions of miles ensuring connectivity that we enjoy nowadays. It is also used in Entanglement for the Quantum key distributions, to improve the security of information during data transmission.

1.2 GRIN rod

Investigation of optical properties of biological samples, crystals and thin films; Raman and Fluorescence microscopy for imaging or in scanning microscope; and many other such systems rely heavily on the optical components. Optical lenses come are one of the most used and needed optical components in many experiments. Optical lenses have been thoroughly investigated for aberrations and associated effects on imaging, propagation and wavefront changes. Various techniques have been developed to compensate for the aberrations associated with lenses. Nowadays adaptive optics is at the forefront, right from designing to implementation for aberration-free images and phase-corrected wavefronts. Stability, space constraints and small optical fiber connectors/couplers are some of the many reasons for the requirement of smaller optical components. The small sizes of lenses are achieved by replacing thickness variation of glass with refractive index variation across the cross-section of cylindrically symmetric glass. This process of refractive index variation is straight forward compared to curvature tuning for small lenses by thickness variation. Due to the refractive index variation, these optical lenses are coined as the "Graded-refractive index" or "Graded-refractive index" rod/lens and in short 'GRIN' rod/lens. The following equation governs the refractive index variation

$$n(r) = n_0 \left(1 - \frac{Ar^2}{2} \right)$$

Where A and n_0 are gradient constant and on-axis refractive index of the GRIN rod respectively. The refractive variations can be of different types such as secant function, axial (along propagation direction), spherical negative (Maxwell's

fisheye lens) and can be tailored according to the requirement. The typical size of GRIN rods varies within few mms length with varying pitches. Variation in the pitch of GRIN rod results in imaging, collimating and focusing of the output light. Apart from the small size, GRIN rod offers many advantages over the conventional lens as mentioned below

- a) More comfortable to mount and assemble due to planar input and output surfaces
- b) Good on-axis and off-axis performance
- c) as fiber coupler
- d) non-toxic silver and lithium-ion exchange process

GRIN rods are manufactured through various methods [11-18], have different shapes [19-24] and different material compositions [25-29]. Applications of GRIN rod are vast and dynamic, such as their implementation in holographic endoscopy, optical interconnections, perfect imaging, in-vivo imaging of biological samples, two-photon fluorescence endomicroscopes and in microscopy [30-42]. Grating structured GRIN rod was used for direct coupling of light with the thin films whereas a stack-based GRIN rod was used for nanophotonic chip coupling [43,44]. Conventional materials are substituted with M(m)etamaterials for specific applications such as tight focusing at THz frequency, Broadband microwave Luneburg lens and Maxwell fisheye lens for integrated optics [45-48].

GRIN rod is an inhomogeneously isotropic media with quadratic refractive index variation along the transverse direction. But it does exhibit birefringence with radial and tangential modes [49-55]. It also displays weak-anisotropy through the polarization dependent refractive-index corrections for right and left circular polarization corresponding to variations in propagation direction [102, 103]. This provides an unique opportunity to investigate the spin-orbit and orbit-orbit interactions of light under the influence of both inhomogeneity and weak anisotropy.

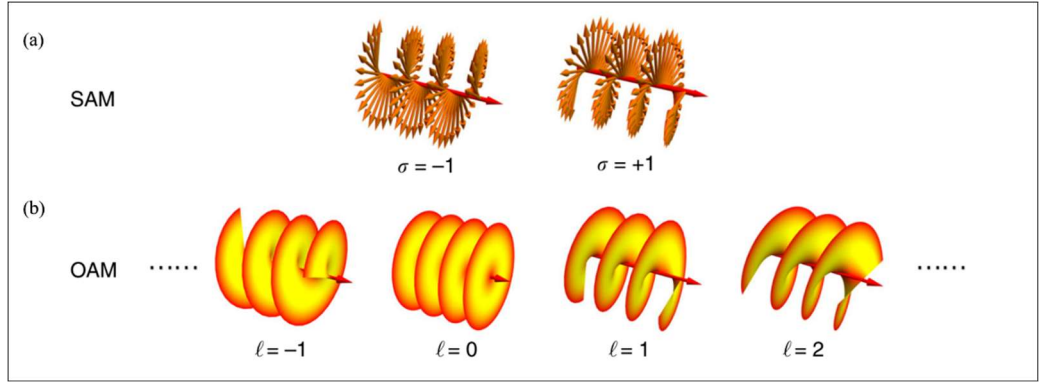


Figure 1. (a) Electric field oscillations of CP with SAM (b) helical phase fronts of Optical vortex beams with OAM. [Shen et al. Light: Science & Applications (2019) 8:90].

1.3 Angular momentum of light

Kepler suggested that light bears angular momentum (AM), based on the observation of comet tail pointing away from the sun's radiation. Almost after two centuries, the angular momentum aspects of light were brought to light by Maxwell. Maxwell's theory of electromagnetism established light as an electromagnetic wave. According to his equations, EM wave (light) has both energy and momentum. Later, Poynting was the one to formulate that circularly polarized (CP) light contains spin angular momentum (SAM) equal to $\sigma\hbar$ [57]. The right (R) and left (L) circularly polarized light has the SAM values \hbar and $-\hbar$ respectively where \hbar is the Planck constant [57]. Generation, detection, and manipulation of both SAM and IOAM beams are omitted here.

1.3.1 Spin angular momentum of light

Einstein de-Haas effect serves as a precursor to the mechanical aspect of AM associated with electron's spin. A change in the magnetic moment of a free body imparts torque to the body, resulting in the rotation of the body conserving the total AM of the system [58]. It was experimentally reported in 1915 by Albert Einstein and Wander Johannes de Haas [58]. After two decades, in 1936, Beth experimentally realized the angular momentum associated with circular polarization of light [59]. In his experiment, Birefringent plate was held by an optical fiber for precision measurement. The Birefringent plate rotates upon passage of right circularly polarized light. This rotation is attributed to exchange of AM between light and Birefringent plate to conserve the total AM of light. Unlike circularly polarized light the linearly polarized light carries no SAM. SAM of light is independent of the axis, making it intrinsic AM.

Optical tweezer's usage in the late '70s and '80s by Ashkin, wherein a microscopic particle was trapped in 3-dimensions due to a single-beam gradient force generated by tightly focusing the Gaussian beam. The use of linearly polarized Gaussian beam with zero SAM in optical tweezer setup traps the particle whereas the circularly polarized light with SAM results in spinning of the particle. The implementation of Optical tweezers for probing the intrinsic nature of SAM while trapping the absorptive particles gave clear insights into AM aspects of light [60]. The size of the particle and focussed beam diameter are critical in determining the location of trapping. The particle is trapped along the beam axis if its size is larger than focused beam and otherwise trapped at off-axis position. For both cases the particle spins around its axis due to transfer of AM, and this establishes intrinsic nature of SAM. Optical tweezers with SAM beam contributed to realization of optical driven pumps and ultrafast rotation of particles trapped in vacuum [61,62]. The SAM of CP light was also used to study the angular doppler effects. The propagation of CP light through the rotating body with an angular velocity Ω yielded a frequency shift of the CP light by $\pm\Omega$ depending on the polarization handedness of CP and rotating body. These frequency shifts associated with angular Doppler effect have been effectively used to measure the rotational velocity of particle.

1.3.2 Orbital angular momentum of light

In 1992, Allen et al., in their seminal work established that light beams with helical phasefronts carry orbital angular momentum (OAM) equal to ±1h [63]. The OAM value can take far higher values than SAM associated with circular polarization [63]. Due to the helical phase structure, the OAM beam does not have a defined phase at the beam axis, indicating phase singularity. Therefore, OAM beams are also known as optical vortex (OV) or phase singular beams. The spatial structure of OV beam is distinct with annular profile resembling a donut. The sense in which helical phase rotates around the beam axis is distinguished with +lh for clockwise and -lh for counter-clockwise rotation. Interference of optical vortex with a Gaussian beam is marked by signature spiral (on-axis) or fork (off-axis) pattern. The OAM of an OV beam depends on the beam axis and thus can be described as quasi-intrinsic. Optical tweezers with OV beams resulted in different outcomes compared to SAM beams where the size of the focussed beam is greater than the particle. The particle trapped at an off-axis position is rotated around the beam axis due to azimuthal scattering force of OV beam. An optical beam with both SAM and OAM has been used in optical tweezers, enabling stop and start spin switch functionality by manipulating the

handedness of both SAM and OAM resulting in zero or $2\hbar$ total angular momentum of light beam respectively [64].

Doppler effect associated with frequency shift due to the motion of either observer or source is also affected by OAM of OV beam. Angular doppler effect of OV beam shifts the frequency by $l\Omega$ [65,66]. Propagation of OV beam through a phase-matched non-linear crystal resulted in frequency doubling. Unlike the fundamental Gaussian beam mode, the OV beam not only undergoes frequency doubling but also doubling of topological charge value due to conservation of angular momentum of light [67]. The total OAM value associated with signal and idler is always equal to pump value in the parametric downconversion. The uncertainty principle states that the accuracy in position measurement is associated with significant uncertainty in momentum of particle and vice-versa for conjugate variables. There exists an equivalent uncertainty relation for the conjugate variables; angular momentum and angular position given by $\Delta \phi \Delta l \ge 1/2$ [68]. Optical vortex beams have also been used in imaging for their gains; the point spread function with term $\exp(il\varphi)$ is used for enhancing the edges of an image [69]. The bright light from the stars is suppressed by using OV beams to observe the neighbouring celestials [70]. The OV beam with unlimited states offers an enticing prospect for optical communications, put into use in variety of systems such as optical fibers, mmwave operations, over city links and free space transmission [71-76].

The AM aspects of light can be divided into two categories.

1. Intrinsic AM

- a) SAM: The SAM related to CP of the Gaussian beam is independent of beam axis. This has been demonstrated in the case of optical tweezers with different particle and beam focus sizes.
- b) OAM: OAM due to the helical phase structure of OV beam is Quasi-Intrinsic (both intrinsic and extrinsic). In the scenario with off-axis particle trapping with OV beam, the particle rotates around the beam axis. The on-axis trapping leads to the particle spinning about beam axis. Therefore, OAM associated with OV beam depends upon the choice of axis location, and thus *Quasi-Intrinsic*.

2. Extrinsic OAM

As with the case of OV's, the AM for a Gaussian beam propagating at angle or shifted with respect to the propagation axis depends on the axis position. This AM is marked by linear phase gradients while the AM associated with OV beams have a rotational counterpart with azimuthal phase gradient.

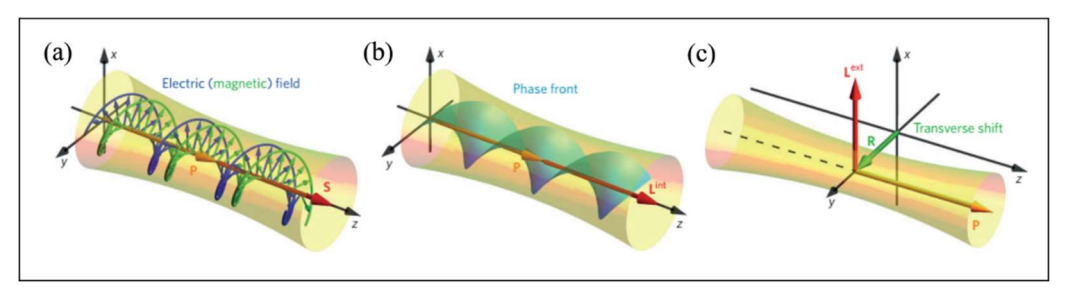


Figure 1. Intrinsic AM (a) SAM associated with the CP Gaussian beam. (b) OAM of an OV beam; Extrinsic AM (c) transverse shift resulting in the EOAM for a Gaussian beam [Nat. Photonics 9, p796 (2015)].

1.4 Geometric phase

The evolution of the dynamical systems in relation to phase was largely neglected by the scientific community. Berry, in an influential paper published in 1984 titled "Quantum phase factors accompanying adiabatic changes" gave a detailed description of the phase changes associated with geometry of the path taken by the system in parameter space or state space [77,81]. Initially, the geometric phase (GP) is studied in the context of quantum systems and later extended to classical systems as well. Berry's work considered the cyclic adiabatic evolution under unitary transformation. Upon the return of system to the initial position in parametric space, the system acquires an additional geometry-dependent phase. A more general case with non-cyclic, non-adiabatic, and non-unitary evolution of the system in parametric space was investigated for real-world scenarios [78-80]. Bartolotti in 1926 and Sergei M. Rytov in 1938 arrived at a conclusion regarding the rotation of polarization vector for propagation along a coiled ray. The rotation of polarization vector is analysed using the geometry of the coiled ray. V.V. Vladimirskii was the first to experimentally measured the effect in 1941. After a decade, Pancharatnam realized the polarization related phase for propagation through the anisotropic media in 1956, known as Pancharatnam Berry (PB) phase [84]. Later in 1985, John Hannay experimentally measured the classical analogue of Quantum Berry phase, related to the precision of a Foucault pendulum. Under the small-angle oscillations of Harmonic oscillator, it was found that the origin of rotation of invariant plane of Foucault pendulum was geometric in nature and equal to modulo 2π times the solid angle subtended by path and known as *Hannay angle* [82]. The geometric phase is independent of the rate of evolution of path, and also the Hannay angle does not depend on the angular velocity of the rotating body. Hannay angle and Berry phase are classical and quantum analogues of geometric phase.

Though manifestations of the Geometric phase are investigated in physics, chemistry, and engineering fields, it has a profound effect in optics. In optics, the Geometric phase is categorized into two types, namely a) Rytov-Vladimirskii-Berry phase [83] and b) Pancharatnam Berry phase [84].

1.4.1 Rytov-Vladimirskii-Berry phase

For a polarized light, due to a non-planar trajectory, the light acquires geometric phase equivalent to the solid angle subtended by the propagation vector in momentum space [83-88]. The first experimental realization of RVB phase was achieved in optical fibers by Tomita and Chiao [89]. The optical fiber was helically wound around a cylinder with matching initial and final positions in momentum space forming a closed circuit. The rotation of polarization vector was proportional to pitch of helix. Free space demonstration of RVB phase was accomplished by aligning mirrors in such a way that the light gets reflected in all (X, Y and Z) directions.

1.4.2 Pancharatnam-Berry phase

Long before Sir Michael Berry, S. Pancharatnam introduced the concept of geometric phase associated with polarization changes of light, known as Pancharatnam Berry phase [84]. He addressed the question about relative phase difference between two different polarizations, and the origin of this relative phase is geometric in nature. A cyclic variation of the state of polarization of light resulted in a phase shift. Representation of the polarization states onto Poincaré sphere aided Pancharatnam in bringing out the geometric nature of observed phase shift. Birefringent materials with different refractive indices for ordinary and extra-ordinary polarization modes have been used to observe the geometric phase due to polarization. The commonly used optical elements half-wave plate (HWP) and quarter-wave plate (QWP) are examples of birefringent material.

Propagation of linearly polarized light through HWP causes the rotation of polarization vector by 2θ , where θ is change in the orientation of HWP with respect to fast-axis. The propagation of circularly polarized light through HWP flips the helicity of CP irrespective of HWP orientation. The global phase change for propagation through the HWP is the Pancharatnam Berry phase.

Phase	Year	Field	Parameter space	Topological	Adiabatic
Pancharatnam	1956	Optics	Poincaré sphere	No	Yes
Aharonov- Bohm	1959	Quantum electrodynamics	Spacetime	Yes	No
Exchange statistics	1977 1982 1984	Condensed matter	Real space	Yes	Yes
Berry	1983 1984	Quantum mechanics	General	No	Yes
Aharonov- Casher	1984	Quantum electrodynamics	Real space	Yes	No
Hannay angle	1985	Classical mechanics	Real space	No	Yes
Aharonov- Anandan	1987	Quantum mechanics	General	Yes	No
Zak	1989	Condensed matter	Momentum space	No	No

Table: Chronology of manifestations of the geometric phase in different fields. [85]

1.5 Spin-orbit interactions of light

Propagation of Gaussian beam through free-space or isotropic media does not couple the spin and orbital angular momenta of light [90,91]. In contrast, the propagation of the Gaussian beam through an inhomogeneous or anisotropic media or inhomogeneously anisotropic media or by tight focussing in an isotropic media couples spin (polarization) and orbital (path) AM of the light beam due to the transversality condition [91,92]. This leads to path-dependent rotation of plane of polarization due to accumulation of RVB phase. Subsequently, a transverse polarization-dependent splitting of path occurs due to opposite phase gradient for RCP and LCP beams known as spin-Hall effect (SHE) of light. Likewise, a new class of effects were also proposed and realized that are

associated with phase singular OAM carrying LG beams. The dynamics are governed by orbit-orbit interaction of light related to IOAM and EOAM of the light.

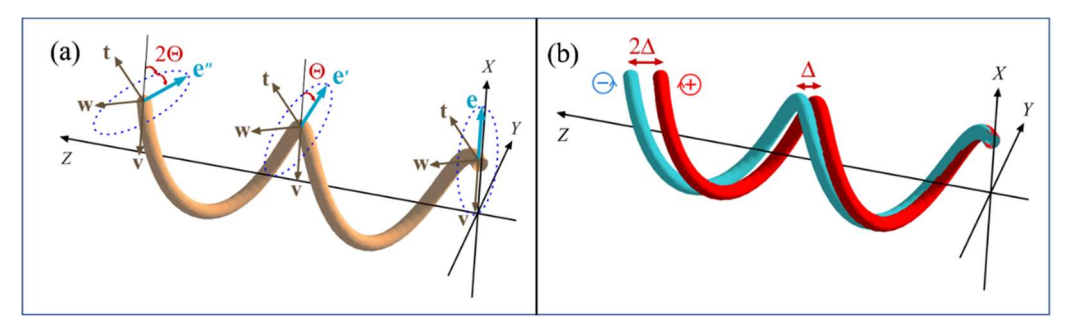


Figure 3. (a) accumulation of geometric Berry phase and (b) SHE of light due to smooth helical trajectory [J. Opt. A: Pure Appl. Opt. 11 (2009) 094009].

1.5.1 SOI due to RVB phase

Under the symmetry paraxial condition, the RVB phase for an incident CP Gaussian beam results in spin to orbital conversion (SOC) of light due to azimuthal phase accumulation in orthogonal CP [94]. The input RCP/LCP generates a LCP/RCP OV beam with topological charge (TC) ±2. The paraxial condition no longer holds under tight focusing leading to non-paraxiality. Non-paraxial propagation due to the tight focusing of CP Gaussian beam also results in the SOC in the orthogonal CP [95]. Under non-paraxial conditions, focusing and scattering by nanoparticle generates OV beams [96,97]. If the direction of the propagation is oblique or shifted with respect to propagation axis, the azimuthal phase transforms into linear phase gradients resulting in SHE of light.

In 1992, Zel'Dovich et al. gave the SOI terminology for the propagation of plane polarized Gaussian beam in an inhomogeneous isotropic medium [98]. They have theoretically anticipated and experimentally demonstrated the optical Magnus effect in an optical fiber. The sharp change in the refractive index during reflection and reflection was also of considerable interest due to spin-dependent shift of Centre of Intensity (COI), known as Imbert-Fedorov effect [99,100]. This effect is also known as Hall effect of light. Onada et al. explained the Hall effect in terms of conservation of angular momentum of light [103]. Bliokh later explained the phenomenon with underlying geometric phase mechanism due to variation in wavevector direction [101,102].

Later, an extension to the Geometric phase dealing with the propagation of OV beams in an inhomogeneous (graded-index) medium was discussed by Bliokh. The GP associated with OV beam is termed Orbital Berry phase (OBP) and is governed by the same parallel transport law that holds for CP Gaussian beam. A topological charge-dependent transverse shift in the OV beam is also proposed due to the OBP accumulation in graded-index medium, labelled as orbital Hall effect (OHE) of light [106]. The sign of TC of the incident OV beams can be reversed through propagation in a coiled optical fiber [107].

1.5.2 SOI due to PB phase

Liquid crystals with inhomogeneous anisotropic properties had a significant role to play in understanding the SOI of light. In 2006, Marrucci et al. demonstrated the SOC for an incident Gaussian beam, by manipulating the orientation of liquid crystals [92]. Q-Plate with its position-dependent orientation of liquid crystals is used to generate specific PB phase profile for orthogonal CP Gaussian beam, offering an advantage over other methods. Propagation of Gaussian beam through Uniaxial crystal also exhibits SOC. The Conoscopic configuration for RCP Gaussian beam through the Uniaxial crystal generates a LCP OV beam of TC +2 and vice-versa [108]. Tilting the Uniaxial crystal or HWP leads to SHE due to circular birefringence [110]. The PB phase is also manipulated to enhance the SHE of light [109]. The PB phase-based optical elements such as Pancharatnam lens are being used for scalability and flexibility and to study novel effects. The patterning of metamaterials similar to Q-plates has proven to be advantageous to control and manipulate light at nanoscale [111]. Metasurface lens is being implemented for spin specific focusing and imaging [112].

Based on the interaction of different AM of light, the associated SOI and OOI effects can be categorized as follows

- a) First order effects coupling between two AM, Ex: SAM and EOAM resulting in SHE and RVB phase accumulation
- b) Second-order effects (SOE) joint effect of two AM on third AM of light, Ex: Effect of SAM and IOAM on EOAM [93].

1.6 Thesis outline

Chapter 2 discusses the on-axis propagation of CP Gaussian and OV beams through GRIN rod. The on-axis propagation of RCP and LCP Gaussian beams through the GRIN rod generates an OV beam with a topological charge of +2 and -2 in orthogonal CP projections respectively. The phase of the generated OV beams is measured using a Mach-Zehnder interferometer setup. Fourier transform fringe analysis method is used to extract the phase of the OV beams. Propagation of zero SAM OV beams with different TCs resulted in weak CP components in the optical output field. Correspondingly, Weak (S3) Stokes parameters were calculated by rotating the polarizer by a small-angle compared to conventional stokes parameters measurement.

In Chapter 3, The propagation dynamics associated with linearly polarized Gaussian beam through the GRIN rod as a function of off-axis position are investigated. The off-propagation breaks rotational symmetry of the system, leading to opposite phase gradients for RCP and LCP beams in momentum space resulting in a polarization-dependent transverse shift in real space. This tiny spin-Hall shift is typically in the order of wavelength of light. The weak measurement method is used to amplify the wavelength- order shifts using a combination of QWP and polarizer. In the next part of the chapter, the rotation of polarization vector of the optical output field as a function of input position is discussed. The weak (S3) Stokes parameters are measured to quantify the small changes associated with polarization.

Chapter 4 discusses the off-axis propagation of OV and zero OAM HG beams through the GRIN rod, in relation to orbit-orbit interaction of light. SOI effects associated with SAM, such as SHE and RVB phase (reciprocal SHE) find their counterparts with the OV and HG beams, which are orbital-Hall effect (topological charge-dependent transverse shift of OV beams) and reciprocal OHE (rotation of spatial intensity structure of the HG beam) respectively. Both effects are independent of polarization and therefore no polarization components were used in capturing the images of the output.

In Chapter 5, we investigate the Second-order effects, the influence of two AM of light on the third and the corresponding outcomes. First, the on-axis propagation of CP OV beams through the GRIN rod is discussed, which results in the algebraic addition and subtraction of topological charge in orthogonal CP projection based on the handedness of TC and SAM. Next, off-axis propagation of CP OV beams is explored, leading to effective TC dependent OHE of light in orthogonal CP projection. Later, the effect of OV beams on the SHE is discussed.

Finally, the polarization changes associated with linearly polarized (LP) OV beam are examined as a function of input position of the GRIN rod.

Chapter 6 deals with OOI of light in a torsion, twist-free two-mode optical fiber. The on-axis propagation of Gaussian beam through the axis of optical fiber excites the fundamental Gaussian beam whereas the off-axis propagation with broken rotational symmetry results in an output HG like LP beam. The output HG beams for diametrically opposite launch positions are π phase shifted, which are marked by a dominant lobe in spatial mode. The azimuthal variation of input launch position resulted in the rotation of the output HG mode due to orbital Berry phase. The rotation of HG beams and OBP accumulation is understood via orbit-orbit interaction of constituent LG beams with TCs +1 and -1 respectively. A Mach-Zehnder interferometer setup is constructed to measure the phase changes through a reference Gaussian beam. The cumulative phase changes due to rotation of HG beams for all the input positions are mapped onto position-dependent grid which revealed a topological character.

In Chapter 7, we summarize the effects discussed above, drawing conclusions from each result and providing possible applications.

References:

- 1. https://photonterrace.net/en/photon/history/
- 2. <u>Toomer, G. J.</u> (December 1964), "Review: Ibn al-Haythams Weg zur Physik by Matthias Schramm", Isis, **55** (4): 463–465, doi:10.1086/349914
- 3. Erasmus Bartholin, *Experimenta crystalli islandici disdiaclastici quibus mira & insolita refractio detegitur* (Copenhagen ("Hafniæ"), Denmark: Daniel Paulli, 1669).
- 4. <u>Newton, Isaac</u> (1998). Opticks: or, a treatise of the reflexions, refractions, inflexions and colours of light. Also, two treatises of the species and magnitude of curvilinear figures. Commentary by Nicholas Humez (Octavo ed.). Palo Alto, Calif.: Octavo. *ISBN 1-891788-04-3.* (Opticks was originally published in 1704).
- 5. Huygens, Christiaan. Treatise on light. tredition, 2012.
- Young, Thomas. "I. The Bakerian Lecture. Experiments and calculations relative to physical optics." *Philosophical transactions of the Royal Society of London* 94 (1804): 1-16.
- 7. Maxwell, James Clerk. *A treatise on electricity and magnetism*. Vol. 1. Clarendon press, 1881.
- 8. Planck, Max. "On the law of distribution of energy in the normal spectrum." *Annalen der physik* 4.553 (1901): 1.
- 9. Einstein, Albert. "On a heuristic point of view about the creation and conversion of light." *Annalen der Physik* 17.6 (1905): 132-148.
- 10. Kenyon, Ian R. *The light fantastic: a modern introduction to classical and quantum optics*. Oxford University Press, USA, 2008.
- 11. Houde-Walter, Susan N., and Duncan T. Moore. "Gradient-index profile control by field-assisted ion exchange in glass." *Applied optics* 24.24 (1985): 4326-4333.
- 12. Ohmi, Sigeaki, et al. "Gradient-index rod lens made by a double ion-exchange process." *Applied optics* 27.3 (1988): 496-499.
- 13. Messerschmidt, Bernhard, Torsten Possner, and Rolf Goering. "Colorless gradient-index cylindrical lenses with high numerical apertures produced by silver-ion exchange." *Applied optics* 34.34 (1995): 7825-7830.
- 14. Huang, Yingyan, and Seng-Tiong Ho. "Superhigh numerical aperture (NA> 1.5) micro gradient-index lens based on a dual-material approach." *Optics letters* 30.11 (2005): 1291-1293.
- 15. Liu, Jui-Hsiang, and Yi-Hong Chiu. "Process equipped with a sloped UV lamp for the fabrication of gradient-refractive-index lenses." *Optics letters* 34.9 (2009): 1393-1395.
- 16. Lv, Hao, et al. "Multistep ion exchange processes of gradient refractive index rod lens." *Optics letters* 36.1 (2011): 28-30.
- 17. Zakeri, Banafsheh, and Arash Sabatyan. "Theoretical considerations for anticipating of function analysis on a gradient index-lens fabrication through double ion-exchange process." *Applied optics* 51.26 (2012): 6290-6294.
- 18. Hernandez-Serrano, A. I., et al. "Fabrication of gradient-refractive-index lenses for terahertz applications by three-dimensional printing." *JOSA B* 33.5 (2016): 928-931.

- 19. Koike, Yasuhiro, Hiroshi Hidaka, and Yasuji Ohtsuka. "Plastic axial gradient-index lens." *Applied optics* 24.24 (1985): 4321-4325.
- 20. Koike, Yasuhiro, Yuji Sumi, and Yasuji Ohtsuka. "Spherical gradient-index sphere lens." *Applied optics* 25.19 (1986): 3356-3363.
- 21. Asahara, Yoshiyuki, et al. "Gradient-index slab lens with high numerical aperture." *Applied optics* 25.19 (1986): 3384-3387.
- 22. Song, Deqiang, et al. "Micro gradient-index conical lenses: simulation and fabrication methods." *Applied optics* 44.18 (2005): 3747-3751.
- 23. Lv, Hao, et al. "Gradient refractive index square lenses. I. Fabrication and refractive index distribution." *JOSA A* 26.5 (2009): 1085-1089.
- 24. Liu, Aimei, et al. "Gradient refractive index square lenses. II. Imaging." *JOSA A* 26.12 (2009): 2512-2514.
- 25. Kindred, Douglas S. "Gradient-index silver alumina phosphate glasses by exchange of Na+ for Ag+." *Applied optics* 29.28 (1990): 4051-4055.
- Fujii, Kiyosumi, Syuya Ogi, and Noboru Akazawa. "Gradient-index rod lens with a high acceptance angle for color use by Na+ for Li+ exchange." *Applied optics* 33.34 (1994): 8087-8093
- 27. Koike, Yasuhiro, et al. "Spherical gradient-index polymer lens with low spherical aberration." *Applied optics* 33.16 (1994): 3394-3400.
- 28. Liu, Jui-Hsiang, and Hung-Tsai Liu. "Gradient refractive-index optical rod prepared from methacrylate derivatives." *Optics letters* 22.10 (1997): 668-670.
- 29. Ji, Shanzuo, et al. "A bio-inspired polymeric gradient refractive index (GRIN) human eye lens." *Optics express* 20.24 (2012): 26746-26754.
- 30. von Bally, Gert, et al. "Gradient-index optical systems in holographic endoscopy." *Applied Optics* 23.11 (1984): 1725-1729.
- 31. von Bally, Gert, E. Brune, and W. Mette. "Holographic endoscopy with gradient-index optical imaging systems and optical fibers." *Applied optics* 25.19 (1986): 3425-3429.
- 32. Song, Seok Ho, et al. "Gradient-index planar optics for optical interconnections." *Optics letters* 23.13 (1998): 1025-1027.
- 33. Gordon, Jeffrey M. "Spherical gradient-index lenses as perfect imaging and maximum power transfer devices." *Applied Optics* 39.22 (2000): 3825-3832.
- 34. Kotsidas, Panagiotis, Vijay Modi, and Jeffrey M. Gordon. "Gradient-index lenses for near-ideal imaging and concentration with realistic materials." *Optics express* 19.16 (2011): 15584-15595.
- 35. Huland, David M., et al. "In vivo imaging of unstained tissues using long gradient index lens multiphoton endoscopic systems." *Biomedical optics express* 3.5 (2012): 1077-1085.
- Matz, Gregor, Bernhard Messerschmidt, and Herbert Gross. "Design and evaluation of new color-corrected rigid endomicroscopic high NA GRIN-objectives with a sub-micron resolution and large field of view." *Optics express* 24.10 (2016): 10987-11001
- 37. Reed, William A., Man F. Yan, and Mark J. Schnitzer. "Gradient-index fiber-optic microprobes for minimally invasive in vivo low-coherence interferometry." *Optics letters* 27.20 (2002): 1794-1796.
- 38. Göbel, Werner, et al. "Miniaturized two-photon microscope based on a flexible coherent fiber bundle and a gradient-index lens objective." *Optics letters* 29.21 (2004): 2521-2523.

- 39. Xie, Tuqiang, et al. "GRIN lens rod-based probe for endoscopic spectral domain optical coherence tomography with fast dynamic focus tracking." *Optics express* 14.8 (2006): 3238-3246.
- 40. Wang, Chen, and Na Ji. "Pupil-segmentation-based adaptive optical correction of a high-numerical-aperture gradient refractive index lens for two-photon fluorescence endoscopy." *Optics letters* 37.11 (2012): 2001-2003.
- 41. Huland, David M., et al. "Three-photon excited fluorescence imaging of unstained tissue using a GRIN lens endoscope." *Biomedical optics express* 4.5 (2013): 652-658.
- 42. Wang, Chen, and Na Ji. "Characterization and improvement of three-dimensional imaging performance of GRIN-lens-based two-photon fluorescence endomicroscopes with adaptive optics." *Optics express* 21.22 (2013): 27142-27154.
- 43. Wang, Qian, et al. "Thin-film stack based integrated GRIN coupler with aberration-free focusing and super-high NA for efficient fiber-to-nanophotonic-chip coupling." *Optics express* 18.5 (2010): 4574-4589.
- 44. Fricke-Begemann, Thomas, and Jürgen Ihlemann. "Direct light-coupling to thin-film waveguides using a grating-structured GRIN lens." *Optics express* 18.19 (2010): 19860-19866.
- 45. Neu, Jens, et al. "Metamaterial-based gradient index lens with strong focusing in the THz frequency range." *Optics express* 18.26 (2010): 27748-27757.
- 46. Loo, Yoke Leng, et al. "Broadband microwave Luneburg lens made of gradient index metamaterials." *JOSA A* 29.4 (2012): 426-430.
- 47. Gabrielli, Lucas H., and Michal Lipson. "Integrated Luneburg lens via ultra-strong index gradient on silicon." *Optics express* 19.21 (2011): 20122-20127.
- 48. Bitton, O., R. Bruch, and U. Leonhardt. "Two-dimensional Maxwell fisheye for integrated optics." *Physical Review Applied* 10.4 (2018): 044059.
- 49. Su, Wei, and John A. Gilbert. "Birefringent properties of diametrically loaded gradient-index lenses." *Applied optics* 35.24 (1996): 4772-4781.
- 50. Rouke, Jennifer L., and Duncan T. Moore. "Birefringence measurements in gradient-index rod lenses." *Applied optics* 38.31 (1999): 6574-6580.
- 51. Montoya-Hernández, Marcial, and Daniel Malacara-Hernández. "Polarization effects in interferograms of radial GRIN rods." *Optics communications* 175.4-6 (2000): 259-263.
- 52. Montoya-Hernández, Marcial, and Daniel Malacara-Hernández. "Spiral Fringes and Fringe Dislocations in GRIN Rod Testing." *Interferometry in Speckle Light*. Springer, Berlin, Heidelberg, 2000. 551-556.
- 53. Rouke, Jennifer L., and Duncan T. Moore. "Birefringence in gradient-index rod lenses: a direct measurement method and interferometric polarization effects." *Applied optics* 40.28 (2001): 4971-4980.
- 54. Tentori, Diana, and Javier Camacho. "Conoscopic evaluation of the birefringence of gradient-index lenses: infidelity sources." *Applied optics* 41.34 (2002): 7218-7228.
- 55. Tentori, Diana, and Javier Camacho. "Ordinary and extraordinary rays in gradient-index lenses." *Applied optics* 42.22 (2003): 4452-4462.
- 56. Poynting, John Henry. "XV. On the transfer of energy in the electromagnetic field." *Philosophical Transactions of the Royal Society of London* 175 (1884): 343-361.

- 57. Poynting, John Henry. "The wave motion of a revolving shaft, and a suggestion as to the angular momentum in a beam of circularly polarised light." *Proceedings of the Royal Society of London. Series A, Containing Papers of a Mathematical and Physical Character* 82.557 (1909): 560-567.
- 58. Einstein, A., and W. J. De Haas. "Experimental proof of the existence of Ampere's molecular currents." *Proc. KNAW*. Vol. 181. 1915.
- 59. Beth, Richard A. "Mechanical detection and measurement of the angular momentum of light." *Physical Review* 50.2 (1936): 115.
- 60. M. E. J. Friese, T. A. Nieminen, N. R. Heckenberg, and H. Rubinsztein-Dunlop, "Optical alignment and spinning of laser-trapped microscopic particles," Nature **394**(6691), 348–350 (1998)
- 61. Simpson, N. B., et al. "Mechanical equivalence of spin and orbital angular momentum of light: an optical spanner." *Optics letters* 22.1 (1997): 52-54.
- **62.** O'neil, A. T., et al. "Intrinsic and extrinsic nature of the orbital angular momentum of a light beam." *Physical review letters* 88.5 (2002): 053601.
- 63. L. Allen, M. W. Beijersbergen, R. J. C. Spreeuw, and J. P. Woerdman, "Orbital angular momentum of light and the transformation of Laguerre-Gaussian laser modes," Phys. Rev. A **45**(11), 8185–8189 (1992)
- 64. N. B. Simpson, K. Dholakia, L. Allen, and M. J. Padgett, "Mechanical equivalence of spin and orbital angular momentum of light: an optical spanner," Opt. Lett. **22**(1), 52–54 (1997).
- 65. Bialynicki-Birula, Iwo, and Zofia Bialynicka-Birula. "Rotational frequency shift." *Physical review letters* 78.13 (1997): 2539.
- 66. Courtial, J., et al. "Rotational frequency shift of a light beam." *Physical review letters* 81.22 (1998): 4828.
- 67. Dholakia, N. B. Simpson, M. J. Padgett, and L. Allen, "Second-harmonic generation and the orbital angular momentum of light," Phys. Rev. A **54**(5), R3742–R3745 (1996).
- 68. S. Franke-Arnold, S. M. Barnett, E. Yao, J. Leach, J. Courtial, and M. Padgett, "Uncertainty principle for angular position and angular momentum," New J. Phys. 6, 103 (2004).
- 69. S. Fürhapter, A. Jesacher, S. Bernet, and M. Ritsch-Marte, "Spiral phase contrast imaging in microscopy," Opt. Express **13**(3), 689–694 (2005).
- G. A. Swartzlander, Jr., E. L. Ford, R. S. Abdul-Malik, L. M. Close, M. A. Peters, D. M. Palacios, and D. W.Wilson, "Astronomical demonstration of an optical vortex coronagraph," Opt. Express 16(14), 10200–10207 (2008).
- N. Bozinovic, Y. Yue, Y. Ren, M. Tur, P. Kristensen, H. Huang, A. E. Willner, and S. Ramachandran, "Terabitscale orbital angular momentum mode division multiplexing in fibers," Science 340(6140), 1545–1548 (2013).
- 72. Wang, L. Zhu, S. Chen, C. Du, Q. Mo, and J. Wang, "Characterization of LDPC-coded orbital angular momentum modes transmission and multiplexing over a 50-km fiber," Opt. Express **24**(11), 11716–11726 (2016).
- Y. Yan, G. Xie, M. P. J. Lavery, H. Huang, N. Ahmed, C. Bao, Y. Ren, Y. Cao, L. Li, Z. Zhao, A. F. Molisch, M. Tur, M. J. Padgett, and A. E. Willner, "High-capacity millimetre-wave communications with orbital angular momentum multiplexing," Nat. Commun. 5, 4876 (2014)

- 74. M. Krenn, J. Handsteiner, M. Fink, R. Fickler, and A. Zeilinger, "Twisted photon entanglement through turbulent air across Vienna," Proc. Natl. Acad. Sci. U.S.A. 112(46),14197–14201(2015).
- 75. Krenn, J. Handsteiner, M. Fink, R. Fickler, R. Ursin, M. Malik, and A. Zeilinger, "Twisted light transmissionover 143 km," Proc. Natl. Acad. Sci. U.S.A. **113**(48), 13648–13653 (2016).
- G. Xie, Y. Ren, Y. Yan, H. Huang, N. Ahmed, L. Li, Z. Zhao, C. Bao, M. Tur, S. Ashrafi, and A. E. Willner, "Experimental demonstration of a 200-Gbit/s free-space optical link by multiplexing Laguerre-Gaussian beams with different radial indices," Opt. Lett. 41(15), 3447–3450 (2016).
- 77. Berry, Michael Victor. "Quantal phase factors accompanying adiabatic changes." *Proceedings of the Royal Society of London. A. Mathematical and Physical Sciences* 392.1802 (1984): 45-57.
- 78. Anandan, J. "Non-adiabatic non-abelian geometric phase." *Physics Letters A* 133.4-5 (1988): 171-175.
- 79. Berry, M. V., and J. H. Hannay. "Classical non-adiabatic angles." *Journal of Physics A: Mathematical and General* 21.6 (1988): L325.
- 80. Mostafazadeh, Ali. "Noncyclic geometric phase and its non-Abelian generalization." *Journal of Physics A: Mathematical and General* 32.46 (1999): 8157.
- 81. Aharonov, Yakir, and J. Anandan. "Phase change during a cyclic quantum evolution." *Physical Review Letters* 58.16 (1987): 1593.
- 82. Hannay, John H. "Angle variable holonomy in adiabatic excursion of an integrable Hamiltonian." *Journal of Physics A: Mathematical and General* 18.2 (1985): 221.
- 83. Tomita, Akira, and Raymond Y. Chiao. "Observation of Berry's topological phase by use of an optical fiber." *Physical review letters* 57.8 (1986): 937.
- 84. Pancharatnam, Shiva Ramakrishnan. "Generalized theory of interference and its applications." *Proceedings of the Indian Academy of Sciences-Section A*. Vol. 44. No. 6. Springer India, 1956.
- 85. Cohen, Eliahu, et al. "Geometric phase from Aharonov–Bohm to Pancharatnam–Berry and beyond." *Nature Reviews Physics* (2019):
- 86. S. M. Rytov, *Dokl. Akad. Nauk SSSR*, **28**, 263 (1938); English translation in: B. Markovski and S. I. Vinitsky (Eds.), *Topological Phases in Quantum Theory*, World Scientific, Singapore (1989), p. 6.
- **87.** V. V. Vladimirsky, *Dokl. Akad. Nauk SSSR*, **31**, 222 (1941); English translation in: B. Markovski and S. I. Vinitsky (Eds.), *Topological Phases in Quantum Theory*, World Scientific, Singapore (1989), p. 11.
- 88. Bhandari, Rajendra. "Light propagation through a coiled optical fiber and Pancharatnam phase." *JOSA B* 24.9 (2007): 2343-2348.
- 89. Tomita, Akira, and Raymond Y. Chiao. "Observation of Berry's topological phase by use of an optical fiber." *Physical review letters* 57.8 (1986): 937.
- 90. Bhandari, Rajendra. "Geometric phase in interference experiments." (1994).
- 91. Bliokh, Konstantin Yu, et al. "Spin-orbit interactions of light." *Nature Photonics* 9.12 (2015): 796.
- 92. Marrucci, Lorenzo, C. Manzo, and D. Paparo. "Optical spin-to-orbital angular momentum conversion in inhomogeneous anisotropic media." *Physical review letters* 96.16 (2006): 163905.

- 93. Abdulkareem, Sarkew, and Nataliya Kundikova. "Joint effect of polarization and the propagation path of a light beam on its intrinsic structure." *Optics express* 24.17 (2016): 19157-19166.
- 94. Andrews, David L., and Mohamed Babiker, eds. *The angular momentum of light*. Cambridge University Press, 2012.
- 95. Rodríguez-Herrera, Oscar G., et al. "Optical nanoprobing via spin-orbit interaction of light." *Physical review letters* 104.25 (2010): 253601.
- 96. Vuong, L. T., et al. "Electromagnetic spin-orbit interactions via scattering of subwavelength apertures." *Physical review letters* 104.8 (2010): 083903.
- 97. Bliokh, Konstantin Y., et al. "Angular momenta and spin-orbit interaction of nonparaxial light in free space." *Physical Review A* 82.6 (2010): 063825.
- 98. Liberman, V. S., and B. Ya Zel'dovich. "Spin-orbit interaction of a photon in an inhomogeneous medium." *Physical Review A* 46.8 (1992): 5199.
- 99. Fedorov, F. I. To the theory of total reflection. J. Opt. 15, 014002 (2013).
- 100.Imbert, C. Calculation and experimental proof of the transverse shift induced by total internal reflection of a circularly polarized light beam. *Phys. Rev. D* **5,** 787–796 (1972).
- 101.Bliokh, K. Yu, and Yu P. Bliokh. "Optical magnus effect as a consequence of berry phase anisotropy." *Journal of Experimental and Theoretical Physics Letters* 79.11 (2004): 519-522. Bliokh, K. Yu, and Yu P. Bliokh. "Modified geometrical optics of a smoothly inhomogeneous isotropic medium: the anisotropy, Berry phase, and the optical Magnus effect." *Physical Review E* 70.2 (2004): 026605.
- 102.Bliokh, K. Yu, and Yu P. Bliokh. "Topological spin transport of photons: the optical Magnus effect and Berry phase." *Physics Letters A* 333.3-4 (2004): 181-186.
- 103.Onoda, Masaru, Shuichi Murakami, and Naoto Nagaosa. "Hall effect of light." *Physical review letters* 93.8 (2004): 083901.
- 104.Bliokh, Konstantin Y., et al. "Geometrodynamics of spinning light." *Nature Photonics* 2.12 (2008): 748.
- 105.Bliokh, Konstantin Y. "Geometrodynamics of polarized light: Berry phase and spin Hall effect in a gradient-index medium." *Journal of Optics A: Pure and Applied Optics* 11.9 (2009): 094009.
- 106.Bliokh, Konstantin Yu. "Geometrical optics of beams with vortices: Berry phase and orbital angular momentum Hall effect." *Physical review letters* 97.4 (2006): 043901.
- 107. Alexeyev, C. N., et al. "Inversion of the topological charge of optical vortices in a coil fiber resonator." *Optics letters* 41.7 (2016): 1526-1529.
- 108.Samlan, C. T., Dinesh N. Naik, and Nirmal K. Viswanathan. "Isogyres— Manifestation of Spin-orbit interaction in uniaxial crystal: A closed-fringe Fourier analysis of conoscopic interference." *Scientific reports* 6 (2016): 33141.
- 109.Ling, Xiaohui, et al. "Realization of tunable photonic spin Hall effect by tailoring the Pancharatnam-Berry phase." *Scientific reports* 4 (2014): 5557.
- 110.Bliokh, Konstantin Y., et al. "Spin-Hall effect and circular birefringence of a uniaxial crystal plate." *Optica* 3.10 (2016): 1039-1047.
- 111.Xiao, Shiyi, et al. "Spin-dependent optics with metasurfaces." *Nanophotonics* 6.1 (2016): 215-234.
- 112. Wang, Sen, et al. "Spin-selected focusing and imaging based on metasurface lens." *Optics express* 23.20 (2015): 26434-26441.

2

Spin-to-orbital and orbital-to-spin angular momentum conversion of light in inhomogeneous media

The fundamental manifestation of the spin-orbit interaction (SOI) of light in an inhomogeneous medium is investigated in this chapter. First, we consider the propagation of circularly-polarized (CP) Gaussian beam, launched parallel to the axis of a cylindrically and radially symmetric GRIN rod. Upon propagation, the beam acquires Rytov-Vladimirskii-Berry (RVB) type geometric phase due to differential propagation vector of the constituent plane waves of the optical beam, resulting in the spin-orbit coupling (SOC) of light. Next, we demonstrate reciprocal orbit-to-spin angular momentum conversion of light, resulting in the appearance of non-zero spin angular momentum (SAM) at the output for the propagation of zero SAM input Laguerre-Gaussian beam with different topological charge. The SOC is revealed through the interference of orthogonal CP output beam with a Gaussian beam of same polarization handedness in the reference arm of a Mach-Zehnder interferometer. The geometric phase signifying the SOC is extracted using Fourier fringe analysis method, revealing phase singularity of the filtered optical vortex in the orthogonal spin projection of the beam. The reciprocal SOC on the other hand is characterized by weak (S3) Stokes parameter extracted from the CP components.

2.1 Introduction

The celebrated work by Beth in 1936 established that light with circular state of polarization carries SAM equal to σh , with $\sigma = 0, \pm 1$ respectively for linear and right- and left-circular polarization. The propagation of CP light through a birefringent plate resulted in the transfer of the SAM to birefringent plate producing a torque as a consequence of conservation of total angular momentum of light [1]. More than half a century later, observations such as chaotic rotation, increased rotation frequency and competition between the SAM and OAM by the Naples optics group in a series of experiments (1980 - 2003) probing the transfer of light's angular momentum to liquid crystals, pointed towards the idea of SOC [2-8]. A decade earlier (in 1992), the seminal work by Alan et al., introduced the concept of orbital angular momentum (OAM) arising due to helical wave front of an optical beam bearing a phase singularity at the beam cross section [9]. Unlike the SAM, the OAM value *lh* could take any integer value theoretically. In 1995, rotation of absorptive particle about the axis of the beam was demonstrated using the phase singular optical vortex (OV) beams, signifying the transfer of light's OAM to the target particles [10]. An OV beam with circular polarization has both SAM and intrinsic orbital AM (IOAM) of light.

The separation of the angular momentum (AM) of light into SAM and IOAM is based on the light-matter interactions. Birefringent material such as liquid crystal served as a candidate that could distinguish between the angular momenta based on the mechanical results arising due to light-matter interaction [3-8]. Later, such light-matter interactions formed the basis to define the AM related to spin and optical vortex beams, the SAM and OAM. The SAM transfer to the particle resulted in the rotation of particle around its own axis while the OAM transfer resulted in the rotation around the beam axis [11] and both the rotational effects are independent of the axis location. Meanwhile Nieminen *et al.*, in their simulation work "Angular momentum of a strongly focused Gaussian beam" presented the SAM to OAM transfer of light [12].

The inter-conversion of SAM and OAM was demonstrated by Marrucci *et al.*, in 2006 in an inhomogeneous anisotropic media (known as the *q*-plate) providing the fundamental understanding of the underlying SOI [13]. The *q* plate is a liquid crystal device assembly, where, the orientation of liquid crystals is varied around the center (quantified by 'q' ranging from fraction to integer) enabling SAM to influence the OAM generation. Following this, the SOC resulting at the focal plane of a strongly focussed CP-OV beam in a homogeneous and isotropic medium was reported in 2007 [14]. In 2011, Bliokh *et al.*, provided

a comprehensive theoretical framework for the SOC and the spin-Hall effect (SHE) of light, for propagation of circularly polarized Gaussian beam through homogeneous media such as lens due to scattering, focusing and in imaging systems [15]. Notably, all the SOC processes are mediated by the geometric phase.

Based on a pair of SOI effects in different media pertaining to the accumulation of geometric phase and spin-Hall beam shifts, we anticipate that the effect of the OAM on the SAM should also be present in inhomogeneous anisotropic media due to SOI. Recently, the reciprocal SOC of light – OAM-to-SAM conversion was demonstrated due to scattering of linearly polarized (LP) OV beam by a nanoparticle, revealing a *l*-dependent spatial output intensity profile and helicity density at the focal volume of the beam [16].

The GRIN rod is an optical element used extensively in light coupling between two optical components, imaging in free-space and coupling light into the fiber [17]. The physical features of the GRIN rod such as flat entry and exit planes, cylindrically symmetric shape, physical dimensions in mm scale makes it an ideal candidate for use in many applications. The GRIN rod is an inhomogeneous media with space-variant refractive index. It also exhibits weak anisotropy due to its construction and manufacturing process (ion-doping exchange methods) resulting in radial and azimuthal polarization modes, making the GRIN rod inhomogeneous and anisotropic [18-21]. The off-axis trajectory of light through GRIN rod is curved leading to the accumulation of RVB phase, resulting in SOI effects due to the refractive index gradient. Thus, the inhomogeneity and anisotropic properties makes the GRIN rod preferable to study the SOI effects. The low-cost and ready availability makes the GRIN rod a good and viable alternative to the *q*-plate to study the SOI related fundamental interactions between the different angular momenta of light.

In the first part of the chapter, the SOI of light in inhomogeneous-anisotropic GRIN media is investigated wherein on-axis propagation of RCP / LCP Gaussian beam results in orthogonal polarized LCP / RCP IOAM beam of topological charge $l=\pm 2$ along with a collinear RCP / LCP Gaussian beam, which can be polarization filtered. The phase of the OAM beam was measured in a Mach-Zehnder interferometer. The output optical field from the GRIN rod is projected in orthogonal CP state, generating an IOAM beam which is interfered with a reference beam of same polarization state, exhibiting signature fork pattern in the interferogram. This pattern is opposite for the RCP and LCP input Gaussian beams. The phase from the interferogram is extracted by using Fourier transform fringe analysis method [30]. The Reciprocal SOC, orbital-to-spin conversion

(OSC) of light is subsequently investigated via on-axis propagation of OV beams with different $l = \pm (1,2,3)$ topological charges through the GRIN rod. The spin content of the output is extracted by measuring the weak (S3) Stokes parameter and thereby the net S3 (spin) content in the beam.

2.2 SOI of light in inhomogeneous media

In systems with cylindrical symmetry, the rotational transformation due to Hermitian operator Jz is invariant. Thus, the associated quantity, the angular momentum of the field is conserved [16,22,28]. This is due to conservation of the projection (of the total OAM (J) of a beam on the rotational symmetry axis z[^] [16, 28, 29]. Therefore, the SOI of light in rotationally symmetric systems typically manifest itself as conversion of the incident SAM to OAM, resulting in the generation of spin-dependent optical vortex beam [16]. A simple clockwise rotation of light results in differential phase accumulation for RCP and LCP beams and this differential phase is termed as the geometric phase. The SOI effects in inhomogeneous anisotropic q plate is attributed to the Pancharatnam-Berry (PB) type geometric phase while in inhomogeneous anisotropic GRIN rod, the effects are due to path dependent RVB phase [25, 26]. The GRIN rod is an inhomogeneous medium, with space-variant refractive index across the transverse XY plane with parabolic refractive index distribution. The transverse radially varying refractive index distribution is expressed $n(r) = n_0 \left(1 - \frac{A_1 r^2}{2}\right)$, where A_1 is the gradient constant, determining the rate of

$$n(r) = n_0 \left(1 - \frac{A_1 r^2}{2}\right)$$
, where A_1 is the gradient constant, determining the rate of

change in refractive index. The refractive index is distributed along the transverse XY plane, while the beam propagation direction is along Z axis. The propagation of light through the GRIN rod is divided into two parts: (1) on-axis with symmetry and (2) off-axis with broken symmetry. In this chapter, we discuss the propagation of CP Gaussian and linearly polarized OV or Laguerre-Gaussian beams along the axis of the GRIN rod while the off-axis propagation and the resulting effects will be discussed in subsequent chapters.

2.3 Theoretical formalism

2.3.1 Spin-to-orbital AM conversion

The Gaussian beam with zero IOAM and circular polarization having net SAM is considered first for propagation through the GRIN rod. The radial refractive index value determines the direction of propagation of light in the GRIN rod. The deviation in the direction of propagation of light is smooth for the GRIN rod owing to the corresponding variation in the refractive index. The smooth refractive index is governed by a parabolic equation which changes the direction of propagation continuously without any abrupt changes. The non-planar trajectory of light in the momentum space results in the accumulation of Rytov-Vladimirskii-Berry (RVB) type geometric phase. This RVB phase is understood as being due to parallel transport law of light [23-27]. For right circularly polarized light propagating along a curved trajectory, geometric phase is acquired equivalent to the solid angle subtended or area covered by the path in the momentum space or k-sphere [26]. The refractive index gradient changes the direction of the constituent plane waves of the Gaussian beam, resulting in both planar (meridional) and non-planar (sagittal) trajectory of the plane waves in the medium.

The cylindrical symmetry of the GRIN rod offers an advantage that enables usage of geometric rotation matrices for on-axis propagation of light. Essential to the transformation is the transversality condition, which states that the propagation vector and the electric field (polarization) vector of light are to be orthogonal to each other [26]. This condition results in the coupling of the propagation and polarization vector and thus emerge the SOI effects [26]. The propagation of Gaussian beam through the GRIN rod is understood via its constituent plane waves propagating at different angles with respect to the central wave vector. The incident plane waves undergo azimuthal rotation and refraction by an angle θ due to the refractive index change and azimuthal rotation to compensate for the first rotation [15]. The rotation matrices are noncommutative, leading to the appearance of geometric phase factor, resulting in the generation of OAM beam in orthogonal circular polarization. The generation of IOAM beam implies that the total AM of the light is conserved. The geometric transformation due to the above-mentioned rotations is written as [15]

$$\hat{U}(\theta,\varphi) = \hat{R}_z(-\varphi)\hat{R}_y(-\theta)\hat{R}_z(\varphi)$$

$$= \begin{bmatrix} a & -be^{-2i\varphi} & -\sqrt{2ab}e^{-i\varphi} \\ -be^{2i\varphi} & a & \sqrt{2ab}e^{i\varphi} \\ \sqrt{2ab}e^{i\varphi} & -\sqrt{2ab}e^{-i\varphi} & a-b \end{bmatrix}$$
(1)

Where $\hat{R}_{a1}(b1)$ is the rotation matrix about the axis a1 (x, y, z) by an angle b1. To keep the treatment simple, we consider paraxial beams wherein the longitudinal fields are ignored. The transverse optical field after the transformation in the circular polarization basis is written as

$$\tilde{E} = \sqrt{\cos(\theta)} \ \hat{U} E_{i}$$

$$E_{o} = \frac{A(\theta_{c})}{\sqrt{\cos \theta_{c}}} \begin{bmatrix} a & -be^{-i2\phi} \\ -be^{i2\phi} & a \end{bmatrix} \begin{bmatrix} E_{ri} \\ E_{li} \end{bmatrix}$$
(2)

Where $A(\theta_c) = \frac{2\pi}{15} \Big[8 - (\cos\theta_c)^{3/2} (5 + 3\cos\theta_c) \Big]$ is the aperture dependent coefficient [15], $a = \cos^2(\theta_c/2), b = \sin^2(\theta_c/2)$ with θ_c being the input cone of angle describing the azimuthal variation of plane waves with respect to a fixed polar coordinate, φ is the azimuthal angle describing the phase singularity of optical vortex beam with helical wave front and E_{ri}, E_{li}, E_o are the incident right circular, left circular polarizations and output optical field respectively. The parameter 'b' controls the SOC efficiency which is related to the input cone of angle of light and can be modulated by the GRIN rod having higher effective focal length.

It is important to note that the right CP input Gaussian beam propagation results in a combination of RCP Gaussian beam and an LCP optical vortex beam with topological charge +2 exhibiting the SOC due to SOI and vice-versa. The term $e^{-i2\varphi}$ is the accumulated RVB phase in orthogonal CP. The total AM of light is conserved for the propagation of CP Gaussian beam through the axis of the GRIN rod. An incident RCP Gaussian beam carries $SAM = \sigma \hbar = \hbar$, and OAM = 0 (l = 0) with total incident AM, $TAM_i = \hbar$ and the output RCP Gaussian beam AM is same as the input beam, the LCP optical vortex carries $SAM = \sigma \hbar = -\hbar$, $OAM = 2\hbar$ and the net total angular momentum $TAM_0 = SAM + OAM = -\hbar + 2\hbar = \hbar$, thus the AM of the total optical field is

conserved during the process. The AM transitions due to SOC of the transverse optical field can be written as [15]

$$|l\hbar, \sigma\hbar\rangle \rightarrow \lceil a|l\hbar, \sigma\hbar\rangle - b|l\hbar + 2\sigma\hbar, -\sigma\rangle \rceil \tag{3}$$

The above transformation can also be applied to the propagation of CP vortex beam through the GRIN rod which will be discussed later. From eqn. (2), it is clear that the interaction strength between light and the GRIN rod is weak due to smaller value of θ_c resulting in lowSOC conversion efficiency. Thus only by filtering the input polarization content can we realize optical vortex beam.

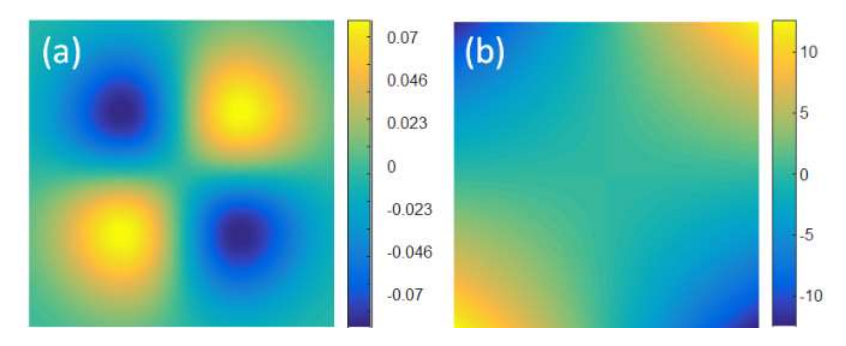


Fig. 1. (a) The orthogonal projection (H) of the output optical field for input Gaussian beam with vertical polarization, (b) the phase acquired by the output optical beam at the exit plane due to parallel transport of polarization vectors. Dimensions of each image is $(X*Y - 1.8 \times 1.8)$ mm.

The output electric field expressions for CP Gaussian beam can be extended to linear polarization as well with appropriate algebra. The output optical field for incident vertically polarized Gaussian beam is written as

$$\mathbf{E}_{\mathbf{v}}^{\mathbf{o}} = -i \frac{A(\theta_{c})}{\sqrt{\cos \theta_{c}}} \begin{bmatrix} \left(aE_{ri} + be^{-i2\varphi}E_{li} \right)_{r} \\ \left(-be^{i2\varphi}E_{ri} - aE_{li} \right)_{l} \end{bmatrix}$$

$$\mathbf{E}_{\mathbf{h}}^{\mathbf{o}} = -i \frac{A(\theta_{c})}{\sqrt{\cos \theta_{c}}} \begin{bmatrix} \left(be^{-i2\varphi}E_{li} \right)_{r} \\ \left(-be^{i2\varphi}E_{ri} \right)_{l} \end{bmatrix}$$

$$(4)$$

Where \mathbf{E}_{v}^{o} and \mathbf{E}_{h}^{o} are the output vertical polarized optical field and orthogonal, horizontal projection of the output field respectively. The linear vertical polarized Gaussian input beam generates a pair of oppositely charged ± 2 optical vortices

in RCP/LCP basis, with zero OAM in the output field. Projection of the output in orthogonal linear polarization basis results in the superposition of ± 2 LG beams, generating the well-known four-lobed pattern, also known as isogyre pattern. The isogyre pattern is used as a standard to distinguish different crystal types [31]. The dark Maltese cross in isogyre pattern indicates the region without polarization change, implying planar trajectory of constituent plane waves, discussed earlier. Each dark line signifies phase discontinuity and thus, all the adjacent lobes are π phase shifted with respect to each other as shown in the Fig. 1 (a). An iterative analysis is carried out to find the net change in the propagation vector direction and angle [32]. By matching the GRIN rod diameter at the exit plane with the beam waist of the output beam, the isogyre pattern was calculated for net deviation in the position and angle of the constituent plane waves with respect to the input plane due to refractive index gradient and was used to extract the residual phase as shown in the Fig 1 (b).

2.3.2 Reciprocal Spin-orbit Coupling

The linearly polarized light with zero SAM can be expressed as a superposition of RCP and LCP eigen modes. The RCP and LCP state of polarization (SOP) of the light have slightly different non-planar phase structure which results in differential electric field distribution during propagation. The spatial separation of the constituent beams would result in the net SAM flux across beam waist. The optical vortex beams with opposite topological charges, having clockwise and counter-clockwise helical wave fronts, have slightly different spatial propagation path and consequently would also have a net SAM flux.

The coupling of propagation direction vector and the polarization state of light is a prerequisite to observe the SOI phenomenon of light. In free space light propagation, this coupling is achieved by tightly focussing the light through microscopic objective of high numerical aperture. However, the propagation of light through inhomogeneous or anisotropic or chiral media does not warrant a need for tight focussing for the SOI to take place. The inhomogeneity and weak anisotropy of the media couples the polarization and propagation vectors of paraxial light beam, enabling SOI and associated phenomena.

Under the tight focusing condition, the reciprocal SOC or orbit-to-spin coupling (OSC) is anticipated for LP optical vortex beam at the focal plane. In general, the LP Gaussian beam has purely transverse SAM density with no longitudinal SAM density in the focal plane [16]. However, the presence of helical phase of OAM bearing OV beams causes a net longitudinal SAM density in the focal plane. This SAM density occurrence for a spin-free linear polarized

OV beam is termed as orbit-to-spin angular momentum conversion of light and the total SAM is zero [33]. At the focal plane, the LP Gaussian beam has no variation in the SOP, while for LP OV beam, changes in orientation and ellipticity in the SOP are observed. This occurrence of spin content in the focal plane was studied for other beams as well [34, 35].

The reciprocal SOC, conversion of orbital AM to spin AM of light due to helical phase is anticipated for a LP optical vortex beam with IOAM, upon propagation through an inhomogeneous-anisotropic media – the GRIN rod. The transverse translational symmetry is broken due to focusing of optical fields which can also be applied to propagation of light beam through the GRIN rod [28]. The focused LG beams have zero helicity density K in the far-field while having complex spatial distribution in the focal plane. Thus, the local operator transformation affects the helicity and the SAM of the optical beam globally. The focusing of (zero SAM) linearly polarized LG beam shows an *l*-dependent helicity density K values in the focal plane [16]. Therefore, the refractive index gradient and curved trajectory of the GRIN rod should also exhibit an *l*-dependent helicity density K values which in the far-field is the average SAM per plane wave component. The SAM in the far-field is however zero due to equal right and left circular components.

The net spin content generated due to the propagation of LP optical vortex beam through the inhomogeneous media, the GRIN rod would be zero as evidenced by equal RCP and LCP content in the output optical field. The Stokes (S3) parameter reveal the spin content of the optical field owing to conservation of total AM of light. The spin (S3) content due to reciprocal SOC is however hard to discriminate due to weak anisotropy in the GRIN rod and ensuing light-matter interaction owing to SOI. Therefore, weak (S3) Stokes parameter is extracted from the output optical field.

2.4 Experimental details

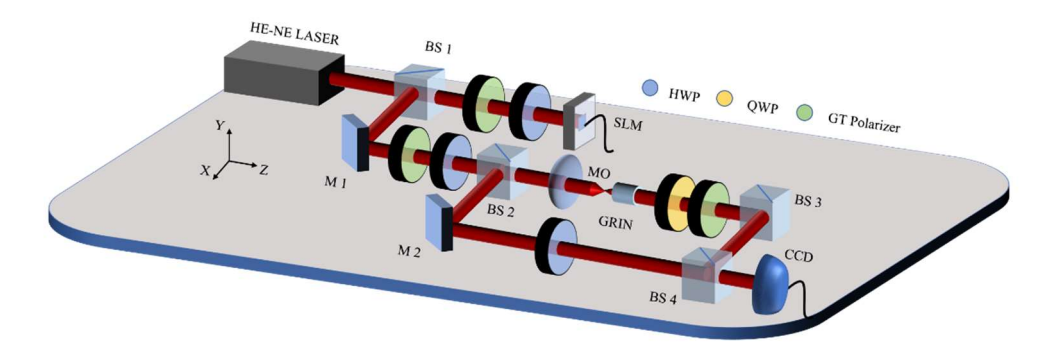


Figure 2. Experimental scheme. *SOC*: The state of polarization of incident Gaussian beam selected as (R / L) circular using GT polarizer, HWP and QWP combination. *Reciprocal SOC*: The QWP is removed and the input polarization of OV beam is selected to be vertical. Beam splitters (BS1-BS4), Mirrors (M1-M2), microscope objective lens (MO), spatial light modulator (SLM) and CCD (camera) are used in the experimental setup to observe the SOC and reciprocal SOC effects. (i) polarimetry and projection and (ii) interferometry set up to extract the phase of generated LG beams.

Spin-Orbit Coupling: The incident Gaussian beam polarization is selected as right-/left- circular using the Glan-Thompson (GT) polarizer, quarter-wave plate (QWP) and half-wave plate (HWP) combination for the spin-orbit coupling measurements. The CP Gaussian beam is passed through the GRIN rod using a microscope objective (MO) lens. The length, diameter, gradient constant of the GRIN rod (Edmund optics, USA) are 3.93 mm, 1.8 mm, $A_1 = 0.132 \text{ mm}^{-2}$ respectively. The on-axis refractive index of the GRIN rod is 1.629, its effective focal length is 1.71 mm, and the numerical aperture is 0.55. The GRIN rod is placed on a V- groove fixed on to a 5-axis precision alignment stage to accurately launch the light beam along the axis of the GRIN rod with respect to the geometric center of the laser beam. The distance between the GRIN rod and the MO lens is varied to nearly collimate the output beam. The output from the GRIN is then projected in orthogonal CP with respect to the input CP state using a QWP-GT polarizer combination. A reference beam split using the beam splitter (BS2) and reflected from the mirror (M2) is passed through a HWP to match the CP of the beam in another arm of the Mach-Zehnder interferometer. The resulting interference pattern of the reference Gaussian beam and beam passing through the GRIN rod is captured using the CCD camera to extract phase structure of the orthogonally projected LG beam.

Reciprocal SOC or OSC: Next, the polarization of the input Gaussian beam is set horizontal using the GT polarizer and HWP combination. The SLM is used to generate the optical vortex beam with horizontal oriented singular axis. If the incident beam polarization on the SLM is horizontal, the reflected beam transforms depending on the phase mask used – it can be Gaussian or Laguerre-Gaussian beam with appropriate spatial intensity profile. However, if the incident beam polarization is vertical, the reflected beam is always Gaussian beam without any change in spatial intensity profile. This behaviour is attributed to the weak anisotropy of the SLM construction itself and is considered in all the experiments reported. The horizontal polarization of the LG beam generated by the SLM is changed to vertical using HWP and GT polarizer and is then passed through a microscope objective lens to launch into the GRIN rod. The output from the exit plane of the GRIN rod is passed through a combination of QWP and analyser and captured using a CCD camera connected to computer. The spin content due to propagation of linearly polarized LG beam through the GRIN rod is measured using weak Stokes polarimetry.

2.5 Results and discussion

2.5.1 Spin-to-orbital AM conversion

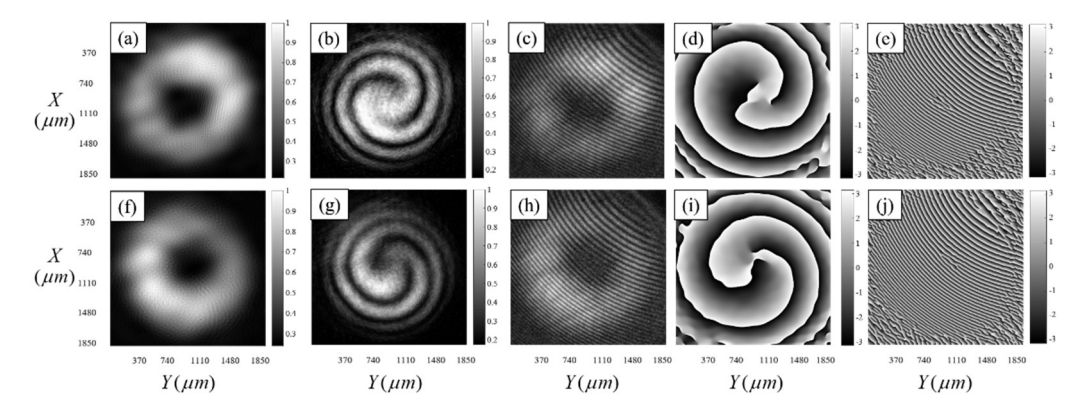


Figure 3. Orthogonal polarization projected output beam from the GRIN rod after passing through QWP and analyzer for incident (a) RCP and (f) LCP Gaussian beams. Interference pattern of generated LCP / RCP OV beams with the reference Gaussian beam for RCP (b), (c) and LCP (g), (h). Spiral fringes in (b) and (g) are due to on-axis and oppositely oriented forklet fringes due to off-axis interference. Corresponding phase structures for RCP (d), (e) and LCP (i), (j) incident beams, extracted from the interferograms.

The propagation of CP Gaussian beam through the axis of the GRIN rod generates a phase singular optical vortex beam with topological charge ± 2 in orthogonal CP with respect to the incident CP, due to SOC of the light beam. The

spin-orbit coupling of light transforms the homogeneously polarized Gaussian beam into inhomogeneously polarized beam at the exit plane of the GRIN rod. The inhomogeneous polarization of the output beam from the GRIN rod is due to SOC. The inhomogeneity in the SOP is attributed to the refractive index distribution experienced by the incident Gaussian beam. The differential rotation of the plane wave components of incident Gaussian beam causes geometric phase accumulation. The plane wave components superpose and results in small magnitude orthogonal polarization component along with incident polarization. This conversion depends on the refractive index variation and the length and hence the optical phase parameter of the GRIN rod. Thus, for an incident RCP Gaussian beam, the output optical field after the GRIN rod is composed of RCP Gaussian beam and LCP OV beam and vice-versa. Since the magnitude of the LCP content is small, the OV beam is measurable only by projecting in the orthogonal CP state, a standard way to characterize weak SOI interactions.

Figure 2 shows the experimental scheme used to study the features related to SOC of light. As shown in the experimental setup, a Mach-Zehnder interferometer is constructed to characterize the optical vortex beam and to extract the phase structure of the OV beam. Figure 3 shows the experimental results obtained: top row (a) to (e) and bottom row (f) to (j) correspond respectively to incident RCP and LCP Gaussian beam. The generated LG beams for input RCP and LCP is shown in Fig. 3 (a) and (f). The on-axis and off-axis interference of the generated OV beam with reference Gaussian beam with same CP state of OV is carried out to extract the phase structure of the generated OV beam. The on-axis and off-axis interferograms are shown in Fig 3 (b), (c) for incident RCP and (g), (h) LCP Gaussian beams. The on-axis interference of LCP / RCP OV beam with the reference LCP Gaussian beam results in spiral interference pattern due to slight divergence of the superposed beams. The direction of spiral fringes is used to distinguish the charge of the OV beams. The LCP OV beam with +2 topological charge resulted in counter clock-wise spiral fringe pattern, shown in Fig 3 (b), while the RCP OV beam with -2 topological charge forms a clock-wise spiral fringe pattern as shown in Fig 3 (g). The offaxis interference patterns are marked by the oppositely oriented forklet fringe pattern seen in Fig 3 (c) and 3 (h), a pattern commonly used to identify phase singular beams. Fourier transform fringe analysis technique is carried out on the measured patterns to extract the phase information from the interferograms to characterize the OV beams. The extracted phase of LCP and RCP OV beams for input RCP and LCP Gaussian beam are shown the Fig. 3 (d), (i) on-axis and (e), (j) off-axis interference respectively [30].

2.5.2 Orbital-to-spin AM conversion

The emergence of topological charge dependent spin component in the output beam for incident zero SAM LP OV beam propagation through the GRIN rod is referred as the reciprocal SOC or Orbital-to-spin AM conversion. The reciprocal SOC is experimentally realized through the propagation of a zero SAM linear vertically polarized OV beams with different topological charges $(l = \pm 1, 2, 3)$ through the GRIN rod. The appearance of non-zero SAM in the output beam field is characterized by measuring the Stokes parameters. The weak light-matter interaction due to weak anisotropy in the GRIN rod results in the appearance of small spin content in the output optical beam, making it hard to analyse through standard Stokes polarimetry measurement. The small spin content due to reciprocal SOC is however measured and quantified via weak (S3) Stokes parameter. Conventionally, the spin content is measured by fixing QWP fast-axis at 90° and the analyser pass axis at 45° and 135° with respect to X-axis, corresponding respectively to the measurement of RCP and LCP components in the output beam. However, due to weak interaction and hence weak circular SOP content in the output beam, the analyser is instead rotated by 90°±5° for measuring weak right- and left- elliptical polarization content through weak Stokes measurement. Figure 4 shows the measured weak S3 parameter for input OV beams with different topological charges. The measured weak S3 parameters are π phase shifted for +l and -l values of the incident linearly polarized OV beams. The weak S3 patterns appear to rotate with change in the l value and the direction flips for -l values of the OV beams. The spatial variation in the weak S3 component is a signature of the reciprocal SOI. The size of LG beam depends on the l value and so the measured weak S3 pattern size increase with increase in the l value. The cumulative weak S3 information measured in the far field of the output OV beams is however zero, owing to the symmetry and conservation of AM.

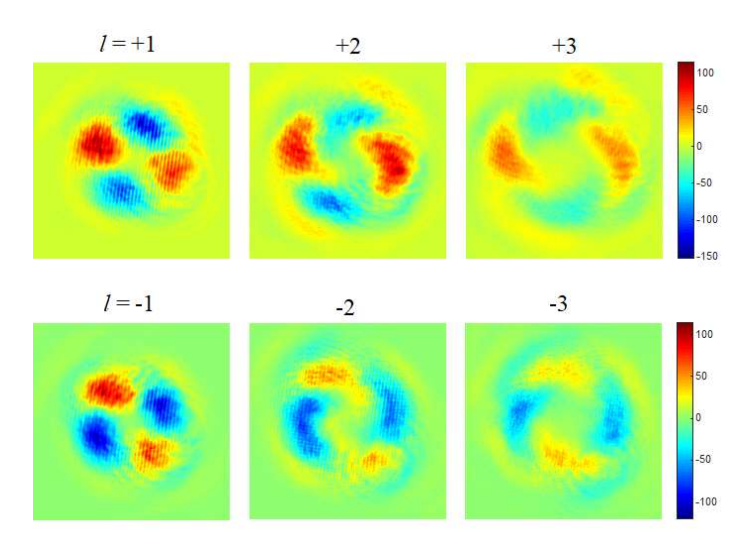


Figure 4. Experimentally measured weak (S3) Stokes parameter for different IOAM values $(l=\pm 1,\pm 2 \text{ and }\pm 3)$ of input beam with vertical polarization (zero SAM). Red and blue colour correspond to right and left elliptical polarization components in the output optical beam from the GRIN rod.

2.6 Summary

This chapter presents our investigation of the SOC and reciprocal SOC phenomenon arising due to spin-redirection RVB phase, due to the non-planar trajectory of propagation vectors in a GRIN rod. The geometric rotational matrices have been used to understand the propagation of RCP / LCP Gaussian beam through the GRIN rod. The non-commutativity of rotational matrices leads to geometric phase factor in the orthogonal CP component with respect to the incident CP state. An LCP / RCP optical vortex beam for input RCP / LCP Gaussian beam is generated due to RVB phase with an underlying geometric phase, known as SOC, conserving the total AM of light. The output optical beam from the GRIN rod is projected in orthogonal CP using a QWP and analyser resulting in a phase singular LG beam. The OV beam is superposed with reference Gaussian beam of same CP state. The interferograms are analysed to reveal the phase structure of the OV beams. Counter rotating spiral fringe pattern and oppositely oriented forklet patterns are observed in the interferograms of OV beams.

Reciprocal SOC, generating local non-zero SAM in the output optical beam due to propagation of linearly polarized LG beams with zero SAM is termed as orbital-to-spin AM conversion of light. This reciprocal SOC is experimentally demonstrated by measuring weak (S3) Stokes parameter due to weak spin content arising due to light-matter interaction. The net SAM in the output beam is zero

owing to conservation of total AM. The results greatly enhance/improve our understanding of higher-order effects, the effect of two angular momenta on the third (considering spin AM and intrinsic and extrinsic orbital AM), which are discussed in subsequent chapters.

References:

- 1. Beth, Richard A. "Mechanical detection and measurement of the angular momentum of light." *Physical Review* 50.2 (1936): 115.
- 2. Piccirillo B and Santamato E 2004 Light angular momentum flux and forces in birefringent inhomogeneous media *Phys. Rev. E* 69 056613.
- 3. Abbate G, Maddalena P, Marrucci L, Saetta L and Santamato E 1991 Photodynamical effects induced by the angular momentum of light in liquid crystals *Phys. Scr.* T39 389–93.
- 4. Santamato E, Daino B, Romagnoli M, Settembre M and Shen Y R 1986 Collective rotation of molecules driven by the angular momentum of light in a nematic film *Phys. Rev. Lett.* 57 2423–6.
- 5. Marrucci L, Abbate G, Ferraiuolo S, Maddalena P and Santamato E 1992 Self-induced stimulated light scattering in nematic liquid crystals: theory and experiment *Phys. Rev.* A 46 4859–68.
- 6. Marrucci L and Paparo D 1997 Photoinduced molecular reorientation of absorbing liquid crystals *Phys. Rev. E* 56 1765–72.
- 7. Piccirillo B, Toscano C, Vetrano F and Santamato E 2001 Orbital and spin photon angular momentum transfer in liquid crystals *Phys. Rev. Lett.* 86 2285–8.
- 8. Piccirillo, B., A. Vella, and E. Santamato. "Competition between spin and orbital photon angular momentum transfer in liquid crystals." *Journal of Optics B: Quantum and Semiclassical Optics* 4.2 (2002): S20.
- 9. L. Allen, M. W. Beijersbergen, R. J. C. Spreeuw, and J. P. Woerdman, *Phys. Rev. A* 45, 8185 (1992).
- 10. He, H., et al. "Direct observation of transfer of angular momentum to absorptive particles from a laser beam with a phase singularity." *Physical review letters* 75.5 (1995): 826.
- 11. O'neil, A. T., et al. "Intrinsic and extrinsic nature of the orbital angular momentum of a light beam." *Physical review letters* 88.5 (2002): 053601.
- 12. Nieminen, Timo A., et al. "Angular momentum of a strongly focused Gaussian beam." *Journal of Optics A: Pure and Applied Optics* 10.11 (2008): 115005.
- 13. L. Marrucci, C. Manzo, and D. Paparo, "Optical spin-to-orbital angular momentum conversion in inhomogeneous anisotropic media," *Phys. Rev. Lett.* 96(16), 163905 (2006).
- 14. Zhao, Yiqiong, et al. "Spin-to-orbital angular momentum conversion in a strongly focused optical beam." *Physical Review Letters* 99.7 (2007): 073901.
- 15. K. Bliokh, E. A. Ostrovskaya, M. A. Alonso, O. G. Rodríguez-Herrera, D. Lara, and C. Dainty, "Spin-to-orbital angular momentum conversion in focusing, scattering, and imaging systems," *Opt. Express* 19(27), 26132–26149 (2011).
- 16. Nechayev, Sergey, et al. "Orbital-to-spin angular momentum conversion employing local helicity." *Physical Review B* 99.7 (2019): 075155.
- 17. Tomlinson, W. J. "Applications of GRIN-rod lenses in optical fiber communication systems." *Applied Optics* 19.7 (1980): 1127-1138.
- 18. 33. W. A. Wozniak, "Birefringence of gradient-index lenses of SELFOC® type," *Proc. SPIE* 2169, 156–167 (1994).
- 19. M. Montoya and D. Malacara, "Polarization effects in interferograms of radial GRIN rods," *Opt. Commun.* 175(4-6), 259–263 (2000).

- 20. J. L. Rouke and D. T. Moore, "Birefringence in gradient-index rod lenses: a direct measurement method and interferometric polarization effects," *Appl. Opt.* 40(28), 4971–4980 (2001).
- 21. D. Tentori and J. Camacho, "Conoscopic evaluation of the birefringence of gradient-index lenses: infidelity sources," *Appl. Opt.* 41(34), 7218–7228 (2002).
- Bliokh, Konstantin Y., Justin Dressel, and Franco Nori. "Conservation of the spin and orbital angular momenta in electromagnetism." New Journal of Physics 16.9 (2014): 093037.
- 23. S. Rytov, "On transition from wave to geometrical optics," *Dokl. Akad. Nauk SSSR* 18, 263–266 (1938); Tr. Fiz. *Inst. Akad. Nauk SSSR* 2, 1 (1940).
- 24. V. Vladimirskii, "The rotation of a polarization plane for curved light ray," *Dokl. Akad. Nauk SSSR* 21, 222–225 (1941).
- 25. K. Y. Bliokh and Y. P. Bliokh, "Modified geometrical optics of a smoothly inhomogeneous isotropic medium: The anisotropy, Berry phase, and the optical Magnus effect," *Phys. Rev. E* 70(2), 026605 (2004).
- 26. K. Bliokh, A. Niv, V. Kleiner, and E. Hasman, "Geometrodynamics of spinning light," *Nat. Photonics* 2(12), 748–753 (2008).
- 27. K.Y. Bliokh, A. Aiello, and M.A. Alonso, "Spin-orbit interactions of light in isotropic media," in The Angular Momentum of Light, David L. Andrews and Mohamed Babiker, eds. (*Cambridge University Press*, 2012), chap. 8, pp. 174–245
- 28. Fernandez-Corbaton, Ivan, Xavier Zambrana-Puyalto, and Gabriel Molina-Terriza. "Helicity and angular momentum: A symmetry-based framework for the study of light-matter interactions." *Physical Review A* 86.4 (2012): 042103.
- 29. Sergey Nechayev and Peter Banzer "Mimicking Chiral Light-Matter Interaction", arXiv:1904.01910v1 [physics.optics] 3 Apr 2019
- 30. M. Takeda, H. Ina, and S. Kobayashi, "Fourier-transform method of fringe-pattern analysis for computer-based topography and interferometry," *J. Opt. Soc. Am.* 72(1), 156–160 (1982).
- 31. C. T. Samlan, D. N. Naik, and N. K. Viswanathan, "Isogyres—manifestation of spin-orbit interaction in uniaxial crystal: A closed-fringe Fourier analysis of conoscopic interference," *Sci. Rep.* 6(1), 33141 (2016).
- 32. A. Javier and G. D. Boreman, "On-axis and off-axis propagation of Gaussian beams in gradient index media," *Appl. Opt.* 29(19), 2944–2950 (1990).
- 33. Yu, Panpan, et al. "Orbit-induced localized spin angular momentum in the tight focusing of linearly polarized vortex beams." *Optics letters* 43.22 (2018): 5677-5680.
- 34. Li, Manman, et al. "Orbit-induced localized spin angular momentum in strong focusing of optical vectorial vortex beams." *Physical Review A* 97.5 (2018): 053842.
- 35. Han, Lei, et al. "Catalystlike effect of orbital angular momentum on the conversion of transverse to three-dimensional spin states within tightly focused radially polarized beams." *Physical Review A* 97.5 (2018): 053802.

3

Reciprocity of spin-Hall effect of light in GRIN rod

In Chapter-2, we investigated symmetric propagation of circularly-polarized (CP) Gaussian beam and linear-polarized (LP) optical vortex (OV) beam along the axis of the graded-index (GRIN) rod. This chapter deals with off-axis propagation of polarized light and the effects arising due to broken rotational (azimuthal) symmetry in the GRIN rod system. The propagation of CP Gaussian beam along an asymmetric, off-axis position of the GRIN rod and the resulting accumulation of Rytov-Vladimirskii-Berry (RVB) phase gradient across the beam leads to the appearance of transverse, spin-Hall effect (SHE) of light. For the LP input beam the separation into right- and left- circular polarized components in the transverse plane, orthogonal to the direction of induced asymmetry is the SHE of light. Subsequently, we demonstrate the reciprocal SHE, a change in the state-ofpolarization (SOP) of light due to rotation of the linear SOP of light due to accumulation of RVB phase, caused by torsion experienced by constituent plane waves of the Gaussian beam. The SHE of light arising in the above-mentioned scenario are optically amplified using the weak measurement technique, while the Berry phase accumulation is measured via the weak (S3) Stokes parameter of the output optical beam-field using OWP-polarizer and a CCD camera combination.

3.1 Introduction

The Hall effect – orthogonal directional pairing of electrons in magnetic field in a current-carrying conductor results in a net voltage, the Hall voltage perpendicular to magnetic field direction, was observed in 1879. This led to the realization of many related effects, the spin Hall effect (SHE), the quantum Hall effect (QHE) and the anomalous Hall effect (AHE) [1-9]. The fundamental property of the electron that resulted in the SHE due to SOI is the spin, which paved way for the development of spintronics to produce, operate and detect the nanoscale spin effects [10-13].

The photonic counterpart of the SHE deals with wavelength scale effects associated with the spin of light. The SHE of light refers to spin-dependent transverse splitting or shift of the trajectory of light arising due to spin-orbit interaction (SOI) of light. Initially, the photonic SHE was investigated by Imbert and Fedorov for reflection/refraction at a sharp interface and subsequently in graded-index media referred to as the optical Magnus effect [14-15]. It was interpreted and explained by employing the conservation of angular momentum (AM) and the SOI of light [14-18]. Subsequently, the phenomenon is understood as a consequence of the geometric phase and named as Hall effect of light [19]. These spin-dependent shift is so small of the wavelength scale, and therefore are hard to observe and measure directly. Under single reflection / refraction the observation of the very small shift is quite challenging, demanding special measurement techniques. The small shift can however be amplified and differentiated directly from the multiple reflections, as demonstrated in the cylindrical glass [20,21]. Significant SHE was also realized under a unique circumstance such as in the case with the use of non-paraxial light beam or near Brewster angle in the reflection of light [22-30]. Hosten and Kwiat measured the wavelength scale shift using the weak measurement introduced by Aharonov-Anandan-Vaidman (AAV) [31]. The weak measurement amplifies the small shift by orders of magnitude to be realized experimentally.

The SHE of light is sensitive to the sample characteristics such as the refractive index, and therefore can be used to distinguish the variation in the thickness of the thin films at nanoscales [32]. Thus, the SHE of light has also been used as a sensor to characterize the thin films. It is also capable of detecting phase changes associated with the thickness of the thin films [32-34]. Tailoring the material thickness, it is possible to generate specific profile for the SHE with thickness as a parameter, which can be manipulated [32]. Additionally, the nanoscale spin Hall shift aids better manipulation of light at the scale of wavelength

with precision and for subsequent use in precision metrology. This also opens up a new field, the spin-optics, wherein optical spin Hall device implementation can be expected to be similar to the spintronic devices associated with electrons and its charge [10-13,20,21,35-41].

The SOI effects of light came to the fore much before the SOI terminology usage, with the discovery of the Rytov-Vladimirskii-Berry (RVB) phase. The RVB phase, also referred to as spin-redirection phase is the phase change associated with the light propagation direction in momentum space. Likewise, the phase change arising due to polarization manipulation is known as the Pancharatnam-Berry (PB) phase. Sir Michael Berry laid out the theoretical foundation and popularized the Geometric phase through his seminal work in 1984 only to realize that it was already explored in crystals with polarization associated phase changes by S. Pancharatnam in 1956 [42]. Although the spinredirection phase was known from 1938, it took 50 years to realize it experimentally in a helically wound optical fiber by Chiao and Wu, taking inspiration from Berry's 1984 paper on the Geometric phase. Within a short while, in 1991, the optical Magnus effect was realized in an optical fiber (inhomogeneous medium) due to the SOI by Zel'Dovich and others [14,15]. Later, all the SOI effects are brought under one umbrella of geometric phase with a unified approach by Bliokh [43,44]

This chapter deals with the effects arising due to the transition of optical modes from symmetric on-axis propagation to off-axis propagation with broken rotational (azimuthal) symmetry of light through a GRIN rod. The photonic SHE, resulting from the propagation of CP Gaussian beam along the off-axis position of the GRIN rod, is discussed. The nano-scale spin-dependent shifts are measured by using weak measurement scheme wherein the shifts are amplified due to the post-selection process. The reciprocal SHE is discussed with respect to the input position of the Gaussian beam. The small changes in the polarization of the output optical field due to reciprocal SHE are quantified by measuring the weak (S3) Stokes parameter of the output optical beam.

3.2 SHE in inhomogeneous media

An insight to and discussion of results on the phase changes associated with propagation of CP Gaussian and OV beams along the axis of the GRIN rod was given in Chapter 2. Here, the off-axis propagation and the effect of associated changes in the output beam's spatial structure and phase are discussed. Breaking the cylindrical symmetry transforms the system into a mixture of partial cylindrical symmetry and rectangular symmetry. We anticipate that breaking of rotational (azimuthal) symmetry would have an impact on the beam's modal characteristics as a function of the input beam position. The GRIN rod is an inhomogeneous but weakly anisotropic media with quadratically varying refractive index in the transverse (XY) plane. The direction of light propagation also changes the refractive index experienced by light leading to weak local anisotropy with two independent eigen modes having distinctive trajectories. The theoretical formalism necessary to understand the effects arising in such a scenario are presented and discussed in subsequent sections of the chapter.

3.3 Theoretical formalism

3.3.1 Spin-Hall effect of light

The Gradient index rod serves as a classic example of smooth inhomogeneous media with weak anisotropy due to non-degenerate eigen polarization modes. The equation describing the propagation of light through smooth inhomogeneous media is written as

$$\vec{\nabla}^2 \vec{E} + k^2 \vec{E} - \vec{\nabla} \left(\vec{\nabla} \cdot \vec{E} \right) = 0 \tag{1}$$

With $k=k_0n$ the wave number in the inhomogeneous medium. In Eq (1), the last term signifies the spin and orbital AM coupling of light resulting in wavelength scale effects. Due to weak refractive index gradient of the GRIN rod, the propagation of light through it remains predominantly transverse with negligible longitudinal effects. Expressing the electric field as the sum of transverse and longitudinal components i.e., $\vec{E} = \vec{E}_{\perp} + \vec{E}_{\parallel}$ and omitting the longitudinal component as $\vec{E}_{\parallel} \ll \vec{E}_{\perp}$, the wave equation can be modified as [46]

$$\vec{\nabla}^2 \vec{E}_{\perp} + k^2 \vec{E}_{\perp} + 2 \left[\left(\vec{\nabla} \ln n \right) \times \vec{\nabla} \right] \times \vec{E}_{\perp} = 0$$
 (2)

Where \vec{E}_{\perp} and \vec{E}_{\parallel} denote transverse and longitudinal electric field components. The propagation of LP light is analysed by considering it to be superposition of RCP and LCP light beams through the GRIN rod. The superposition of RCP and LCP light through the media is expressed as, $\vec{E}_{\perp} = \vec{E}^+ e^+ + \vec{E}^- e^-$, where $\vec{E}^{\pm} = \left(\vec{E}_1 \mp i \vec{E}_2\right)/\sqrt{2}$ and $e^{\pm} = \left(e_1 \pm i e_2\right)/\sqrt{2}$. Substitution of the above transforms Eq. (2) as the following [46]

$$k_0^{-2} \vec{\nabla}^2 \vec{E}^{\sigma} + n^2 \vec{E}^{\sigma} - 2ik_0^{-2} \mathbf{t} \cdot \left[\left(\vec{\nabla} \ln n \right) \times \vec{\nabla} \right] \times \vec{E}^{\sigma} = 0$$
 (3)

Where σ symbolizes helicity of the circular polarization, $\sigma = +1$ for RCP and $\sigma = -1$ for LCP light. The wave function for circularly polarized photons is $\vec{E}^{\sigma} = A(r) \exp[ik_0 \psi(r)] \exp(-i\sigma \pi/4)$, and the eikonal equation and amplitude transport equation are obtained in the first-order geometrical optics approximation as [46]

$$(\vec{\nabla}\psi)^{2} - n^{2} - \sigma \left(\frac{2\vec{\nabla}n \times \vec{\nabla}\psi}{k}\right) \cdot t = 0$$

$$2\vec{\nabla}\psi \cdot \vec{\nabla}A + A\vec{\nabla}^{2}\psi - \sigma \left(\frac{2\vec{\nabla}n \times \vec{\nabla}A}{k}\right) \cdot t = 0$$

$$(4)$$

Where, t = dr/ds is the direction of propagation of the light through the medium. The ray equation can be derived from the eikonal equation and subsequently the optical matrix for the propagation of light through smoothly inhomogeneously media. However, the 2×2 optical matrix does not have polarization contributions i.e., the resulting spin dependent deviation of the output beam, the SHE. Therefore, a 4×4 optical matrix is required for the two orthogonal directions to describe the spin-Hall effect of light. Combining the optical matrix and Huygens-Fresnel equations, we can investigate the propagation of circularly polarized light under the paraxial approximation [46].

Traditionally the propagation of light through optical elements is modelled by 2x2 matrix which is generalized by Collin's integral using the matrix elements [45]. The 4x4 matrix describing the propagation of circularly polarized Gaussian light beam through the GRIN rod is given by [46]

$$T = \begin{bmatrix} A_{x} & B_{x} & E_{x} & F_{x} \\ C_{x} & D_{x} & G_{x} & H_{x} \\ E_{y} & F_{y} & A_{y} & B_{y} \\ G_{y} & H_{y} & C_{y} & D_{y} \end{bmatrix}$$
 (5)

$$\begin{bmatrix} A_{x} & B_{x} \\ C_{x} & D_{x} \end{bmatrix} = \begin{bmatrix} A_{y} & B_{y} \\ C_{y} & D_{y} \end{bmatrix} = \begin{bmatrix} A & B \\ C & D \end{bmatrix}$$

$$= \begin{bmatrix} \cos(z\sqrt{2\alpha}) & -\sqrt{2\alpha}\sin(z\sqrt{2\alpha}) \\ \sin(z\sqrt{2\alpha})/\sqrt{2\alpha} & \cos(z\sqrt{2\alpha}) \end{bmatrix}$$

$$\begin{bmatrix} E_{x} & F_{x} \\ G_{x} & H_{x} \end{bmatrix} = -\begin{bmatrix} E_{y} & F_{y} \\ G_{y} & H_{y} \end{bmatrix}$$

$$= \begin{bmatrix} \beta(C + Az) & \beta(D + Bz) \\ \beta Cz & \beta Dz \end{bmatrix}$$
(6)

Where $\beta = 2\sigma\alpha/k$. Based on Collin's integral, the propagation of circularly polarized paraxial light beam through the GRIN rod follows the expression [45, 46]:

$$E(x,y,z) = -\frac{ik}{2\pi C} \exp(ikz) \iint dx_0 dy_0 E(x_0, y_0, z = 0) \exp\{\frac{ik}{2C} [D(x_0^2 + y_0^2) + A(x^2 + y^2) - 2(x_0 x + y_0 y) + 2\beta z(x_0 y - xy_0) + 2\beta Cxy]\}$$
(7)

Using Eq. (7), we investigate the evolution of circularly polarized Gaussian beam propagating through the GRIN rod. The electric field distribution for the Gaussian beam at the input plane is [46]

$$E(x_0, y_0, z = 0) = \exp\left[\frac{ik(x_0^2 + y_0^2)}{2q_0}\right]$$
 (8)

Substituting Eq. (8) into Eq. (7), an analytical expression for the propagation of circularly polarized Gaussian be is obtained as,

$$E(x, y, z) = \frac{\omega_0}{\omega_z} \exp\left[-\frac{\left(x - \delta_x\right)^2 + \left(y - \delta_y\right)^2}{\omega_z^2}\right] \exp\left\{\frac{ik}{2R_z} \left[\left(x - \delta_x\right)^2 + \left(y - \delta_y\right)^2\right]\right\}$$

$$\times \exp\left(ik\beta z\right) \exp\left\{i\left[kz - \arctan\left(\frac{C}{LD}\right)\right]\right\}$$
(9)

Where, $\delta_x = \beta z y, \delta_y = \beta z x, R_z = \left(C^2 + L^2 D\right) / \left(AC + L^2 BD\right),$

 $\omega^2(z) = \omega_0^2 (C^2 + L^2 D)/L^2$ denote the radius of curvature and beam waist of Gaussian beam respectively.

The off-axis propagation of LP Gaussian beam through the GRIN rod apart from the SHE also results in distortion of output Gaussian beam. Elongation of the beam waist occurs perpendicular to the direction of off-axis position as shown in the Fig 1. This results in elliptical spatial intensity profile of the output Gaussian beam and is related to eccentricity of ellipse. The eccentricity varies linearly as a function of input launching position and incident angle of input beam [51]. The beam waist along the x and y directions are modelled as

$$\omega_{x}(z,x) = \omega(z)$$

$$\omega_{y}(z,x) = \omega(z)(1 + d\omega_{y} * x_{0}^{2})$$
(10)

Here, $d\omega_y$ is a correction to the beam waist for off-axis launch position x_0 in the x-direction and the beam waist scales as square of input position.

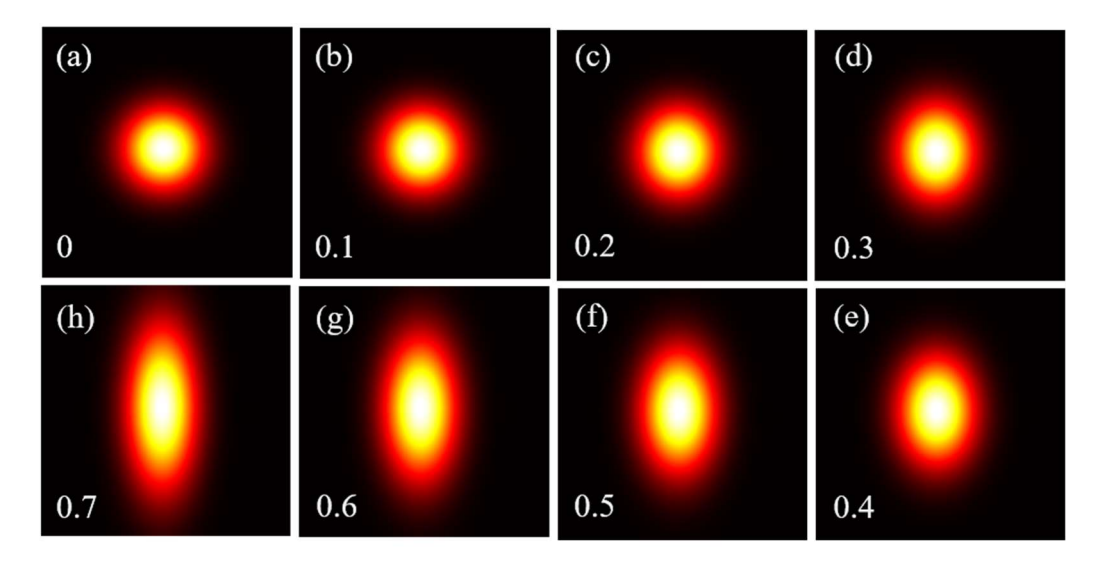


Figure 1. The Gaussian beam intensity at the exit plane of the GRIN rod as a function of input beam position. Input beam position is varied from on-axis (0 mm) to off-axis (0.7 mm) in steps of 0.1 mm.

The refractive index profile influences the trajectory of the Gaussian beam in the medium and it depends on the initial launch position and the z- plane where it is calculated. The trajectory (XZ) of the propagating Gaussian beam in a graded-index medium is approximated as

$$x(x_0, z_1) = x_0 \cos\left(\sqrt{A}z_1\right) \tag{11}$$

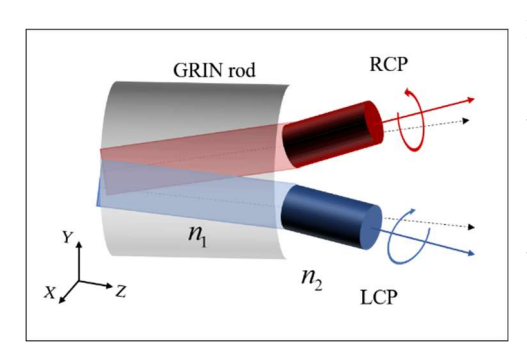


Figure 2. (a) Refraction of transversely shifted Gaussian output beam at GRIN-air interface. Red and blue colours represent RCP and LCP output beams. The solid arrows depict the change in the direction of propagation due to refraction of output optical field at the end face of GRIN rod. The dotted line represents the propagation of the beam without refraction.

At the exit plane of the GRIN rod, the outgoing Gaussian beam undergoes refraction and results in an increased shift as shown in the Fig 2 (a). The deflected output beam propagates at an angle in the YZ plane, and the angle of deviation

can be calculated as $\theta(y_0, z_1) = \frac{\delta_y(x_0, z_1)}{z_1}$ with z_1 the length of the GRIN rod.

The deviation in the refracted angle is

$$n_1 \theta_1 = n_2 \theta_2$$

$$\theta_2 = n_1 \theta_1 \approx 1.629 \times \theta_1 \quad [\because n_2 = 1]$$
(12)

Where θ_1, θ_2 are angle of deviation in the GRIN rod and air, and n_1, n_2 are refractive index of GRIN rod and air respectively. From this, the modified SH shift for free-space propagation at a distance z_2 is written as

$$\delta_{y}(x_{0}, z_{2}) = \theta_{2}z_{2} = 1.629 * \theta_{1}z_{2}$$

$$= 1.629 \frac{\delta_{y}(x_{0}, z_{1})}{z_{1}}z_{2}$$
(13)

Eq. (14) describes the transverse spin shift at the centre of intensity of the beam and the phase change of beam due to propagation in the GRIN rod. Apart from the transverse spin-Hall shift of the output beam, the propagation of beam changes its direction in the XZ plane also due to curved trajectory.

If the input beam is launched at a position (x,0) along x axis, the beam is compressed in x direction and elongated in y direction. Thus, the beam waist of the output Gaussian beam is scaled according to initial launch position. The off-axis propagation of Gaussian beam in x direction results in SHE and beam waist elongation in y direction and a change in the beam's trajectory. The intensity of the output Gaussian beam is,

$$I = \left(\frac{\omega_0}{\omega_z}\right)^2 \exp\left\{-2\left(\frac{\left(x - x\left(x_0, z_1\right)\right)^2 + \left(y - \delta_y\right)^2}{\omega_x^2}\right)\right\}$$
(14)

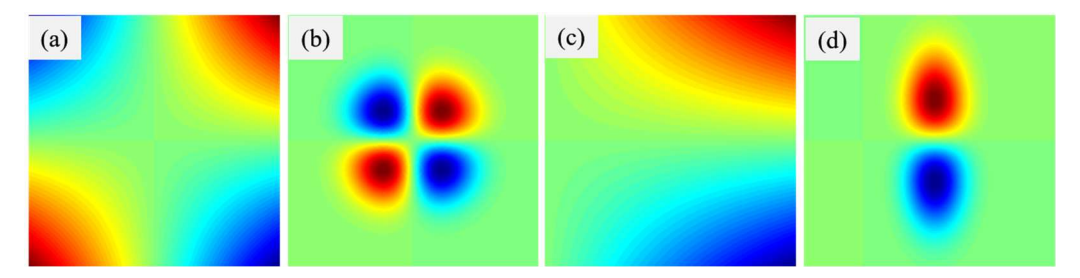


Figure 3. RVB phase accumulation due to (a) on axis (c) off-axis propagation of LP Gaussian beam through the GRIN rod. Corresponding orthogonal polarization projection for (b) on-axis and (d) off-axis propagation.

3.3.2 Reciprocal spin-Hall effect of light

It is known that propagation of plane polarized Gaussian beam in isotropic, homogeneous, and non-dispersive medium does not affect polarization up to first-order approximation [52]. While the propagation in an inhomogeneous or anisotropic medium leads to substantial changes in the state of polarization and degree of polarization [47,50]. In this context reciprocal spin-Hall effect of light refers to the rotation of plane of polarization due to path dependent accumulation of Rytov-Vladimirskii-Berry phase in the GRIN rod or in optically active media.

The off-axis launching of plane polarized Gaussian beam leads to propagation of beam along curved trajectory, determined by the refractive index gradient resulting in a decrease in the radius of curvature which increases the curvature of path as one moves from on-axis to off-axis position. The off-axis propagation results in two types of Berry phase due to i) torsion or twist of helical trajectory of constituent plane waves [48] and ii) curvature of the beam's trajectory [49]. The curvature of the beam's trajectory changes the bi-normal component of electric field and there by resulting in curvature dependent geometric Berry phase accumulation. The central plane wave does not experience any change in the polarization due to its planar trajectory, but the neighbouring plane waves propagating at a different angle undergo a twist in its trajectory, resulting in a net torsion, leading to rotation of the plane of polarization. The accumulated Berry phase is found to be proportional to the square of input beam position or the incident angle of the Gaussian beam for a helical trajectory in a graded-index fiber [50].

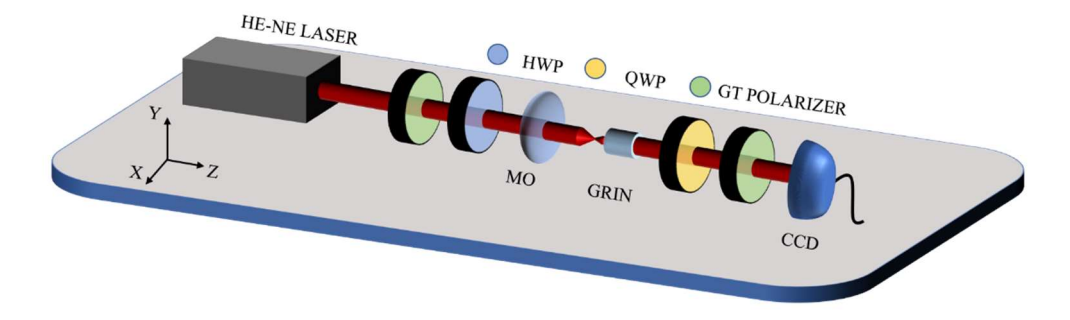


Figure 4. Schematic of the experimental setup used to study the spin-Hall and reciprocal SH effect of light in the GRIN rod. MO: Microscope objective lens, CCD: camera.

3.4 Experimental details

The optical output from the He-Ne Laser is polarized using Glan-Thompson polarizer and is then passed through a 0-order HWP to select input vertical state of polarization. Vertically polarized input Gaussian beam is propagated through the GRIN rod, which is precision-positioned on a V-Groove. The GRIN rod is aligned with a 5-axis stage (3-directional, 2-inclinational arms) by matching the output with the geometric centre of the beam without the GRIN rod. The GRIN rod is then carefully moved in + y direction to induce a phase gradient, breaking the symmetry of the system. The off-axis launching causes the Gaussian beam to experience phase gradient due to refractive index profile of the GRIN rod. This results in smooth curved trajectory of Gaussian beam, modifying the direction of the propagation. The output from the GRIN rod propagates at angle with respect to the Z-axis in XZ plane and the angle is determined by the input launch position. The optical components are carefully placed perpendicular to output Gaussian beam direction of propagation. This process was repeated for all the different off-axis launch positions.

The output Gaussian beam is then passed through a QWP and GT polarizer combination for measuring SHE and reciprocal SHE. The QWP and GT polarizer are used in weak measurement scheme to amplify the small shift and the change in the SoP of the output beam. The QWP is positioned at 90° and the analyser is rotated from $90^{\circ} + \Delta$ to $90^{\circ} - \Delta$ and corresponding output intensity are captured in the CCD camera using LabView program controlling the devices. From the captured images, the weak (S3) Stokes parameter is calculated for different input beam positions.

3.5 Results and discussion

3.5.1 Spin-Hall effect of Light

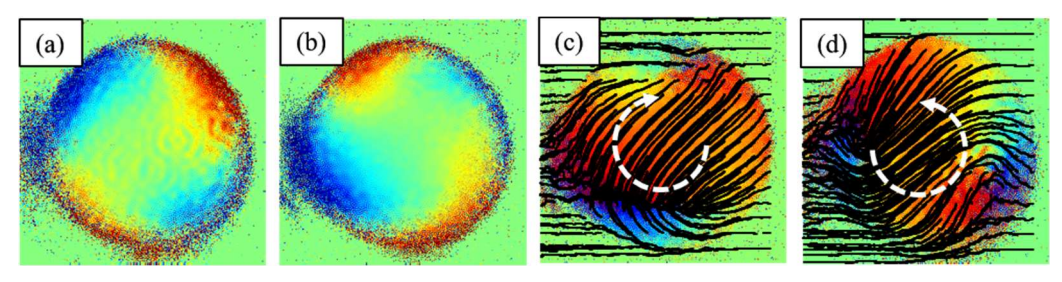


Figure 5. Experimentally measured Stokes parameter S_1 , (a), (b) and ellipticity orientation (c), (d) for RCP (a), (c) and LCP (b), (d) input polarization.

The on-axis propagation of polarized Gaussian beam through the GRIN rod can be analysed by dividing the GRIN into 4 quadrants grouped under the curvaturedependent phase. The Stokes parameters are calculated for incident RCP and LCP Gaussian beams. The phase changes associated with RCP and LCP Gaussian beams propagation can be seen in Fig 5 (a) and (b) from the Stokes parameter S₁. The red and blue colour represents $\pi/2$ phase difference between them and as can be seen each quadrant is $\pi/2$ phase shifted with respect to the adjacent quadrant. The S_1 parameter for the output Gaussian beam reveals a polarization dependent phase distribution as can be seen in the Fig 5 (a) and (b). Not only the phase difference but the energy circulation through the GRIN also depends on polarization [46]. A similar kind of effect was observed in the polarization ellipticity orientation of the output beam. Ellipticity orientation mapped as streamlines for RCP and LCP Gaussian beams is shown in Fig 5 (c) and (d) reveal the clockwise and counter-clockwise rotation, indicating helicity and energy circulation in the beam cross-section. These effects reported here are observed without introducing any asymmetry via off-axis or skewed launching of the input Gaussian beam.

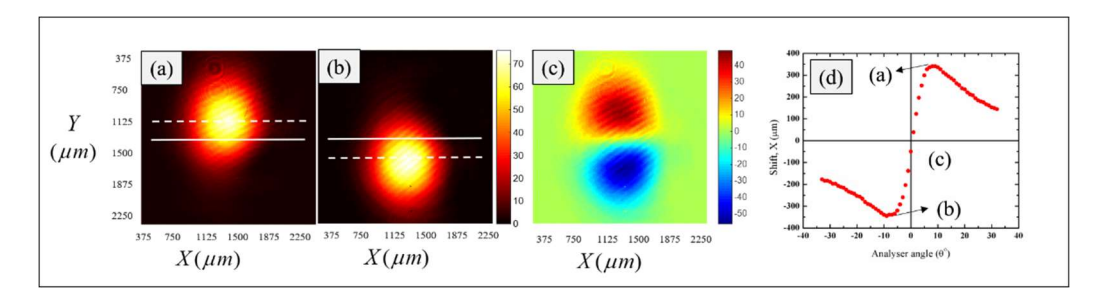


Figure 6. Spin-Hall shift measured using weak measurement technique. (a) RCP and (b) LCP components of output beam for LP input Gaussian beam, (c) spin-Hall shift and (d) spin-Hall shift as a function of analyser angle for input position 0.7 mm. The red and blue colour represent right and left polarization components. Solid white line indicates centre of intensity (CoI) of the output beam with two lobes and the dotted lines indicate change in CoI for (a) RCP and (b) LCP components of the beam in transverse direction.

The transverse spin-dependent shift of the output Gaussian beam is amplified via weak measurement technique. The output from the GRIN rod is passed through QWP and GT polarizer combination. The analyser is rotated from $90^{\circ} - \Delta$ to $90^{\circ} + \Delta$, and the centre of intensity (CoI) distribution is calculated as a function of the analyser angle as shown in the Fig. 6 (d) for the input beam position $x = 0.7 \ mm$. The output beam after passing through QWP and GT polarizer has a HG beam like spatial intensity profile as shown in Fig. 6 (c). The clockwise (+), counter-clockwise (-) rotation of analyser selects the oppositely displaced LCP and RCP beam respectively as shown in Fig. 6 (b) and (a). The images in Fig. 6 (a) and (b) correspond to maximum displacement of RCP and LCP beams. The solid line represents the CoI prior to analyser rotation and the dashed line represent the shifted CoI position of the beam. The maximally displaced RCP and LCP beams are used to extract the weak (S3) Stokes parameter as shown in the Fig. 6 (c). The amplified shifts for RCP and LCP components are $341.5 \ \mu m$ and $344.7 \ \mu m$.

The optical output fields for various launch positions are shown in Fig 7, input launch position is mentioned at the bottom left of each image. The four-lobe pattern for on-axis propagation is the signature pattern observed in conoscopic inspection of uniaxial crystals. The on-axis to off-axis propagation transforms the output from four-lobe to two lobe HG-like pattern after passing through the QWP-analyser combination. The above transition is also accompanied by changes in the beam waist along y direction, perpendicular to off-axis launch direction. This change in the spatial intensity profile also signifies the asymmetry and the SHE associated with it. The ellipticity parameter of the output beam fields can also be used identify the input beam position induced

asymmetry. The output Gaussian beam has asymmetry in both spatial intensity profile and polarization distribution. The SHE shifts are measured for different input off-axis positions. The nonlinear curve (Fig. 8 (b)) associated with the SHE as a function of input position can be attributed to the weak anisotropy of the GRIN rod. The spin-dependent angular momentum density is a manifestation of the SHE due to spin-orbit coupling of light in the GRIN rod.

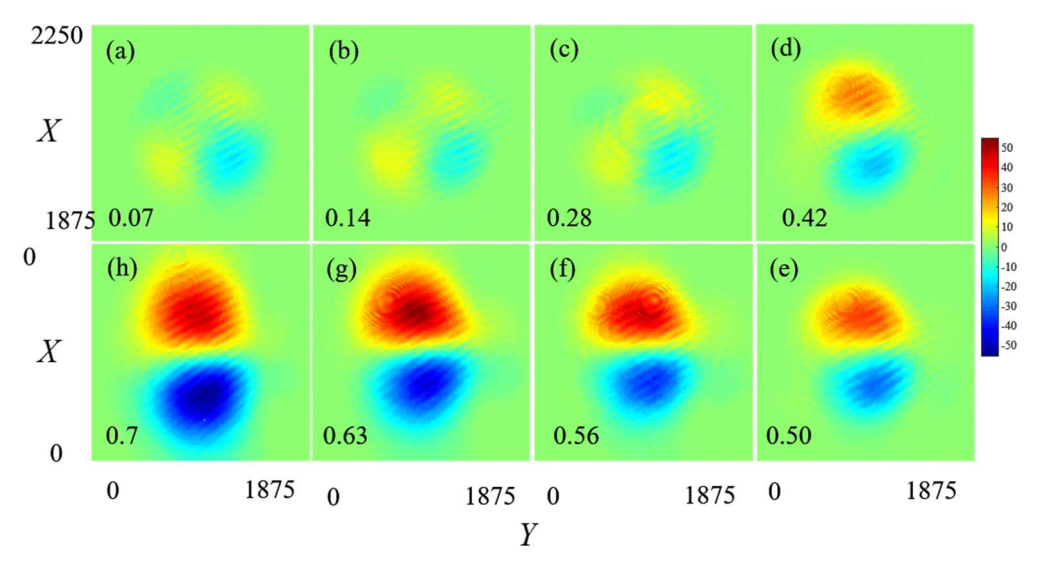


Figure 7. Experimentally measured weak (S3) Stokes parameter for different input launch positions. Red and blue colour correspond to right and left circular polarization components in the output optical field.

3.5.2 Reciprocal spin-Hall effect of Light

The reciprocal or inverse SHE is the accumulation of Berry phase due to the trajectory of the constituent plane waves of the Gaussian beam resulting in the rotation of the plane of polarization of the output beam. The torsion independent trajectory of the central plane does not affect the polarization but the neighbouring plane waves propagating at different angles experience a net torsion leading to the accumulation of the RVB phase. The RVB phase changes the polarization structure of the output beam. The weak interaction restricts the usage of the conventional Stokes parameter used for extracting the output beam polarization parameters. Therefore, modified Stokes parameter measurement, known as weak (S3) Stokes parameters measurement, is employed for the measurement of small changes in the SoP. The analyser is oriented quasi-

orthogonal to the input polarization, and it is rotated by a small angle $\pm \Delta$ enabling us to measure small changes in the polarization ellipse orientation. From the captured images, weak S3 values are extracted and plotted as a function of the input position as shown in Fig 8. The behaviour of the weak (S3) Stokes parameter is shown in Fig 8 for all the different input launch positions mentioned. The phase-gradient and the torsion experienced by the Gaussian beam increases as the input position is changed from 0.1 mm to 0.7 mm. An increase in torsion increases the rotation of the plane of polarization and thus altering the polarization content of the output beam. The intensity of colour changes associated with off-axis propagation can be seen in Fig 7 (a)-(h). The resulting change in the weak (S3) content as a function of input position is plotted as shown in Fig. 8 and it is a nonlinear due to weak anisotropy of the GRIN rod.

The SH shift in inhomogeneous isotropic medium scales linearly with the change of input position and angle of Gaussian beam [52]. With the inclusion of anisotropy, the SH shift for a Gaussian beam in a cylindrical glass exhibits a nonlinear behaviour as a function of input launch angle [52]. Thus, SH shift offers a way to distinguish the isotropic and anisotropic materials. Further, it can help to differentiate weak anisotropy due to different manufacturing processes, defects, contamination of the sample etc. The SH shift is experimentally measured for different off-axis positions by fixing the analyser angle in post-selection process of the weak measurement as shown in the Fig. 6 (a) and (b). The SH shift exhibits a non-linear behaviour due to weak anisotropy as shown in the Fig. 8 (b).

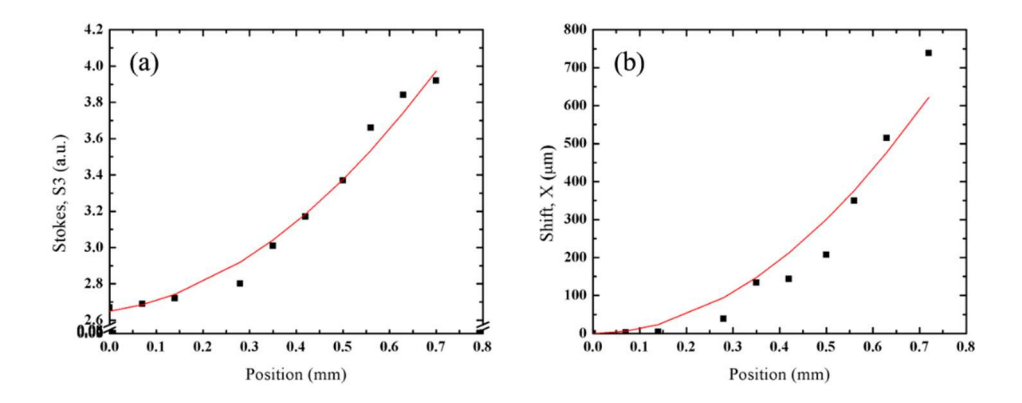


Figure 8. Experimentally measured a) weak (S3) Stokes parameter and b) transverse SHE shifts for different input positions.

3.6 Summary

In this chapter, we investigated the spin-Hall effect arising due to propagation of Gaussian beam in a graded-index medium. Off-axis propagation of vertically polarized Gaussian beam results in spin-dependent transverse shift of output optical beam. Small wavelength scale SHE is amplified using weak measurement technique as a function of input position of the Gaussian beam. The reciprocal SHE – RVB phase is realized and measured using weak (S3) Stokes parameter. Our study helps understanding of the spin-orbit interaction of light in inhomogeneous media in view of spin-Hall effect and reciprocal SHE of the beam.

References:

- Nagaosa N, Sinova J, Onoda S, MacDonald A H and Ong N P 2010 Anomalous Hall effect Rev. Mod. Phys. 82 1539–82
- 2. Haldane F D M 1988 Model for a quantum Hall effect without Landau levels: condensed-matter realization of the 'parity anomaly' *Phys. Rev. Lett.* **61** 2015–8
- 3. Ezawa Z F 2013 *Quantum Hall Effects: Recent Theoretical and Experimental Developments* (Singapore: World Scientific).
- 4. Hirsch, J. E. "Spin hall effect." Physical review letters 83.9 (1999): 1834.
- 5. Kato Y K, Myers R C, Gossard A C and Awschalom D D 2004 Observation of the spin Hall effect in semiconductors *Science* **306** 1910–3
- 6. Sinova J, Culcer D, Niu Q, Sinitsyn N A and Jungwirth T 2004 Universal intrinsic spin Hall effect *Phys. Rev. Lett.* **92** 126603.
- Kane C L and Mele E J 2005 Quantum spin Hall effect in graphene *Phys. Rev. Lett.* 95 226801.
- 8. Qi X L and Zhang S C 2010 The quantum spin Hall effect and topological insulators *Phys. Today* **63** 33–8.
- 9. Chang C Z *et al* 2013 Experimental observation of the quantum anomalous Hall effect in a magnetic topological insulator *Science* **340** 167–70.
- 10. Wolf S A *et al* 2001 Spintronics: a spin-based electronics vision for the future *Science* **294** 1488–95.
- 11. Awschalom D D and Flatte M E 2007 Challenges for semiconductor spintronics *Nat. Phys.* **3** 153–9.
- 12. Chappert C, Fert A and Van Dau F N 2007 The emergence of spin electronics in data storage *Nat. Mater.* **6** 813–23.
- 13. Wunderlich J et al 2010 Spin Hall effect transistor Science 330 1801-4.
- 14. Dooghin A V, Kundikova N D, Liberman V S and Zel'dovich B Y 1992 Optical Magnus effect *Phys. Rev.* A **45** 8204–8.
- 15. Liberman V S and Zel'dovich B Y 1992 Spin—orbit interaction of a photon in an inhomogeneous medium *Phys. Rev.* A **46** 5199–207.
- 16. Schilling H 1965 Die Strahlversetzung bei der Reflexion linear oder elliptisch polarisierter ebener Wellen an der Trennebene zwischen absorbierenden Medien *Ann. Phys.* **16** 122–34.
- 17. Player M A 1987 Angular momentum balance and transverse shifts on reflection of light *J. Phys. A: Math. Gen.* **20** 3667–78.
- 18. Fedoseyev V G 1988 Conservation laws and transverse motion of energy on reflection and transmission of electromagnetic waves *J. Phys. A: Math. Gen.* **21** 2045–59.
- 19. Onoda, Masaru, Shuichi Murakami, and Naoto Nagaosa. "Hall effect of light." *Physical review letters* 93.8 (2004): 083901.
- 20. Bliokh, Konstantin Y., et al. "Geometrodynamics of spinning light." *Nature Photonics* 2.12 (2008): 748-753.
- 21. Nori, Franco. "The dynamics of spinning light." *Nature Photonics* 2.12 (2008): 717-718.
- 22. Haefner D, Sukhov S and Dogariu A 2009 Spin Hall effect of light in spherical geometry *Phys. Rev. Lett.* **102** 123903.
- Rodriguez-Herrera O G, Lara D, Bliokh K Y, Ostrovskaya E A and Dainty C 2010
 Optical nanoprobing via spin—orbit interaction of light *Phys. Rev. Lett.* 104 253601.
- 24. Roy B, Ghosh N, Banerjee A, Gupta S D and Roy S 2014 Manifestations of geometric phase and enhanced spin Hall shifts in an optical trap *New J. Phys.* **16** 083037.
- 25. Ling X *et al* 2014 Realization of tunable spin-dependent splitting in intrinsic photonic spin Hall effect *Appl. Phys. Lett.* **105** 151101.

- 26. Kruk S S *et al* 2014 Spin-polarized photon emission by resonant multipolar nanoantennas *ACS Photonics* 1 1218–23.
- 27. Luo H, Zhou X, Shu W, Wen S and Fan D 2011 Enhanced and switchable spin Hall effect of light near the Brewster angle on reflection *Phys. Rev.* A **84** 043806.
- 28. Kong L *et al* 2012 Spin Hall effect of reflected light from an air–glass interface around the Brewster's angle *Appl. Phys. Lett.* **100** 071109.
- Ling X, Luo H, Tang M and Wen S 2012 Enhanced and tunable spin Hall effect of light upon reflection of onedimensional photonic crystal with a defect layer *Chin. Phys. Lett.* 29 074209.
- 30. Gotte J B and Dennis M R 2013 Limits to superweak amplification of beam shifts *Opt. Lett.* **38** 2295–7.
- 31. Hosten O and Kwiat P 2008 Observation of the spin Hall effect of light via weak measurements *Science* **319** 787–90.
- 32. Zhou X, Ling X, Luo H and Wen S 2012 Identifying graphene layers via spin Hall effect of light Appl. Phys. Lett. 101 251602.
- 33. Zhou X, Xiao Z, Luo H and Wen S 2012 Experimental observation of the spin Hall effect of light on a nanometal film via weak measurements Phys. Rev. A 85 043809.
- 34. Qiu X et al 2014 Determination of magneto-optical constant of Fe films with weak measurements Appl. Phys. Lett. 105 131111.
- 35. Hasman E, Bomzon Z, Niv A, Biener G and Kleiner V 2002 Polarization beamsplitters and optical switches based on space-variant computer-generated subwavelength quasiperiodic structures Opt. Commun. 209 45–54.
- 36. Hasman E, Kleiner V, Biener G and Niv A 2003 Polarization dependent focusing lens by use of quantized Pancharatnam– Berry phase diffractive optics Appl. Phys. Lett. 82 328–30.
- 37. Shitrit N, Bretner I, Gorodetski Y, Kleiner V and Hasman E 2011 Optical spin Hall effects in plasmonic chains Nano Lett. 11 2038–42.
- 38. Shitrit N, Yulevich I, Maguid E, Ozeri D, Veksler D, Kleiner V and Hasman E 2013 Spin-optical metamaterial route to spin-controlled photonics Science 340 724–26.
- 39. Ling X et al 2015 Giant photonic spin Hall effect in momentum space in a structured metamaterial with spatially varying birefringence Light: Sci. Appl. 4 e290.
- 40. Gorodetski Y, Niv A, Kleiner V and Hasman E 2008 Observation of the spin-based plasmonic effect in nanoscale structures Phys. Rev. Lett. 101 043903.
- 41. Lin J et al 2013 Polarization-controlled tunable directional coupling of surface plasmon polaritons Science 340 331–4.
- 42. Pancharatnam S 1956 Generalized theory of interference, and its applications Proc. Indian Acad. Sci. A 44 247–62.
- 43. Bliokh, Konstantin Yu, and Yury P. Bliokh. "Conservation of angular momentum, transverse shift, and spin Hall effect in reflection and refraction of an electromagnetic wave packet." *Physical review letters* 96.7 (2006): 073903.
- 44. Bliokh, K. Yu, and Yu P. Bliokh. "Polarization, transverse shifts, and angular momentum conservation laws in partial reflection and refraction of an electromagnetic wave packet." *Physical Review E* 75.6 (2007): 066609.
- 45. Collins, Stuart A. "Lens-system diffraction integral written in terms of matrix optics." *JOSA* 60.9 (1970): 1168-1177.
- 46. Li, Hehe, et al. "Changes of phase structure of a paraxial beam due to spin-orbit coupling." *Physical Review A* 97.5 (2018): 053843.
- 47. Bliokh, Konstantin Yu, et al. "Spin-orbit interactions of light." *Nature Photonics* 9.12 (2015): 796-808.
- 48. Lai, Meng-Yun, et al. "Electromagnetic wave propagating along a space curve." *Physical Review A* 97.3 (2018): 033843.

- 49. Lai, Meng-Yun, et al. "Geometrical phase and Hall effect associated with the transverse spin of light." *Physical Review A* 100.3 (2019): 033825.
- 50. Petrov, N. I. "Evolution of Berry's phase in a graded-index medium." *Physics Letters A* 234.4 (1997): 239-250.
- 51. Alda, Javier, and Glenn D. Boreman. "On-axis and off-axis propagation of Gaussian beams in gradient index media." *Applied optics* 29.19 (1990): 2944-2950.

4

Orbital-Hall effect of light in GRIN rod

This chapter deals with off-axis propagation of optical vortex (OV) bearing intrinsic orbital angular momentum (IOAM) and the effects arising due to breaking the rotational (azimuthal) symmetry of the GRIN rod system. The application of theoretical formalism developed in Chapter 3, for optical vortex beams, also leads to the understanding of the orbital-Hall effect (OHE) of light, a topological chargedependent splitting of the optical vortex beam in the transverse plane, orthogonal to the direction of induced asymmetry of the system. Subsequently, the reciprocal OHE, the rotation of spatial intensity of the output optical beam, due to orbital Berry phase (counterpart to RVB phase) accumulation leads to the appearance of phase gradient experienced by the zero IOAM beam. The reciprocal OHE is explored in detail and measured as a function of the beam position at the input end of the GRIN rod. The beam shift arising due to the OHE depends on the topological charge of the input IOAM beam and increases linearly as a function of the topological charge of the beam. Akin to the reciprocal SHE, the reciprocal OHE scales as square of the input beam position. These polarization independent effects are experimentally measured, without any polarization components, using a CCD camera for intensity image capture to quantify the effect.

4.1 Introduction

Much before the wide-spread knowledge of optical vortices, vortex solitons were studied thoroughly in hydrodynamics due to a unique feature, the singularity [1-3]. In 1992, in their seminal work, Allen et al., introduced optical beams carrying intrinsic orbital angular momentum (IOAM) bearing a phase singularity in the beam cross-section [4]. Also known as the optical vortex (OV) beams, these are marked by helical wavefronts propagating with the phase singularity at its center. They are characterized by topological charge value $(\pm l)$, corresponding to the number of phase winding turns within one wavelength distance. The OV beams can take positive or negative topological charge values signifying clockwise and counter-clockwise rotation of the beam's helical phase. Though the SAM, associated with circular state of polarization is limited to +1 or -1 values for rightand left-circular polarized beam of light, the OV beams with IOAM can have very large $(l \rightarrow \infty)$ OAM value due to scalability. The unique properties and dynamics associated with OV beam interactions demanded more resources and attention, eventually leading to a new field of study, "Singular Optics" dealing with OV beam interaction with materials and corresponding effects.

As a natural extension to the SHE, the transverse splitting of circular polarization components, the orbital-Hall effect (OHE) of light is the transverse, topological charge-dependent deflection of OV beam due to refractive index phase gradient and curved trajectory, proposed by Bliokh [8-10] for various physical situations. The OHE of light was subsequently realized in the reflection of OV beam at an air-glass interface by Zhang jin et al., [11]. The beam-shift due to the OHE was also observed and measured for the propagation of OV beams through the bi-prism [12]. The orbital-Berry phase, proposed to understand the propagation of OV beam through a helicoidal fiber [9] is been used to understand the experimentally measured off-axis propagation of Gaussian beams through two-mode step-index optical fiber [14]. However, a much simpler experimental realization of the OHE of light due to transmission in a medium remained an open problem. We experimentally measured off-axis propagation of OV beams through a GRIN rod and as a function of the topological charge of the OV beam [13]. The results presented are understood using the orbital Berry phase accumulated by an off-axis beam propagating through a GRIN rod system.

This chapter describes off-axis propagation of OV beams with different topological charge, based on ABCD matrix formalism [15]. The transverse orbital-Hall shift of the OV beam is understood and measured for different input positions [13] on the GRIN rod system. The reciprocal OHE, rotation of the

optical output field due to the orbital-Berry phase is measured for HG beams with zero OAM. These topological charge-dependent transverse shifts of OV beam trajectory are independent of the beam polarization. Thus, only a CCD camera is used for capturing the intensity images of the output. The output optical beam field's rotational changes due to reciprocal OHE are quantified by choosing high-intensity locations as markers for reference. The magnitude of the (r)OH effects associated with IOAM, is much large compared to effects resulting from the SAM of light in the medium. Unless mentioned otherwise, this chapter deals only with off-axis propagation leading to orbital Hall and its reciprocal effect.

4.2 Orbital – Hall effect of light

The previous chapter discussed the spin-dependent transverse shift in the center of intensity distribution for CP Gaussian beam propagating through the GRIN rod for different input off-axis positions and described the RVB phase accumulation as a function of the input beam position. Now we study the OHE shift as a function of the topological charge of the incident OV beam. The reciprocal OHE – rotation of the output optical field due to the Berry phase is discussed for two different cases of HG beam orientation. It is shown that the HG beams possessing zero OAM undergo rotation for off-axis propagation through the GRIN rod. The incident HG beam orientation plays a crucial role in the output HG beams' rotation dynamics. Though the input OV beam and the HG beam are linearly polarized, the beams' polarization aspect will not be mentioned hereafter as the effects under study are independent of polarization.

4.3 Theoretical formalism

4.3.1 Orbital-Hall effect of light

The 4x4 matrix formalism used for the propagation of CP Gaussian beam through the GRIN rod is now applied to the OV beams bearing phase singularity. The 4x4 matrix describing the propagation of the optical vortex beam through the GRIN rod remains the same, with one notable change representing the topological charge (l) of the input OV beam instead of the circular state of polarization of the Gaussian beam. Accordingly, the variable β is modified as $\beta = 2l\alpha/k$. The output optical field at a plane in cylindrical coordinate system is written based on Collin's integral as [16]

$$E(r,\theta,z) = -\frac{ik}{2\pi C} \exp(ikz) \int_{0}^{\infty} \int_{0}^{2\pi} E_{0}(r_{0},\theta_{0},z=0) \times \exp\left\{-\frac{ik}{2C} \left[D(r^{2}) + A(r_{0}^{2}) - 2(r_{0}r\cos\theta_{0}\cos\theta) - 2(r_{0}r\sin\theta_{0}\sin\theta) + 2\beta z(r_{0}\cos\theta_{0}r\sin\theta) - 2\beta z(r\cos\theta r_{0}\sin\theta_{0}) + 2\beta Cr^{2}\cos\theta\sin\theta\right]\right\} r_{0}dr_{0}d\theta_{0}$$

$$(1)$$

Using the above equation, we investigate the evolution of Laguerre-Gaussian beam through the GRIN rod. The electric field distribution for the Laguerre-Gaussian beam in cylindrical coordinates at the input plane is [15]

$$E\left(r_{0}, \varphi_{0}, z=0\right) = \left(\sqrt{2} \frac{r_{0}}{\omega}\right)^{l} L_{p}^{l}\left(2 \frac{r_{0}^{2}}{\omega_{0}^{2}}\right) \exp\left(-\frac{r_{0}^{2}}{\omega_{0}^{2}}\right) \exp\left(-il\varphi_{0}\right)$$
(2)

Upon substitution of Eq (2) in Eq (1), an analytical expression for the propagation of OV beam through the GRIN rod is obtained as [15],

$$E(r,\varphi,z) = q_0^{l+1} \exp(-l\varphi) \exp(ik\beta z) \frac{\left(Aq_0 - C\right)^p}{\left(Aq_0 + C\right)^{p+l+1}} \left(\frac{\sqrt{2}r}{\omega_0}\right)^l$$

$$\exp\left(-\frac{ik\left(r - \delta_r\right)^2}{2q}\right) L_p^l \left[\frac{2\left(r - \delta_r\right)^2}{2\omega^2(z)}\right]$$
(3)

Where $\omega(z) = \omega_0 \sqrt{\left(a^2 + \left(\frac{b\lambda}{\pi\omega_0^2}\right)^2\right)}$ is the beam waist of the output optical field

at a distance z. The output optical field for an input position x, in the rectilinear coordinate system is [16]

$$E(x, y, z) = q_0^{l+1} \exp\left(-l \tan^{-1}(y/x)\right) \frac{(Aq_0 - C)^p}{(Aq_0 + C)^{p+l+1}} \left(\sqrt{2} \frac{(x+y)}{\omega_0}\right)^l \exp\left(-ik \frac{\left((x-\delta_x)^2 + (y-\delta_y)^2\right)}{2q}\right) L_p^l \left[\frac{2\left((x-\delta_x)^2 + (y-\delta_y)^2\right)}{2\omega^2(z)}\right]$$
(4)

Where $\delta_x = \beta zy$, $\delta_y = \beta zx$ are shifts in x- and y- directions due to the orbital-Hall effect of light. As can be seen, the value of the OHE shift increases linearly

with the topological charge and can thus be greater than the value obtained using the SHE. Due to the change in the OV beam trajectory, the beam propagates at an angle to the axis of the system and no longer remains in the XZ plane. As discussed in Chapter 3, the beam undergoes refraction at the GRIN rod's output end, changing its trajectory. The orbital-Hall shift increases linearly with free space propagation due to oblique propagation of the output, as discussed in Chapter 3.

However, unlike the Gaussian beam, the optical vortex beam suffers larger distortions in the phase and spatial intensity structure. The distortions are not only due to the refractive index gradient but also due to the diffraction phenomenon in the GRIN rod. The diffraction is associated with both the refractive index gradient and weak local anisotropy. Apart from the spatial distortions, the OV beam also rotate as they propagate through the GRIN rod.

4.3.2 Reciprocal orbital-Hall effect of light

Akin to the Berry phase accumulation for polarized Gaussian beam propagating along helical trajectory in the GRIN rod, propagation of the optical vortex beam results in the rotation of output optical beam due to orbital-Berry phase accumulation. The handedness of the spatial intensity rotation depends on the sign of the topological charge. The intrinsic helical wavefront structure of the OV serves as an ideal candidate to observe the orbital Berry phase in the modal domain. The orbital Berry phase varies linearly with the OV beams' topological charge. Much like reciprocal SHE, the orbital Berry phase is expected to change as the square of the input beam position at the input face of the GRIN rod.

HG_{10} and HG_{01} beams:

The Hermite-Gaussian (HG) beams with line phase discontinuity do not carry orbital angular momentum, similar to linearly polarized light not carrying spin angular momentum. The HG beams can be expressed as a superposition of oppositely charged Laguerre-Gaussian beams with variable phase. The variable phase controls the orientation of the HG beam. Propagation of the HG beam through the GRIN rod leads to rotation of the output HG beam due to the orbital-Berry phase accumulated by constituent Laguerre-Gaussian modes. The off-axis (x-) propagation through the GRIN rod results in phase gradients along the y-direction. The HG_{10 (01)} beams with 0° and 90° orientation have phase

discontinuity along x- and y- directions, respectively. Since the phase structure due to incident HG beam and refractive index gradient due to off-axis propagation is parallel or anti-parallel, there is no net rotation of the output HG beam.

HG beams with ±45°

HG beams with ±45° orientation become ideal candidates to investigate the OBP. The mutual interaction of the HG beams phase structure and the phase gradient associated with the GRIN rod results in rotation of the output HG beam. The HG beam rotation angle increases as a function of input position owing to increased phase gradient. The input HG beam oriented at ±45° can be written as

$$E_{i} = A' \left[\exp(-il\varphi_{0}) \exp(\pm i\pi/4) + \exp(\mp i\pi/4) \exp(+il\varphi_{0}) \right]$$
 (5)

Where
$$A' = \left(\sqrt{2}\frac{r_0}{\omega}\right)^l L_p^l \left(2\frac{r_0^2}{\omega_0^2}\right) \exp\left(-\frac{r_0^2}{\omega_0^2}\right)$$
 and E_0 is the output electric field

[14]. The constituent LG beams acquire orbital Berry phase $\exp(-il\beta_{l+})$, $\exp(il\beta_{l-})$ for topological charges +l and -l respectively. The output optical field after propagation through the GRIN rod is

$$E_{0} = A'' \left[\exp\left(\pm i \,\pi/4\right) \exp\left(-il\beta_{l+}\right) \exp\left(-il\varphi_{0}\right) + \exp\left(\mp i \,\pi/4\right) \exp\left(il\beta_{l-}\right) \exp\left(+il\varphi_{0}\right) \right]$$
(6)

$$A'' = \left(\sqrt{2}\left(\frac{x_0}{\omega_x} + \frac{y_0}{\omega_y}\right)\right)^l L_p^l \left(2\left(\frac{x_0^2}{\omega_x^2} + \frac{y_0^2}{\omega_y^2}\right)\right) \exp\left(-\left(\frac{x_0^2}{\omega_x^2} + \frac{y_0^2}{\omega_y^2}\right)\right).$$

The constituent LG beams become elliptical with different beam waist along x- and y- directions. The sense in which HG beam rotates depends on the incident HG beam orientation and its input location on the GRIN rod. The GRIN rod can essentially discriminate between the HG modes with different orientations.

4.4 Experimental details

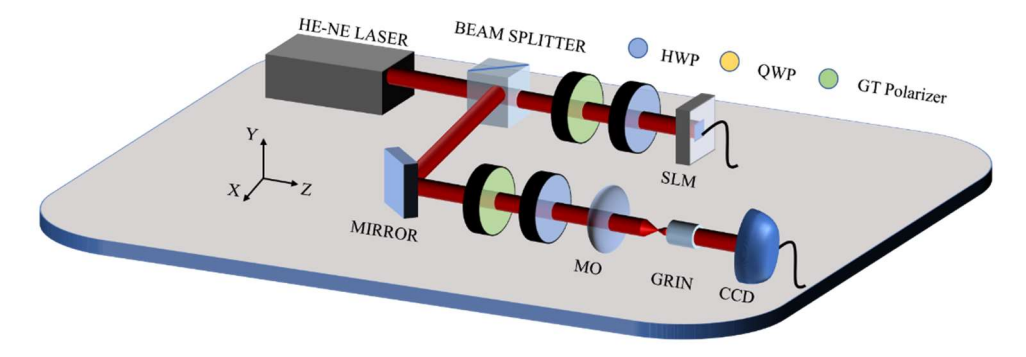


Figure 1. Schematic of the experimental setup used to investigate the OHE and reciprocal OHE due to off-axis propagation of linearly polarized OV beam and HG beam with $\pm 45^{\circ}$ orientation through the GRIN rod.

The optical output from the He-Ne laser is horizontally polarized using Glan-Thompson polarizer and HWP. The horizontally polarized input Gaussian beam is incident on the SLM (horizontal polarization being the active axis) with desired phase masks to generate the OV beams. The reflected beam from the SLM with suitable mode structure is then propagated through the GRIN rod. The GRIN rod is aligned using the 5-axis stage (3- directional,2- inclinational arms) to match the output with the beam's geometric center without the GRIN rod. The GRIN rod is then precisely moved in x (+) direction to induce a phase gradient by breaking the system's symmetry. The output optical beam is captured using the CCD for further analysis.

4.5 Results and discussion

4.5.1 Orbital-Hall effect of light

The GRIN rod with radially varying quadratic refractive index variation provides the flexibility to study the SOI and OOI effects in a laboratory due to its physical dimensions. Positioned on a 5-axis stage offers freedom to shift the GRIN rod precisely and appropriately. Experimentally measured output beam structure from the GRIN rod, for different charge input LG beam, without any polarization component is shown in Fig. 2 for a fixed input beam position of 0.6 mm.

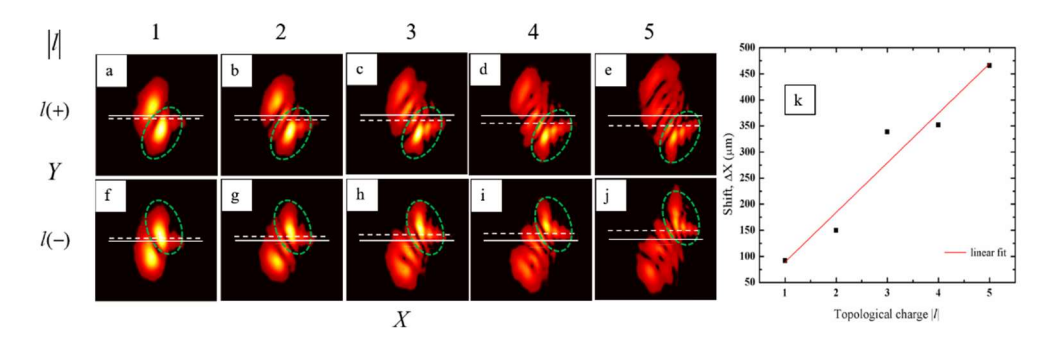


Figure 2. Experimentally measured output beam intensity for different topological charge OV beam propagating through the GRIN rod. The topological charge of the input beam are as indicated. The net transverse orbital-Hall shift (in µm) measured from the images are plotted as a function of the input OV beam's topological charge.

The output beam intensity for the input OV beam with positive TC is shown in Fig. 2 (a)-(e). The output intensity images in Fig. 2 (f)-(j) correspond to input OV beams with negative TC. At appropriate input position, the incident OV beam splits into HG like beams in the output. As can be seen from Fig 3, the orbital-Hall shift of the incident OV beam passing through the GRIN rod increases linearly as a function of the TC of the input OV beam and the OH shift flips from +y to -y with the change in the sign of the TC. Apart from input OV beam, Gaussian beam is also propagated through the same input position and is used to compare the shift associated with input OV beam. The solid lines in the Fig. 2 (a)-(j) are the CoI for the Gaussian beam. The direction of shift is indicated by a high-intensity lobe (highlighted using green dotted ellipse) of the output OV beam. The orbital-Hall shifts are quantified by extracting the centre of intensity (CoI) of the captured output beam. The OH shifts are plotted as a function of the topological charge of the input OV beam as shown in Fig. 2 (k).

Unlike the CP Gaussian beam, the OV beam with IOAM gets affected more measurably due to diffraction during off-axis propagation through the GRIN rod, resulting in the splitting of the optical vortices. The OAM of the beam is not conserved as the beam is split into HG like beams and HG beams do not possess the OAM. The splitting of OV beams results in phase dislocation (dark intensity regions) and the number of dislocation in the beam cross-section reveal information about the topological charge of the input OV beam [17,18]. The phase discontinuities due to splitting are useful to distinguish the optical vortices with different topological charges. The orientation of the output optical field is used to discriminate the sign of topological charge.

4.5.2 Reciprocal orbital-Hall effect of light

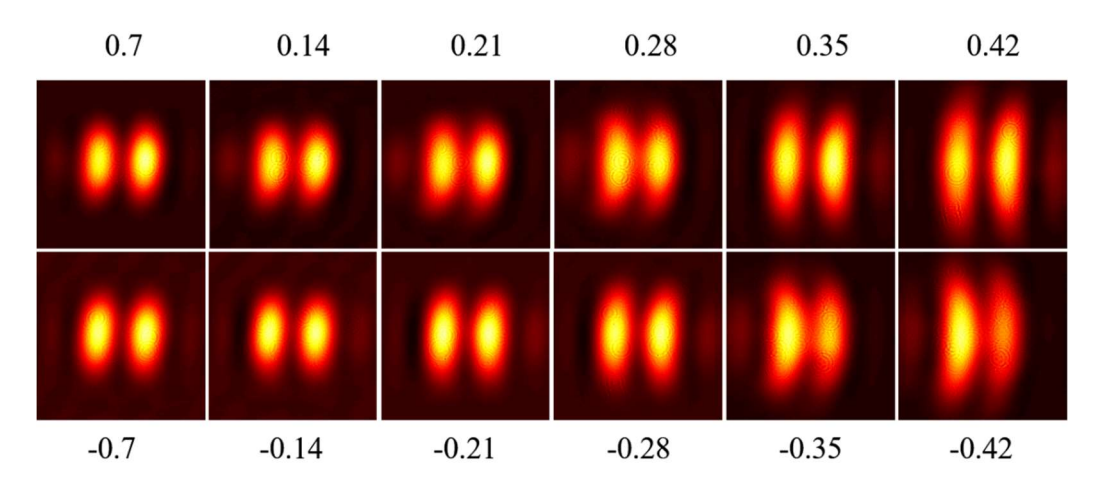


Figure 3. Experimentally measured output intensity for input HG_{10} beam for different input positions on the GRIN rod. The input positions given are in mm with negative values corresponding to the left of on-axis position.

The orientation of an elliptical-shaped Gaussian beam plays a crucial role upon interaction in anisotropic media [19]. The elliptical Gaussian beam does not undergo any rotation if the major axis of the ellipse is parallel to one of the eigen direction of the anisotropic media [19]. Likewise, the input HG beam does not show any rotation if it is oriented parallel or perpendicular to the GRIN rod's refractive index gradient direction [13]. The propagation of HG₁₀ mode, oriented along x-direction for different input positions on the GRIN rod is shown in Fig. 3. The input launch positions are measured in mm and are as indicated in the figure. Negative values for the position refer to the left of the on-axis position. Since the HG₁₀ mode and its phase structure are parallel to the refractive index gradient of the GRIN rod, there appears to be no measurable rotation in the output beam apart from spatial intensity distortion as can be seen.

However, propagation of HG beams oriented 45° to the x-axis upon propagation through the GRIN rod shows rotation of output HG beams as a function of the input beam position in the GRIN rod. The output beam intensity rotation implies that the GRIN rod imparts OAM to the input HG beam (of zero OAM) due to orbital Berry phase as a function of the input position. The incident HG beam orientation plays a vital role in the reciprocal OHE observation. The presence of x- and y- components in the intensity and phase structure of the incident HG beam with 45° orientation results in the mutual interaction between the HG beam phase structure and the phase gradients of the GRIN rod leading to a net rotation of output HG beams. It is known that the propagation of HG beam

through a helical fiber or trajectory results in the rotation of the HG beam due to parallel transport law [9]. The refractive index gradient in the GRIN rod appears to be having a similar effect on HG beam propagation and depends on the HG orientation. The HG beams in-plane trajectory in the GRIN rod appears to mimic the role of helical trajectory in the momentum space for the propagation vectors. The GRIN rod's physical dimension and the cylindrical symmetry prove advantageous and replace complex systems to study the fundamental effects.

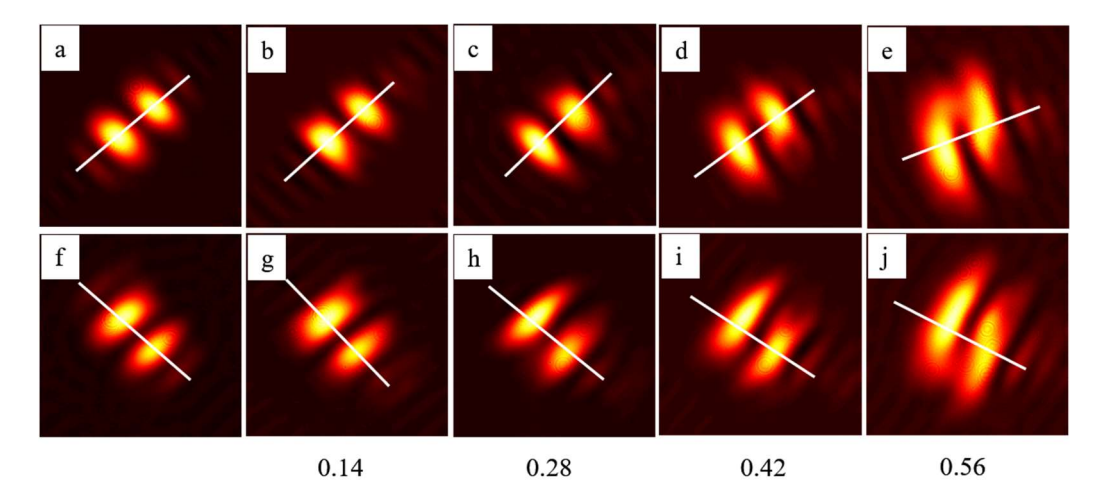


Figure 4. Experimentally measured output intensity from the GRIN rod for input 45° oriented HG beam (top row) and for -45° (bottom row) orientation for different input beam positions as indicated. The images a) and f) are the input HG beams.

The experimentally measured output HG beam for different input positions on the GRIN rod are shown in Fig 4 for (a) –(f) +45° and (g)-(l) –45° input HG beam orientation, respectively. As anticipated, the HG beams oriented at +45°, and –45° with respect to the x-axis experience rotation due refractive index gradient and the associated orbital Berry phase. The handedness of rotation is clockwise and counter-clockwise for the input HG beam with +45° and –45° respectively. The rotation angle of the output HG beam are calculated using a ring based high-intensity filter, as discussed in our paper [13] and will also be discussed in detail in Chapter 6. The rotation angles are plotted as a function of input beam position as shown in Fig. 5 (e), revealing quadratic behaviour, analogous to reciprocal SHE discussed in Chapter 3. The input HG beam intensity and phase plot are shown in the inset of Fig 5 (e).

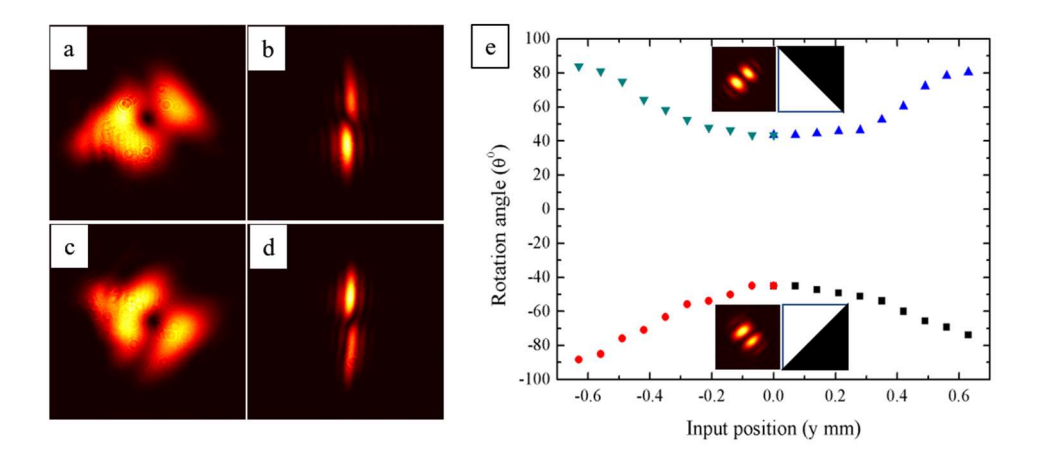


Figure 5. Experimentally measured output HG beams for different input positions for incident HG beams with 45° (top row) and --45° (bottom row) orientations.

The rotation of HG beams indicates that the GRIN rod imparts extrinsic OAM to the HG beam. This implies a possibility of transforming the HG beam to a vortex (LG) beam under appropriate conditions. The GRIN rod's phase gradient for the input position closer to the GRIN rod axis is insufficient to transform the HG to OV beam. On the other side, the distortions and diffraction at farther input position do not support an ideal beam structure. We find that input beam positions of 0.40 - 0.60 mm offer sufficient angle of rotation with manageable distortion, enabling HG to OV like beam transformation. The OV like beam is realized for the input beam position 0.56 mm by collimating the output beam. The clockwise rotation of HG (+45°) beam results in the OV beam with topological charge +1 while OV beam with l = -1 is realized using HG (-45°) input beam. The diffraction pattern measured after a single-slit reveals the signature phase dislocation pattern indicating the presence of phase singularity. The collimated output intensity structure and the diffraction pattern after passing through the single-slit for input HG beams with 45°, -45° orientations are shown in Fig. 5 (a), (c) and (b), (d) respectively.

4.6 Summary

This chapter presented studies on off-axis propagation of optical vortex beams and HG beams through the GRIN rod. The off-axis propagation of OV beam resulted in topological charge-dependent transverse shift in the center of the intensity distribution of the output beam. The splitting of the OV beam into HG like beam of different orders is seen as a manifestation of the orbit-orbit interaction (OOI) of light in the GRIN rod. As the OV beams are split open upon propagation, a part of the OAM is transferred to the medium, resulting in HG like beams and its rotation. The reciprocal OHE on the other hand is where the intensity pattern output HG beam rotates due to accumulation of orbital-Berry phase upon propagation through the GRIN rod. The HG beams with parallel and perpendicular orientations to the axis of the GRIN rod however do not undergo rotation while any other HG beams orientation results in rotation of spatial intensity structure. This rotation of HG beams with zero OAM appears to be due to vector addition of the phase structure of the HG beam and the phase gradient experienced in the GRIN rod. Apart from the rotation, the output beam gets distorted due to propagation close to extreme positions as seen in Chapter 3. Significantly, upon collimation of the output beam for 45° -oriented input HG beam results in an OV beam due to accumulation of orbital Berry phase between the eigen modes. The topological charge of the OV beam depends on the orientation of incident HG beam. The conversion of input OV beam into HG output beam and input HG beam to OV beams implies that the GRIN rod can be thought of to act like a mode converter.

The present study helps one to further understand the orbit-orbit interaction effects of light in inhomogeneous media and its possible extension to other fields of research. All the orbit-orbit interaction related effects are measured directly without using polarization components. The ability of the GRIN rod to distinguish HG beam with different orientations can be used for designing optical elements to enable mode selection or discrimination functionality based on refractive index gradient. The splitting of OV beams into HG beams helps to understand the interconversion of HG – LG beams under different circumstances and their physical implementation using such optical components. These effects also help one to understand second-order effects pertaining to the effect of two AM on the third AM of light upon propagation in the GRIN rod.

References:

- Coullet, P., Gil, L. & Lega, J. Defect-mediated turbulence. Phys. Rev. Lett. 62, 1619–1622 (1989).
- 2. Brambilla, M. et al. Transverse laser patterns. I. Phase singularity crystals. Phys. Rev. A 43, 5090–5113 (1991).
- Brambilla, M. et al. Transverse laser patterns. II. Variational principle for pattern selection, spatial multistability, and laser hydrodynamics. Phys. Rev. A 43, 5114–5120 (1991).
- 4. Allen, L. et al. Orbital angular momentum of light and the transformation of Laguerre-Gaussian laser modes. Phys. Rev. A 45, 8185–8189 (1992).
- V. Bazhenov, M. V. Vasnetsov, and M. S. Soskin, "Laser-beams with screw dislocations in their wavefronts," JETP. Lett. 52, 429–431 (1990).
- 6. C. Tamm, "Frequency locking of two transverse optical modes of a laser," Phys. Rev. A Gen. Phys. 38(11),5960–5963 (1988).
- 7. M. W. Beijersbergen, R. P. C. Coerwinkel, M. Kristensen, and J. P. Woerdman, "Helical-wavefront laser beams produced with a spiral phaseplate," Opt. Commun. 112(5-6), 321–327 (1994).
- 8. Bliokh, Konstantin Y., et al. "Spin-to-orbital angular momentum conversion in focusing, scattering, and imaging systems." Optics express 19.27 (2011): 26132-26149.
- 9. Bliokh, Konstantin Yu. "Geometrical optics of beams with vortices: Berry phase and orbital angular momentum Hall effect." Physical Review Letters 97.4 (2006): 043901.
- Bliokh, Konstantin Y., and Anton S. Desyatnikov. "Spin and orbital Hall effects for diffracting optical beams in gradient-index media." Physical Review A 79.1 (2009): 011807.
- 11. Jin, Zhang, et al. "Orbit-orbit interaction and photonic orbital Hall effect in reflection of a light beam." Chinese Physics B 23.6 (2014): 064215.
- 12. Cisowski, Claire M., and Ricardo RB Correia. "Splitting an optical vortex beam to study photonic orbit—orbit interactions." Optics letters 43.3 (2018): 499-502.
- 13. Chakravarthy, T. Pradeep, and Nirmal K. Viswanathan. "Direct and reciprocal spin-orbit interaction effects in a graded-index medium." OSA Continuum 2.5 (2019): 1576-1589.
- 14. Chakravarthy, T. Pradeep, Dinesh N. Naik, and Nirmal K. Viswanathan. "Geometric phase due to orbit—orbit interaction: rotating LP11 modes in a two-mode fiber." Journal of Optics 19.10 (2017): 105607.
- 15. Cai, Y., and S. He. "Propagation of a Laguerre–Gaussian beam through a slightly misaligned paraxial optical system." Applied Physics B 84.3 (2006): 493.
- 16. Li, Hehe, et al. "Changes of phase structure of a paraxial beam due to spin-orbit coupling." Physical Review A 97.5 (2018): 053843.
- 17. Vaity, Pravin, J. Banerji, and R. P. Singh. "Measuring the topological charge of an optical vortex by using a tilted convex lens." *Physics letters a* 377.15 (2013): 1154-1156.
- Reddy, Salla Gangi, et al. "Propagation of an arbitrary vortex pair through an astigmatic optical system and determination of its topological charge." *JOSA A* 31.6 (2014): 1295-1302.
- 19. Chen, Zhixiao, and Qi Guo. "Rotation of elliptic optical beams in anisotropic media." Optics Communications 284.13 (2011): 3183-3191.

5

Mutual influence of SAM, IOAM and EOAM of light in GRIN rod

In the previous chapters, the mutual effects of SAM-EOAM and IOAM-EOAM pairs were discussed resulting in SHE - reciprocal SHE (RVB phase) and OHE - reciprocal OHE (Orbital Berry phase) for off-axis propagation of circularly polarized Gaussian and Laguerre-Gaussian beams respectively. This paired interaction of different AM can be categorized as first-order effects. The introduction of the third AM to the first-order effects changes the dynamics of interactions, providing more intricate details. The interaction of all three AM bring forward the second-order effects: the effect of two AM on the third AM and the corresponding outcomes. This chapter focuses on such second order effects, for example the effect of SAM and IOAM on EOAM and vice-versa. Initially the effect of SAM and EOAM on IOAM is discussed followed by the effect of SAM and IOAM on EOAM. Later, the combined effect of IOAM and EOAM on the SHE and the polarization effects associated with the IOAM are also investigated. Orthogonal circular polarization projection, optical weak measurement and Stokes parameter methods are used to quantify the changes associated with the mentioned effects.

5.1 Introduction

Much of the spin-orbit interaction (SOI) or orbit-orbit interaction (OOI) effects have been focussed on the mutual effects of SAM – EOAM and IOAM – EOAM pairs, resulting in the SHE - reciprocal SHE and OHE - reciprocal OHE pairs pertaining to off-axis propagation of CP Gaussian and OV beams respectively through the GRIN rod. Though the propagation dynamics of the circularly polarized OV beams in different media is studied or investigated, they were limited to the interaction of AM pairs mentioned. Such paired interaction of AM of light can be categorized as first-order effects [1]. An addition of the missing AM degree of freedom among the three AM of light significantly changes the interaction dynamics and the outcome. This addition of the third AM to the firstorder interaction of AM leads to second-order effects (SOE). The second-order effects: the combined effect of the two AM on the third AM of light, for example, the effect of SAM and IOAM on the EOAM and the possible results are worth investigating to gain more insight into their interactions. The experimental implementation of the second-order effects have rarely been studied, if any [1]. The SOE can serve as a basis to explore further complex light-matter interactions such as third-order or in combination of different media or in complex media. Controlled experimental realization of such complex effects are challenging to measure owing to sensitivity of the effects and their intricate nature.

However, these effects may provide a way to distinguish between the different media via the effects arising. The SOE's can enable different interactions in media to distinguish between the different degrees of freedom associated with light beams. Such systems may include metamaterials, ordered / sequential grouping of optical components used as spin, OAM filters and even as OAM sorters [2,12]. The spin, OAM filters and OAM sorters are gaining demand for possible applications in image processing, information encoding and in optical communications [3-5, 10]. The spin-mediated variation of topological charge of the optical output field in the orthogonal CP projection may prove to be an useful OAM sorter implementation. Previously, the changes in the rotational speed of the trapped particles were investigated using the SAM and IOAM [6] of the light beam. The changes in the OHE shifts in orthogonally CP projected optical output field due to SAM may help unravel novel ways for controlled manipulation of a trapped particle.

The study of the spin and orbital angular momentum intertransfer will provide insight into the fundamental properties of light and allow for a deeper understanding of the mechanical torque exchange, dependent on the AM light [11]. These effects also provide information about the strength of interaction, as to which AM dominates the fundamental effects, steering the effects closer to its dynamics. A careful investigation into the second order effects could potentially help us to understand the fundamental interactions between the three AM of the light beam and could be used for controlled manipulation of AM of the light beams and applications at nanoscale.

The chapter describes on-axis propagation of CP OV beam (symmetric) and off-axis propagation of linearly-polarized (LP) OV beam (asymmetric) through the GRIN rod system. Initially, the investigation of on-axis propagation of CP OV beams related to the creation and annihilation of topological charge (TC) of OV in orthogonal polarization projection of output optical field is discussed. This is followed by results and discussion on spin-induced orbital-Hall effect. Later, the effect of OAM of an OV beam on the SHE of light is discussed for off-axis propagation of spin-free LP OV beams. Finally, the polarization changes due propagation of LP OV beams through the GRIN system are quantified using weak measurement technique.

5.2 Spin-induced effects on OAM of light

Previously, the effect of SAM on IOAM, the spin-orbit coupling (SOC) was studied in focussing, imaging, and scattering phenomena of light [8,9]. It was demonstrated that strong focussing of Gaussian beam leads to the appearance of Z-component of electric field with donut shaped intensity profile, implying spin-to-orbital angular momentum transfer [9]. The Z- component acquired a clockwise and anti-clockwise helical phase structure for input RCP and LCP Gaussian beams respectively [9]. The LCP and RCP OV beams demonstrated a zero and doubled helical phase structure in the Z- component of the electric field. The LCP and RCP have -1 and +1 helical phases in the Z- component while the TC value of the OV beam remains unchanged in the focussing region. Cumulatively, the helical phase due to both CP's and of OV beam resulted in zero and double helical phase for LCP and RCP OV's, respectively.

Taking inspiration from the above-mentioned work, propagation of CP OV beams is investigated in relation to the inter-transfer of SAM and IOAM of the light beams in the GRIN rod system. The inclusion of helical phase to Eq. 3 (in Chapter 2), describes the propagation of OV beam in the GRIN rod. The output for on-axis propagation of CP OV beam through the GRIN rod is expressed as:

$$\tilde{E} = \sqrt{\cos(\theta)} \ \hat{U} E_{i}$$

$$E_{o} = \frac{A(\theta_{c})}{\sqrt{\cos \theta_{c}}} \begin{bmatrix} a & -be^{-i2\varphi} \\ -be^{i2\varphi} & a \end{bmatrix} \begin{bmatrix} E_{ri}e^{il\varphi} \\ E_{li}e^{il\varphi} \end{bmatrix}$$

$$= \frac{A(\theta_{c})}{\sqrt{\cos \theta_{c}}} \left\{ E_{ri} \begin{bmatrix} ae^{il\varphi} \\ -be^{i(2+l)\varphi} \end{bmatrix}_{R} + E_{li} \begin{bmatrix} -be^{i(-2+l)\varphi} \\ ae^{il\varphi} \end{bmatrix}_{L} \right\}$$
(1)

Where $E_{ri}e^{il\varphi}$ and $E_{li}e^{il\varphi}$ are incident RCP and LCP optical vortex beams with topological charge l which can be positive or negative. Let us now consider the propagation of RCP OV beam with different topological charges l:

RCP $LG_0^l(l=1,2,3)$:

$$E_{o} = \frac{A(\theta_{c})}{\sqrt{\cos \theta_{c}}} E_{ri} \begin{bmatrix} ae^{il\varphi} \\ -be^{i(2+l)\varphi} \end{bmatrix}$$

$$= \frac{A(\theta_{c})}{\sqrt{\cos \theta_{c}}} E_{ri} \left\{ \begin{bmatrix} ae^{i\varphi} \\ -be^{i3\varphi} \end{bmatrix}^{1}, \begin{bmatrix} ae^{i2\varphi} \\ -be^{i4\varphi} \end{bmatrix}^{2}, \begin{bmatrix} ae^{i3\varphi} \\ -be^{i5\varphi} \end{bmatrix}^{3} \right\}$$
(2)

In this equation the output optical field for different topological charge is separated by commas, superscripts for square bracket denote the incident topological charge, the top and bottom row represent RCP and LCP, respectively. From Eq (2), we see that the optical output consists of both RCP and LCP components with varying topological charge determined by the SOI. The output RCP beam retains incident topological charge value while the TC value of the output LCP beam changes incrementally. The TC of LCP transform to or take +3,+4,+5 values for incident RCP OV beam with +1,+2,+3 TC values, respectively.

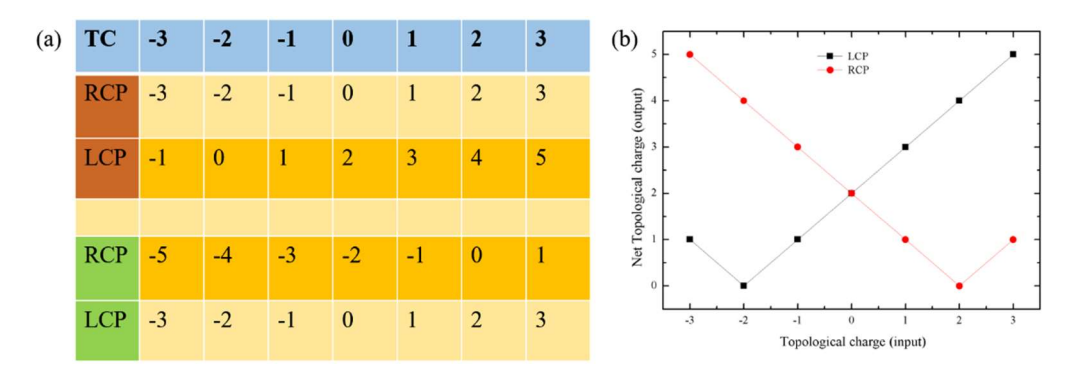


Figure 1. Theoretically calculated (a) effective and (b) net TC values for the on-axis propagation of input RCP and LCP OV beams with different TC values through the GRIN rod. The opposite direction of red and black lines represents positive and negative phases of constituent OV beams. The flip at -2 and +2 signify the phase flip in the output optical field. The red and green colours represent incident RCP and LCP of the OV beam. The orange colour highlighted strips indicate orthogonal polarization projection resulting in the modulation of effective TC of the OV beam.

RCP LG₀^l
$$(l = -1, -2, -3)$$
:

$$E_{o} = \frac{A(\theta_{c})}{\sqrt{\cos \theta_{c}}} E_{ri} \left\{ \begin{bmatrix} ae^{-i\varphi} \\ -be^{i\varphi} \end{bmatrix}^{-1}, \begin{bmatrix} ae^{-i2\varphi} \\ -b \end{bmatrix}^{-2}, \begin{bmatrix} ae^{-i3\varphi} \\ -be^{-i\varphi} \end{bmatrix}^{-3} \right\}$$
(3)

As the helical phase (l=-) and circular polarization $(\sigma=+)$ of the input beam are in opposite directions, the phase structure of the output LCP beam changes significantly compared to the previous case. The incident RCP LG_0^l beam (-1, -2, -3) results in 1, 0, -1 TC of the output LCP beam, respectively. The propagation of circular polarized LG_0^l beams result in algebraic addition and subtraction of topological charges for orthogonal CP output beam.

Changing the polarization to LCP, the incident LCP LG_0^l beam with topological charges -3, -2, -1, 1, 2, 3 modify the TC values of the output RCP beams to -5, -4, -3, -1, 0, 1 respectively. As a general rule of thumb, if the product of TC and SAM value of the input beam, $l\sigma > 0$, the net TC value of orthogonal CP projected output beam increases and decreases if $l\sigma < 0$. The changes in the TC values are manifested in the spatial intensity structure of the output beams (Fig. 2). It will nevertheless be interesting to study the fractional charged optical vortices in this context.

5.2.1 Experimental results and discussion

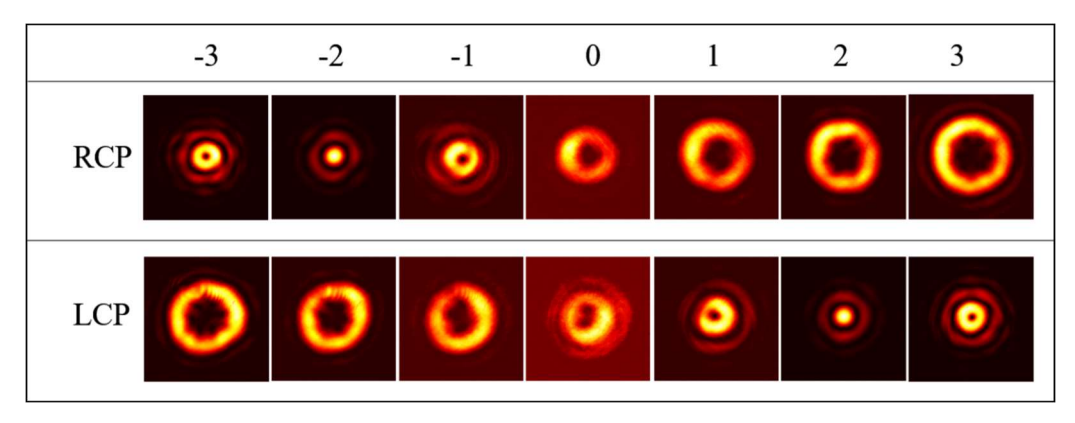


Figure 2. Experimentally measured orthogonal circular polarization projection of output optical field for incident RCP (top row) and LCP (bottom row) LG beams (intensity) for different topological charges (-3:1:+3). The topological charge values of the input CP OV beams are mentioned at the top.

The influence of SAM on IOAM resulting in the SOC is being implemented using the experimental schematic discussed in Chapter 2. The output optical field is passed through the polarization analyser (QWP and GT polarizer) for orthogonal circular polarization projection. The changes in the TC value of the output after the polarization analyser is observed in the spatial intensity structure with size increase / decrease. The overall effect seems to be of creation and annihilation of TC of the incident OV beam. Typical OAM sorters rely on the phase profile structures independent of polarization. The coupling of SAM and IOAM in the GRIN rod system offers a unique way to control the IOAM of the beam with SAM albeit in the orthogonal CP projection. A new type of OAM and polarization sorter can be designed using the above analysis in systems which exhibit SOC. Wherein the output field can be controlled by the product $l\sigma$. The conditionality of $l\sigma$ can be tailored as per the requirement to allow a specific polarization or spatial intensity structure. This type of filters can be employed in an optical fiber, to filter leaky modes having an orthogonal polarization. Wherein not only the polarization but the spatial mode specific to that polarization also is filtered.

The topological charge value of the input beams is given at the top in Fig. 2. RCP and LCP in Fig. 2 indicate the input CP, while the spatial intensity structures in the row represent orthogonal CP projections. A comparison of the output optical fields for RCP and LCP input beam with same TC is quite significant. The modifications in the TC value of the output for input polarization are given in a table [Fig. 1].

5.3 Spin-mediated orbital-Hall effect of light

Taking a closer look at the propagation of CP OV beam through the GRIN rod system, the net TC value of orthogonal CP projected output beam determines the spatial intensity structure changes associated with spin-induced orbital-Hall effect of light (SOHEL). This implies that net OAM value affects both the onaxis and off-axis propagation through the system. The total shift due orbital-Hall effect depends on the incident CP OV beam properties, the topological charge, and helicity values. The off-axis propagation of CP OV through the GRIN rod results in both SHE and OHE, which can be retrieved depending on how the optical output field is measured. Making the necessary changes to incorporate both SAM and IOAM values, the variable β is modified as $\beta = 2(l+l_{\sigma})\alpha/k$, where l_{σ} is the OAM value of the output in the orthogonal CP projection due to SOI. The output optical field for the propagation of circularly polarized LG₀ beam through the GRIN rod is written as

$$E(x, y, z) = q_0^{l+1} \exp\left(-l \tan^{-1}(y/x)\right) \frac{(Aq_0 - C)^p}{(Aq_0 + C)^{p+l+1}} \left(\sqrt{2} \frac{\left((x - \delta_x) + (y - \delta_y)\right)}{\omega_0}\right)^l \exp\left(-ik \frac{\left((x - \delta_x)^2 + (y - \delta_y)^2\right)}{2q}\right) L_p^l \left[\frac{2\left((x - \delta_x)^2 + (y - \delta_y)^2\right)}{2\omega^2(z)}\right]$$
(4)

Where $\delta_x = \beta zy$, $\delta_y = \beta zx$ denote shift in x- and y- directions due to cumulative effect of SAM and IOAM of light. The SOHEL can be realized by filtering incident polarization content by orthogonal CP projection using a combination of QWP and GT polarizer. The net topological charge of the orthogonal spin projected output varies as discussed in the previous section and the total OHE shift value relying on the net TC value gets modified as well.

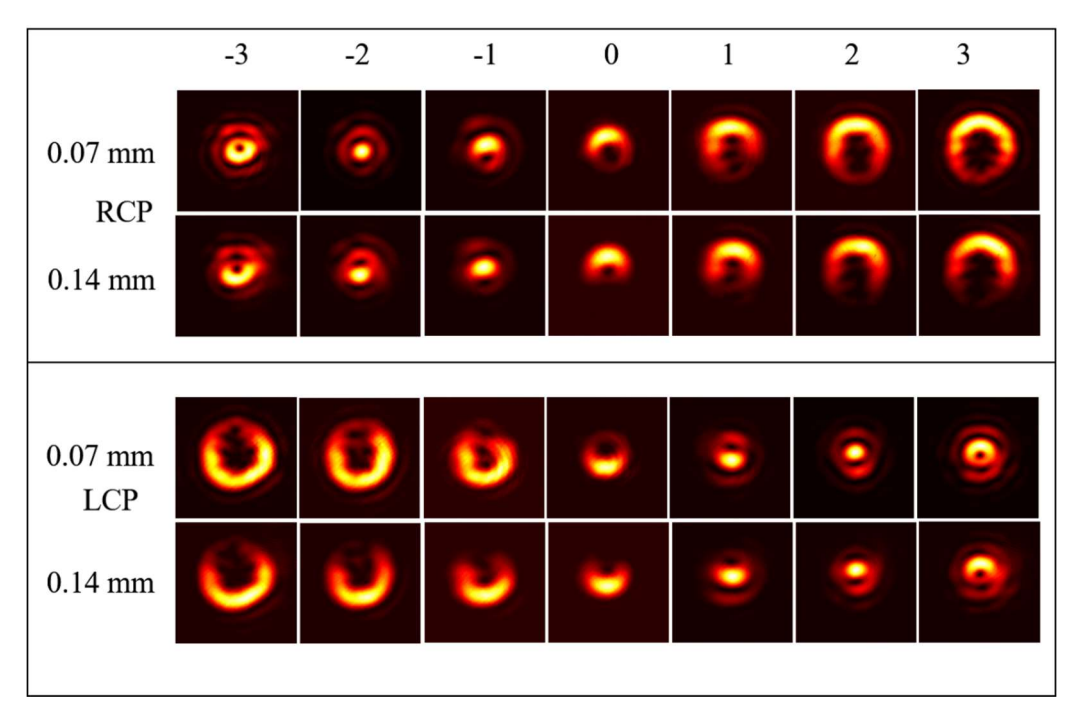


Figure 3. Experimentally measured spatial intensity structures related to SOHEL of light for incident RCP (top) and LCP (bottom) OV beam with different TC values. The topological charge values are varied as -3: +1: +3 and is indicated at the top for all the images. The RCP and LCP mentioned are input CP's, while the images correspond to orthogonal CP projections of the output optical field.

Let us now investigate the off-axis (x-) propagation of RCP LG_0^I through the GRIN rod. The output electric field can be written as

$$E(x, y, z) = q_0^{l+1} \exp\left(-l \tan^{-1}(y/x)\right) \frac{(Aq_0 - C)^p}{(Aq_0 + C)^{p+l+1}} \left(\sqrt{2} \frac{\left((x) + (y - \delta_y)\right)}{\omega_0}\right)^l \exp\left(-ik \frac{\left((x)^2 + (y - \delta_y)^2\right)}{2q}\right) L_p^l \left[\frac{2\left((x)^2 + (y - \delta_y)^2\right)}{2\omega^2(z)}\right]$$
(5)

The variation in the SOHEL shift $\delta_y = (2(l+l_\sigma)\alpha/k)zx$ for different incident RCP topological charges is similar to that shown in the previous section. As the TC of the input RCP LG_0^l is varied as -3, -2, -1, 0, 1, 2, 3, the resulting OHE shift values appear as -1, 0, 1, 2, 3, 4, 5 TC of the beam and vice-versa for LCP LG_0^l beams. At the exit plane of the GRIN rod the output beam refracts and results in

an increased beam shift. The deflected output beam propagates at angle with respect to the YZ plane and the angle of deviation is defined as $\theta(y_0) = \frac{\delta_x(y_0)}{z_g}$ with z_g being the length of GRIN rod.

5.3.1 Experimental results and discussion

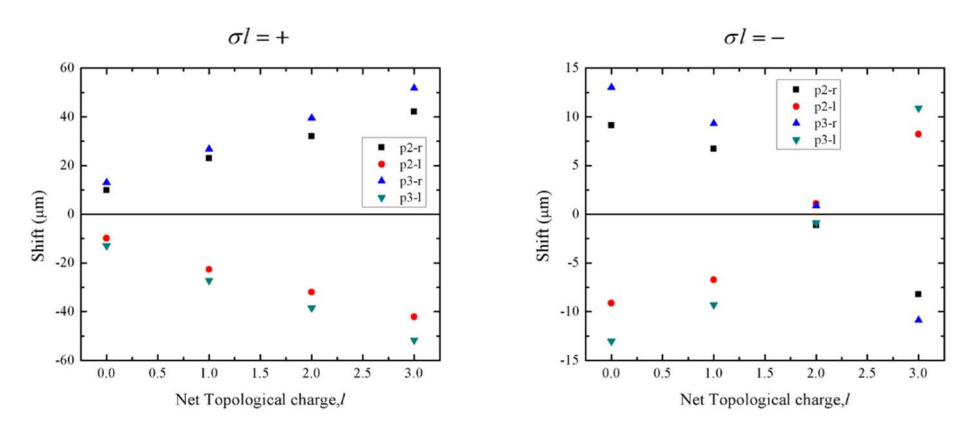


Figure 4. Experimentally measured SOHEL, for off-axis propagation of CP OV beam through the GRIN rod as a function of topological charge.

The transverse beam shift associated with SOHEL is categorized into two, depending on the product of SAM and OAM values, $l\sigma$, with $l\sigma < 0$ or $l\sigma > 0$. The experimentally measured output images are shown in Fig. 3, where RCP, LCP are input beam polarization while the adjacent row of images are for orthogonal CP projections. The TC value of the input beam and its input position is mentioned at the top and left of images.

The spin-induced OH shifts are calculated from the captured images (of Fig 3) and are given in Fig 4. The shifts are plotted as per ($l\sigma$) categorization. Unlike the SHE, the OHE and SOHEL associated shifts are easily noticeable to naked eye and the observed shift values confirm this. From a comparison of the shift values of SHE and OHE, it appears that OAM related effects are dominant here. But the interaction of both SAM and OAM in the GRIN rod system changes the dynamics of the effect significantly. A smallest change in the polarization of the input beam changes the shift dramatically due to multiplying effect of the OAM of the light beam. The extreme case of polarization change, such as RCP to LCP can possibly function as a switch parameter in optical circuits. Not only the polarization, but the ellipticity and orientation also possibly play crucial role in such processes. If the analyser is rotated in both direction by tiny angle, one can

possibly extract the orientation values of the polarization ellipse. A QWP rotation reveals the ellipticity of the output beam. More importantly, any rotation of the QWP or the GT analyser leads to a shift of the CoI attributed to the polarization ellipticity or orientation of the SoP in the beam. The extracted information can in addition reveal the refractive index value or its changes and thus can be extended to study the material properties optically in a non-intrusive way. Even a change in the input orientation or ellipticity or the TC value can be understood by either fixing the QWP and GT analyser angle using the shift or by rotation to get null optical output. Small changes in the polarization ellipse can also be measured using this system. If an interferometer is constructed, with the control of orientation and ellipticity in the reference arm. The interference pattern (either null interference intensity changes or interference fringe shift) could reveal both changes and can be used to relate the shift, and consequently can be associated with changes in material property. Prior calibration of ellipticity and orientation of polarization ellipse by SOHE shift can help one to measure the material properties for different input positions or different materials or in different configuration for the same material.

The other degree of freedom in the system is the TC value of the input beam OAM. Fixing the input polarization, a controllable change in the TC value can be used study the fundamental properties of light in relation to the material properties. A flip in the TC form + to – can possibly achieve an optical switch functionality. Even, a small change in the TC value by 0.1 in a sequential step can help us to understand the effect of TC on polarization, orientation and ellipticity of the output beam in GRIN rod system.

A change in the input off-axis position from x-axis (+) to x-axis (-) leads to a reversal of all the effects due π phase change associated with directionality. All the effects flip the direction from y (+) to y (-) as though the polarization or TC sign is changed from RCP to LCP or + to – TC of the OV for a given position.

5.4 Influence of IOAM on SHE

Recently, the beam shifts associated with polarized optical vortex beam in reflection, refraction have also gained attention due to its ability to control the optical helicity [14-18]. The Fresnel reflection and refraction coefficients have been tuned in systems like graphene to modify the topological charge dependent GH and IF shift for OV beam [19,20]. The observation of both GH and IF shifts were facilitated by setting the input polarization as diagonal or anti-diagonal in the above-mentioned work [21]. Here, we probe the OAM-dependent beam shifts as a function of input position on the GRIN rod system and the topological charge of OV beam. Remarkably, the incident vertical polarization of OV beam resulted in both in-plane and out-of-plane beam shift at the output due to orbital Berry phase (OBP). The beam shifts are categorized as OAM dependent and independent. The in-plane shifts parallel to incident plane are OAM dependent and are symmetric. The out-of-plane shifts (SHE) are composed of two parts (a) polarization dependent (SHE) (b) OAM dependent (SOHEL). The combination of both shifts results in asymmetric spin-Hall shift. The polarization of the OV beam during propagation changes to elliptical polarization and for input elliptical polarization results in asymmetric spin-Hall shifts [22].

The propagation of polarized OV beam through the GRIN rod system offers a unique opportunity to study the underlying dynamics related to weak anisotropy in relation to SOI, OOI and the coupled effects. The source of anisotropy can be material properties or the OV beam structure. The anisotropic OV beams are referred to as non-canonical OV's due to asymmetry in the core shape in the spatial intensity structure. The asymmetry in the OV can be due to both amplitude and phase structure, with phase being the prominent one. A symmetric polarized OV beam upon entering the GRIN rod input face undergoes changes in its phase structure. The OV beam experiences different refractive indices along X and Y directions respectively due to weak anisotropy of the GRIN rod. Under the sufficient conditions such as the length of the GRIN rod and input beam position, the weak anisotropy results in OHE due to OBP. The interaction of the OV's azimuthal phase gradient and the position dependent radial gradient of the GRIN rod results in the mentioned effects due to the OOI of light.

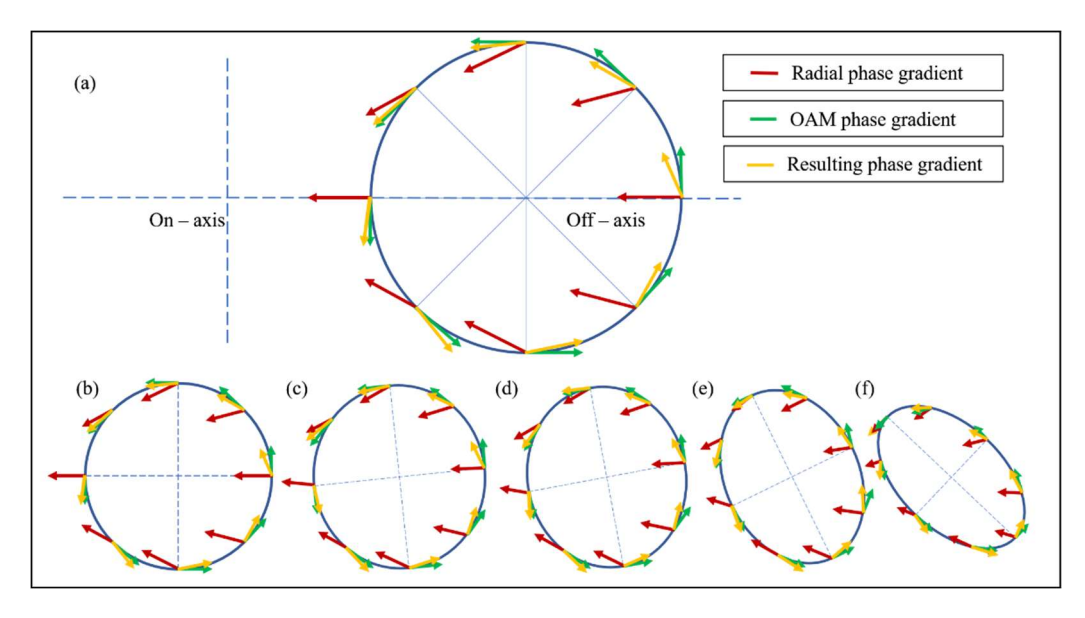


Figure 5. Transformation of OV beam's azimuthal phase gradient for an input off-axis launch position at different propagation planes in the GRIN rod. (a) Off-axis launching of OV beam, (b) -(f) Variation in the phase gradient of OV beam due to weak anisotropy of the GRIN rod at different z – planes along the propagation direction. Note: the images correspond only to phase gradients.

During the propagation of OV, the resulting phase structure of the OV beam gets distorted due to the effect of refractive index gradient. The interaction between b phase gradients results in elliptical phase structure for the OV beam as shown in the Fig. 5. The azimuthal phase gradient for an off-axis position is shown in Fig. 5 (a). The images in Fig. 5 (b-f) correspond to OV beam's phase structure at different z-planes in the GRIN rod along the propagation direction. The transformation of the symmetric azimuthal phase gradient to asymmetric elliptical phase gradient is depicted in Fig. 5 (b-f). The asymmetric phase structure of the OV beam in-turn leads to asymmetric elliptical spatial intensity structure of the OV beam [23,24]. The rotational aspect of the azimuthal phase gradient of OV beam results in the rotation of elliptical OV beam [25,26]. The rotation of output spatial intensity and ellipticity effects of the OV beam are counterpart to SAM associated effect (accumulation of geometric Berry phase due to helical trajectory) as discussed in Chapter 3.

The off-axis (X-) propagation of CP Gaussian beam results in spin-Hall shift, a spin-dependent transverse shift (Y-) of the output beam. A general off-axis (X & Y) propagation leads to rotation of output spatial intensity structure with spin-Hall shift in both directions [27]. The propagation of OV beams through the

GRIN rod also results in the OHE – a topological charge dependent transverse shift in OV trajectory and reciprocal OHE – rotation of the spatial output intensity structure due to orbital Berry phase. The orbital-Hall shift increases with TC value and can flip the direction with the change of TC sign (+ to -). The propagation of CP OV beam with OAM leads to an increase in the SHE because of TC and rotation of output intensity, indicating the spin-Hall shift along both directions.

From the above discussion, it can be inferred that the general off-axis (X & Y) propagation of CP Gaussian beam appears to be analogous to off-axis (X) propagation of OV beam in the GRIN rod system in relation to the output beam rotational characteristics. Thus, the restriction of strict transverse directional SHE is lifted by the OV beam bringing along in-plane shift components leading to SHE in both X and Y directions – implications of rotated output spatial intensity structure due to OAM. The direction of general SHE is dependent on the input position at GRIN rod, topological charge and input polarization of the OV beam.

5.4.1 Experimental results and discussion

The effect of OAM on SHE will be discussed in this section. The incident beam is pre-selected in vertical polarization and the corresponding spin-Hall shifts are measured employing weak measurement technique, by performing quasi-orthogonal post-selection of weakly interacted output using a combination of QWP and GT polarizer.

To understand the dynamics of the OAM on the SHE, the center of intensity (CoI) as a function of analyser rotation angle are plotted on the crossing angle (quasi-orthogonal polarization) image for different OV charge and input beam position. The crossing angle images are arranged as a function of input position and TC of the OV beam as shown in the Fig. 6. The white dots on the images are the CoI for analyser angle rotation. The behaviour of the CoI's reveal the rotational motion of the polarized OV beam in the GRIN rod. All the CoI's on an image can be considered as dot-strip. The shape of the dot-strip is elliptical with different orientations for different input positions and TC of the OV beam. The size of the dot-strip increases as a function of input position, implying an increase in the weak anisotropy experienced by the OV beam affecting its phase structure and the resulting modal intensity structure. The sense of rotation of the dot-strip is clockwise and counter-clockwise respectively for – and + TC values of the input OV beam. The rotation value of the dot-strip for – and + TC values are unequal, and this effect can be associated with the curvature of path taken by the light beam inside the GRIN rod.

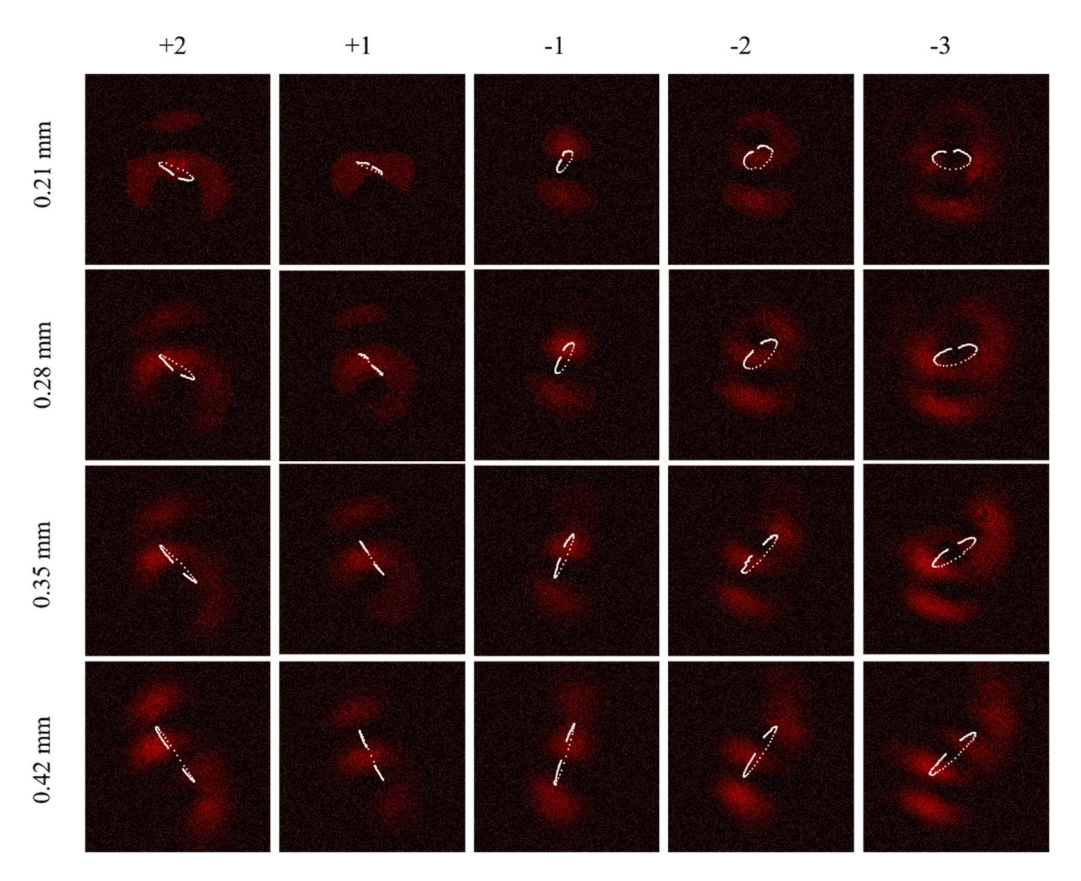


Figure 6. Experimentally measured output optical fields at crossing angle for different TC's of input OV beam at various input positions. The input positions and TC of the OV beam are mentioned to left and top of the image, respectively. The white dotted strip represent the CoI's mapped on crossing angle image for analyser angle rotation.

The curvature of the path is determined by the evolution of CoI of the OV beam through the GRIN rod. The curvature can be + or – depending on the deviation with respect to the Z-axis. The curvature is + for counter-clockwise deviation of CoI in the XZ plane with respect to Z-axis and vice-versa. The curvature of the path induces asymmetry in the rotation values of the quasi-orthogonal projected output optical field. The spin dependent transverse (lateral/out of plane) shift of the CoI's for polarized Gaussian beam is transformed to spin dependent rotational shift with lateral (out-of-plane) and longitudinal (in-plane) shifts for LP OV beam. The orientation of the CoI's plotted on crossing angle images imply complex polarization structure of the output optical field.

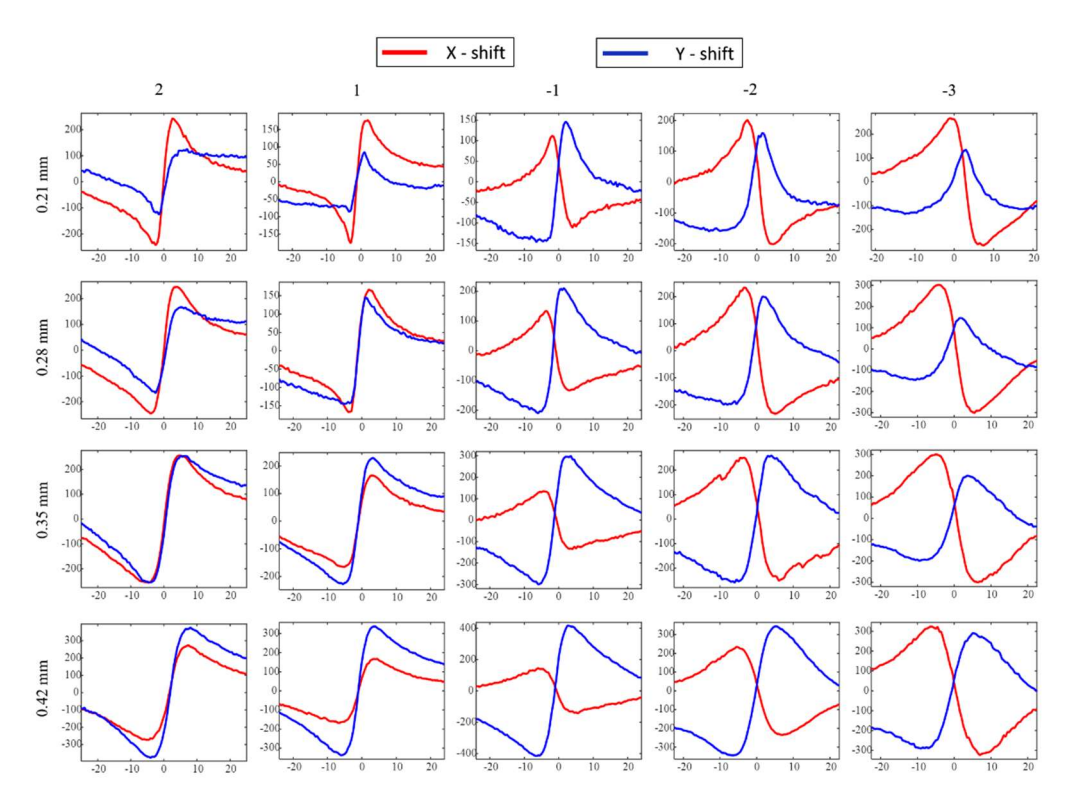


Figure 7. Experimentally measured X and Y shifts for different TC values of incident OV beam as a function of input position.

Further, the general shift of the output optical field is divided into X- and Y-shifts. The images are arranged for different input position and TC values of the input OV beam as shown in Fig. 7. Both X- and Y- shifts are plotted for an input position and TC of OV beam, red colour and blue colour shift curves are associated with X- and Y- shifts, respectively. The origin of X shift is of purely OAM phase and is symmetric for all the input positions and TC values. Similar to asymmetry in the rotational values of dot strip, the X- shift values are unequal for + and – TC values of the input OV beam. The X- shifts for OV beam with + TC value is greater than the shifts for the OV's with – TC values. The source of this asymmetry is related to the curvature of the path inside the GRIN rod. The X shift increases as a function of input beam position and TC values.

The in-plane shifts (longitudinal, -X-) shifts at the input position (0.21 mm) for different TC's are greater than the out-of-plane (transverse, Y-) shifts except for -1 TC. It is also interesting to note that the X shift corresponding to -1 TC value is always lesser than the Y- shift for all input positions. The Y- shifts always increase with the increase in the input off-axis position. The X- and Y- shifts

always increase with the increase in the TC value of the OV beam. The X- shift is caused by the OBP of the OV beam and is corroborated by the flip of the X-shift curve with the change of TC sign. The general shift is oriented along the orientation of CoI's for TC value and input position. The general shift increases with TC value and input position with exceptions for OV beam with -3 and -2 TC value at input positions 0.28, 0.35 mm and 0.42 mm, respectively.

Unlike the X- shift, the behaviour of the Y- shift is quite different with asymmetry. The Y- shift value increases for the OV beams with + TC values and decreases for – TC values. The asymmetry in not only in the shift values for + and – TC values but also in the behaviour for + and – TC values of the OV beam. The shape of the curves representing the Y- shift are asymmetric, implying that the interaction of all three AM – the SAM, IOAM and EOAM degrees of freedom of light in the GRIN rod plays a role. The transverse Y- shift can be divided into two parts: a) OAM dependent and b) SAM dependent. Though they are OAM and SAM dependent, they are also affected by SAM - EOAM and OBP - EOAM pairs, respectively. The OAM dependent shift is termed as general spin-induced orbital-Hall effect (SOHEL) while the SAM dependent shift is the SHE. These shifts arise due to coupling between SAM, IOAM, EOAM degrees of freedom of light. The Y- shifts as a function of OV's TC value and input position is shown in Fig. 8. The red colour curves represent the Y- shifts while the blue and green colour curves depict the SHE and general SOHEL. The Y- shift curves are experimental while the SHE and general SOHEL are extracted values. The asymmetry in the Y- shifts can be attributed to the general SOHEL. The SOHEL shift values were subtracted from the Y- shift values to extract the symmetric SHE curves. The general SOHEL value increases as TC value increase as can be seen in Fig. 8. It is interesting to note that the general SOHEL flips for +1 OV beam with the change in input position as seen in Fig. 8. The overall asymmetry in the Y- shift curves decrease with the increase of input position.

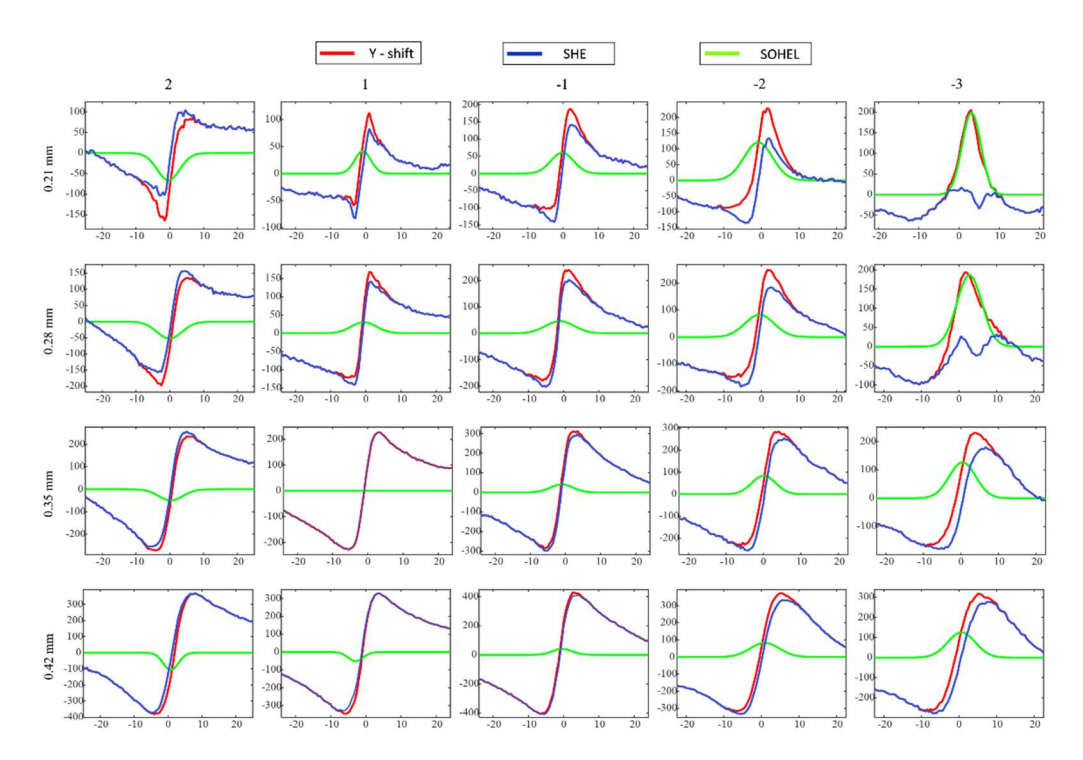


Figure 8. Experimentally measured Y shift curves and the extracted SHE and SOHEL for different TC values of incident OV beam as a function of input position.

Again, the Y- shift values are asymmetric for + and – TC values due to the curvature of the path of CoI of the input polarized OV beam. Apart from TC dependent asymmetry, there exists an asymmetry in the shift curve which depends on the input position and the TC value of the input OV beam. The presence of general SOHEL for different analyser angles indicate weak ellipticity, orientation induced orbital-Hall shifts for quasi-orthogonal polarization projection of output optical field. The results discussed in Section 5.3 represents the SOHEL as a special case of this general SOHEL, observed with the QWP and analyser positioned at crossing angles, maximising the SOHEL. It is important to note that, the general SOHEL is analogous to the SHE but with only one circular polarization leading to the Gaussian kind of shift curve. From the above discussion, it is possible to name the shift as orbit-induced rotational SHE of light due coupling between SAM, IOAM and EOAM.

The different input positions and TC values provide the flexibility to manipulate to control the shift values and its direction. At p3 and p4 input position, the SHE (Y – lateral shift) is completely transformed to X-(longitudinal) shift. This coupling of SAM, IOAM and EOAM provides an advantage for controlling the individual degree of freedom in manipulating the

output of light. Directionality is an added advantage which may be useful for sensing the rotations or rotational sorting of photons at the nano-scale in developing nano-optical devices, links for communications.

5.5 Polarization changes due to IOAM beams

The spin-orbit interaction of light manifested as SOC, orbital-to-spin conversion (OSC), the SHE and geometric Berry phase accumulation in different media under various configurations have been extensively studied during the past two decades, owing to fundamental interest and the application such phenomena in high-resolution imaging, in optical microscopy, nano-scale optical-signal processing, particle trapping, material processing etc [28-31]. Out of the four mentioned SOI effects, the OSC (reciprocal SOC) has not received enough attention until recently when it was reported in tight focussing of cylindrical vector-vortex beams [32]. In 2018, the OSC was theoretically predicted to occur in tight focussing of spin-free linearly polarized vortex beam (LPVB) [33]. The OSC does not change the overall SAM density value of the electric field, but it is manifested as local SAM density variation in the focal region of LPVB as elliptical polarization [33]. The helical phase of LPVB induces longitudinal SAM affecting the distribution of transverse SAM density in the focal region. The distribution of local SAM density due to OSC can be tailored by varying the topological charge value, sign, and the input linear polarization angle [33]. It was theoretically and experimentally demonstrated that linearly polarized Laguerre-Gaussian beams upon scattering by spherical silicone nanoparticle exhibit an l dependent helicity density in the focal volume [33]. Further, the dipole scatterer placed at focal plane to locally manipulate the helicity density resulting in scattered light with defined circular polarization depending on the OAM of the incident light beam demonstrating the OSC [34].

Here, we demonstrate OSC effect by breaking the symmetry of the system with off-axis launching of LPVB through the GRIN rod system. The OSC is manifested as weak (S3) parameter in the output optical field. The off-axis propagation of spin-free Gaussian beam with zero OAM also results in weak (S3) parameter (RVB phase) as discussed in Chapter 3. Here, we experimentally demonstrate that the off-axis propagation of spin-free OV beam with non-zero OAM results in the *l*-dependent weak (S3) parameter. This weak S3 parameter is a sum of contributions from IOAM and EOAM degrees of freedom of light which are coupled to the SAM. The coupling between the SAM and OAM of OV beam is first established by weak (S3) parameter for different TC, depicting the effect of OAM on the SHE as shown in Fig. 9. Figure 9 also reveals the coupling

between SAM, IOAM and EOAM degrees of freedom of light when analysed as a function of TC and off-axis position.

5.5.1 Experimental results and discussion

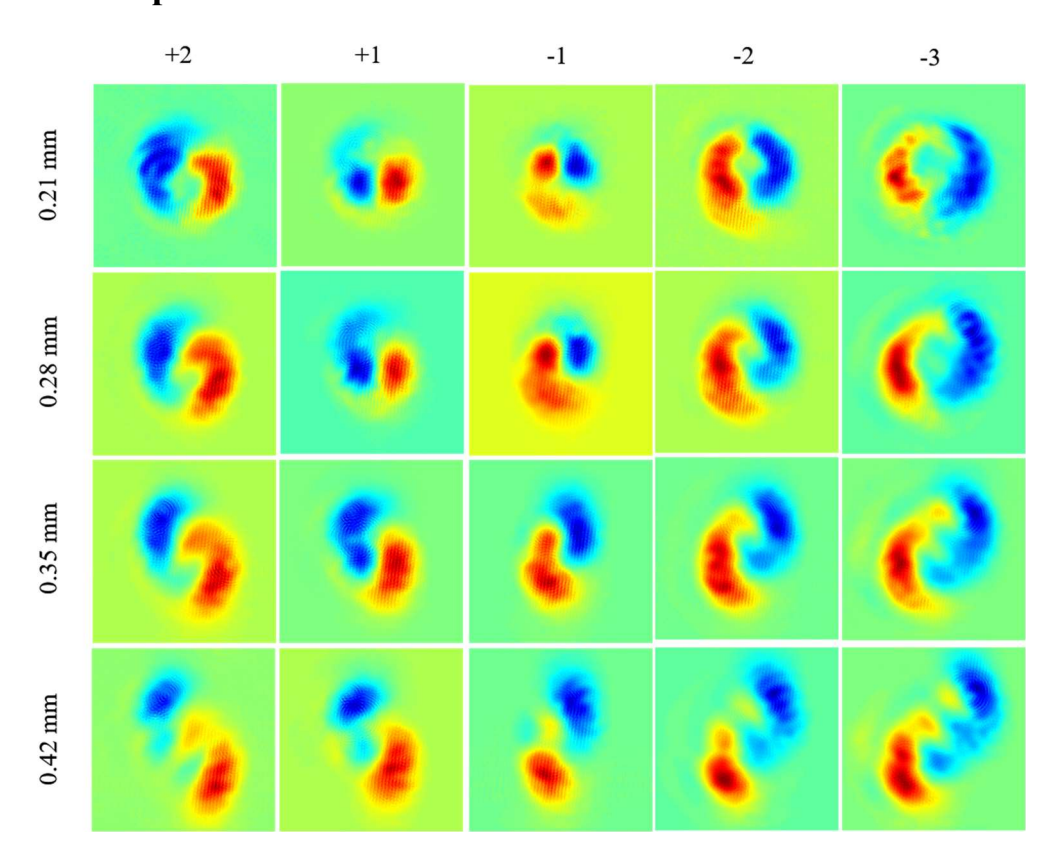


Figure 9. Experimentally measured weak S3 parameter for different input positions as a function of topological charge. The topological charge and input position are mentioned at the top and left of the image, respectively.

The weak S3 parameter extracted for different TC values at different off-axis input position are shown in Fig. 9. The position and TC values are mentioned at left and top of the images. Let us consider the weak S3 parameter for input position 0.21 mm for various TC values. The polarization changes associated with the OAM beams is manifested as changes in the spatial intensity structure for the weak S3 parameter. The flip in the weak S3 parameter for TC sign change confirms the coupling between the SAM and OAM of incident spin-free OV beam. Apart from the flipping, the intensity images also reveal circulation of optical fields with non-vanishing tail for different polarization indicating the

sense of circulation of optical energy circulation. The positive and negative TC's reveal counter-clockwise and clockwise circulation of optical fields. It is important to note that the transverse SHE (lateral - Y) is completely rotated by almost 90°, transforming into longitudinal shift (X-). [This rotation of transverse SHE due to OAM changes with TC value and input position.] As the input is varied from 0.21 mm to 0.28 mm, the SHE appears to be rotated by a small angle with respect TC. Further change of input position not only rotates the output field but also distorts the spatial intensity structure due to anisotropic diffraction. The input position 0.35 and 0.42 mm reveal the general SHE – SHE in both X- and Y- directions. This rotation of SHE due to IOAM and EOAM can prove to be an additional degree of freedom to control the light characteristics at nano-scale. All the images in the Fig. 9 are normalized with respect to maxima of that image weak S3 parameter.

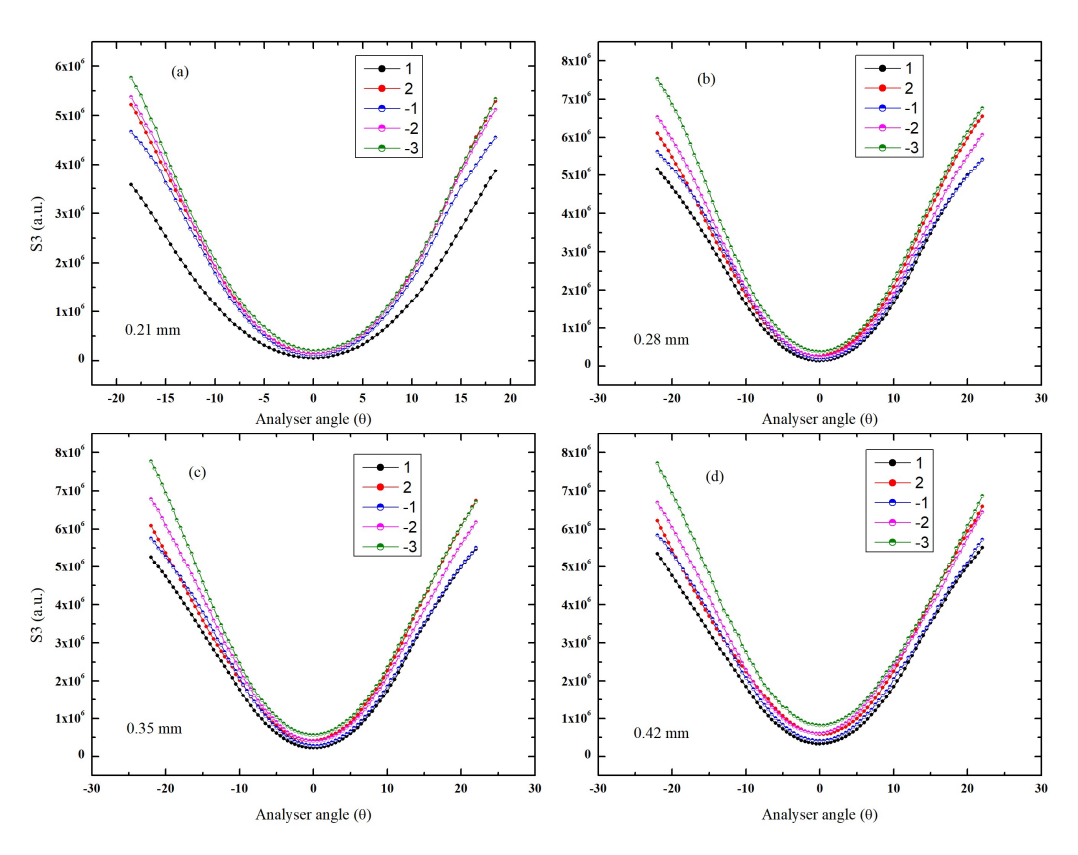


Figure 10. Experimentally measured weak S3 parameter for different input positions as a function of TC value of incident OV beam.

In the previous section, the intensity images associated with weak S3 parameter were shown and discussed. The associated weak S3 parameter as a function of input position for analyser angle variation is shown in Fig. 10. The input position is mentioned in the left bottom of each image. In line with the results previously discussed for Gaussian beam in Chapter 3, the weak S3 parameter for the OV beam increases with the increase in TC value. The curves for positive and negative TC's are asymmetric owing to curvature of CoI of the OV beam propagating in the GRIN rod. This also implies that the OSC (reciprocal SOC) of light is directly related to TC of OV beam along with the input position.

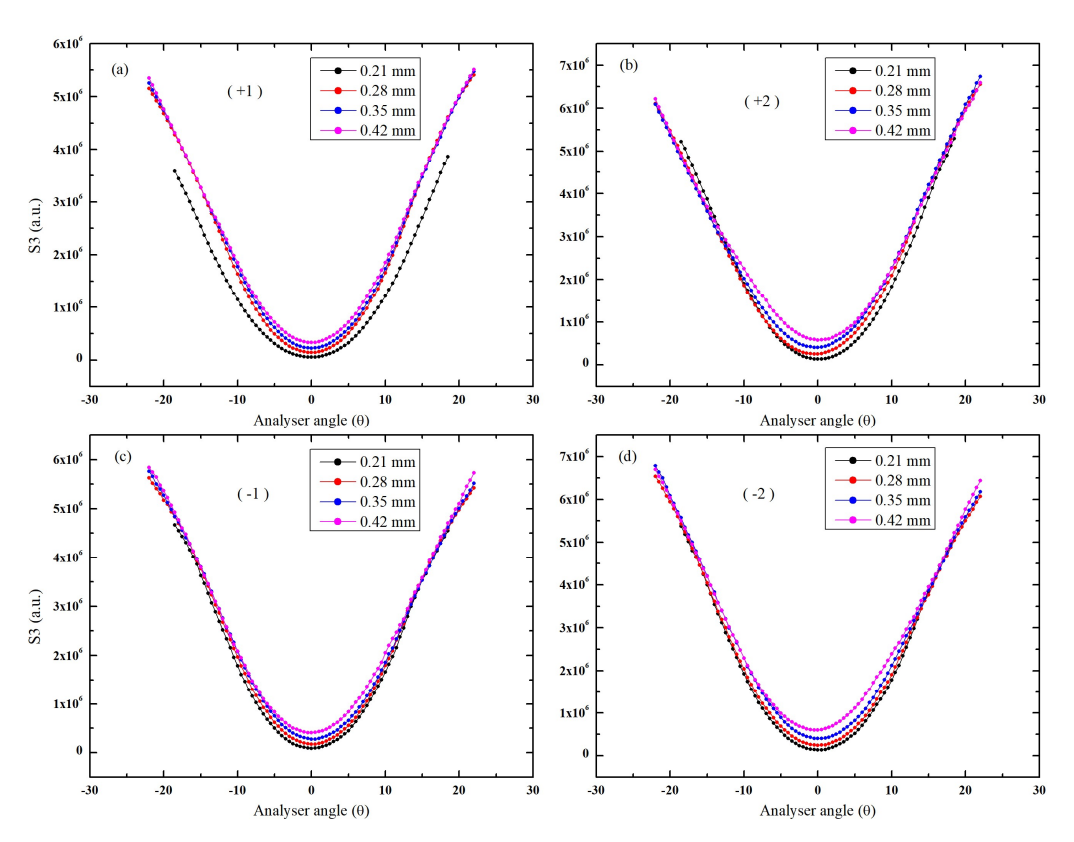


Figure 11. Experimentally measured weak S3 parameter for different TC's of incident OV beam as a function of input position.

Next, the weak S3 parameter is analysed as function of input position for each TC of the incident OV beam. The weak S3 parameter as a function of input position for different TC's of incident OV beam is shown in the Fig. 11. It is understood from the Chapter 3 (reciprocal SOC) and the Fig. 11 that the weak S3 parameter increases as a function of input position. The curves depict clear weak S3 parameter separation for different input positions.

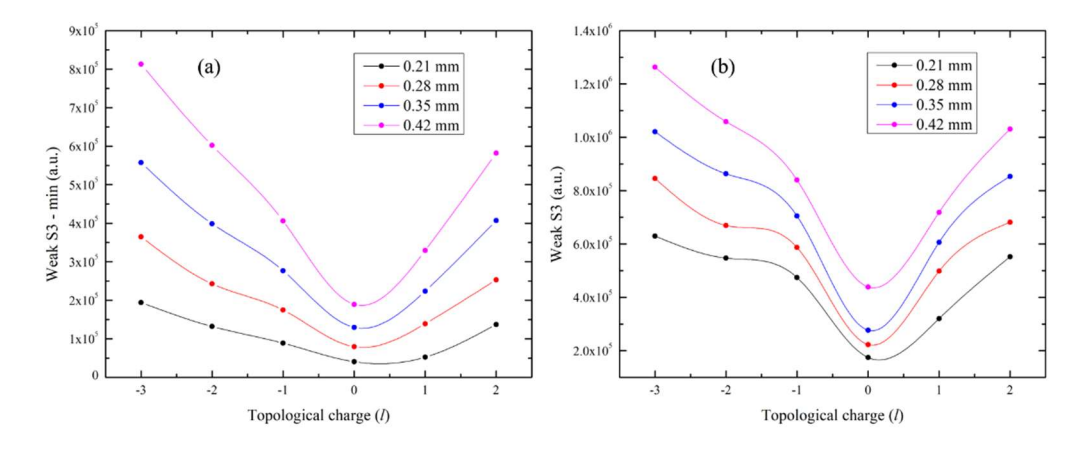


Figure 12. Asymmetry in the a) weak S3 minima at quasi-orthogonal analyser angle and b) weak S3 calculated for $\pm 5^{\circ}$ analyser angle for different input position as a function of TC's for the incident linearly polarized OV beam.

The crossing angle for the Gaussian beam at different off-axis input positions is used as reference during measurement process, for analysing the data related to OV beams. Apart from the asymmetry in Y- shift, it also exhibits asymmetry in the weak S3 parameter value. The weak S3 minima at quasi-orthogonal analyser angle and weak S3 parameter at $\pm 5^{\circ}$ of analyser angle is shown in the Fig. 12 (a) and (b), respectively, for different input position. It is to be noted that the nature of asymmetry for both the weak S3 minima and S3 ($\pm 5^{\circ}$) reveal same behaviour.

5.6 Summary

In this Chapter we investigated second-order effects associated with the mutual interaction of SAM, IOAM and EOAM degrees of freedom of light in a GRIN rod system. Initially the spin-induced modulation of OAM of light for on-axis propagation of CP OV beam is studied for different TC. It was experimentally shown that the effective OAM of light in orthogonal polarization projection of the output optical field is modified by changing the polarization of the incident OV beam. The introduction of asymmetry through off-axis launching of CP OV beam, results in spin-induced orbital-Hall effect of light (SOHEL), the effective change in shift value is similar to the case of effective change in OAM value for on-axis launching. Later, the effect of OAM on the SHE and polarization of the output optical field were investigated. The transverse SHE is modified into general SHE with shift in both X- and Y- directions. Apart from this the Y- shift is asymmetric due to contributions from the general SOHEL. The asymmetry is also exhibited in the X- and Y- shift values. In the case polarization, the spin-free linearly polarized OV beam resulted in OSC (reciprocal SOC) and is dependent on both the input TC value and position of LP OV beam. The OSC was realized through measurement of weak (S3) Stokes parameter. The weak (S3) Stokes parameter also displayed asymmetry for + and – TC values. All the asymmetries in the mentioned effects can be attributed to the optical beam's trajectory curvature. The sense of curvature taken by the incident beam through the GRIN rod modifies the contribution of + and – TC OV beams in general SHE and OSC.

The above dynamics further our understanding related to coupled interaction of the different AM degrees of freedom of light in inhomogeneous weakly anisotropic media which can be extended to other media as well. The overall understanding of the 3 DoF's of light in relation to coupled interactions may find applications in designing nano-optical devices, OAM sorting, optical signal processing, optical communications, optical links, optical trapping etc.

References:

- Sadykov, Nail Rakhmatullovich. "Polarization effects due to the mutual influence of trajectory parameters and polarization." *Theoretical and mathematical physics* 149.1 (2006): 1354-1365.
- Wen, Yuanhui, et al. "Monolithic integrated optical vortex sorter based on cascaded metasurface structures." 2017 Asia Communications and Photonics Conference (ACP). IEEE, 2017.
- 3. L. Torner, J. Torres, and S. Carrasco, "Digital spiral imaging," Opt. Express 13(3), 873–881 (2005).
- 4. S. R. P. Pavani and R. Piestun, "Three-dimensional tracking of fluorescent microparticles using a photon-limited double-helix response system," Opt. Express 16(26), 22048–22057 (2008).
- 5. A. Jesacher, M. Ritsch-Marte, and R. Piestun, "Three-dimensional information from two-dimensional scans: a scanning microscope with post acquisition refocusing capability," Optica 2(3), 210–214 (2015).
- 6. Y. Arita, M. Mazilu, and K. Dholakia, "Laser-induced rotation and cooling of a trapped microgyroscope in vacuum," Nat. Commun. 4, 2374 (2013).
- 7. Rodríguez-Herrera, Oscar G., et al. "Optical nanoprobing via spin-orbit interaction of light." Physical review letters 104.25 (2010): 253601.
- 8. Bliokh, Konstantin Y., et al. "Spin-to-orbital angular momentum conversion in focusing, scattering, and imaging systems." *Optics express* 19.27 (2011): 26132-26149.
- 9. Zhao, Yiqiong, et al. "Spin-to-orbital angular momentum conversion in a strongly focused optical beam." Physical Review Letters 99.7 (2007): 073901.
- 10. Willner, Alan E., et al. "Optical communications using orbital angular momentum beams." Advances in Optics and Photonics 7.1 (2015): 66-106.
- 11. O'neil, A. T., et al. "Intrinsic and extrinsic nature of the orbital angular momentum of a light beam." *Physical review letters* 88.5 (2002): 053601.
- 12. Ke, Yougang, et al. "Photonic spin filter with dielectric metasurfaces." *Optics express* 23.26 (2015): 33079-33086.
- 13. Shao, Zengkai, et al. "Spin-orbit interaction of light induced by transverse spin angular momentum engineering." *Nature communications* 9.1 (2018): 1-11.
- 14. K. Y. Bliokh and A. Aiello, "Goos-Hänchen and Imbert-Fedorov beam shifts: an overview," J. Opt. 15, 014001 (2013).
- 15. K. Y. Bliokh, I. V. Shadrivov, and Y. S. Kivshar, "Goos-Hänchen and Imbert-Fedorov shifts of polarized vortex beams," Opt. Lett. 34, 389–391 (2009).
- 16. M. Merano, N. Hermosa, J. P. Woerdman, and A. Aiello, "How orbital angular momentum affects beam shifts in optical reflection," Phys. Rev. A 82, 023817 (2010).
- 17. W. Löffler, A. Aiello, and J. P. Woerdman, "Observation of orbital angular momentum sidebands due to optical reflection," Phys. Rev. Lett. 109, 113602 (2012).
- 18. M. Jiang, W. Zhu, H. Guan, J. Yu, H. Lu, J. Tan, J. Zhang, and Z. Chen, "Giant spin splitting induced by orbital angular momentum in an epsilon-near-zero metamaterial slab," Opt. Lett. 42, 3259–3262 (2017).
- 19. L. Zhuo, W. Long, M. Jiang, W. Zhu, H. Guan, J. Tang, J. Yu, H. Lu, J. Zhang, and Z. Chen, "Graphene-based tunable Imbert-Fedorov shifts and orbital angular momentum sidebands for reflected vortex beams in the terahertz region," Opt. Lett. 43, 2823–2826 (2018).

- 20. W. Zhu, M. Jiang, H. Guan, J. Yu, H. Lu, J. Zhang, and Z. Chen, "Tunable spin splitting of Laguerre-Gaussian beams in graphene metamaterials," Photon. Res. 5, 684–688 (2017).
- 21. Long, Wenjin, et al. "Optimized weak measurement of orbital angular momentum-induced beam shifts in optical reflection." *Photonics Research* 7.11 (2019): 1273-1278.
- 22. Zhou, Xinxing, and Xiaohui Ling. "Unveiling the photonic spin Hall effect with asymmetric spin-dependent splitting." *Optics express* 24.3 (2016): 3025-3036.
- 23. Liang, Guo, et al. "Anisotropic diffraction induced by orbital angular momentum during propagations of optical beams." Optics express 26.7 (2018): 8084-8094.
- 24. Liang, Guo, and Wenjing Cheng. "Splitting and rotating of optical vortices due to non-circular symmetry in amplitude and phase distributions of host beams." Physics Letters A 384.2 (2020): 126046.
- 25. Liang, Guo, Wenjing Cheng, and Qing Wang. "Rotations of elliptic vortex beams in media with and without anisotropy." Journal of Optics 21.3 (2019): 035607.
- 26. Liang, Guo, Tingjian Jia, and Zhanmei Ren. "Controllable rotations of spiraling elliptic beams in anisotropic linear media." IEEE Photonics Journal 9.5 (2017): 1-8.
- 27. Li, Hehe, et al. "Changes of phase structure of a paraxial beam due to spin-orbit coupling." Physical Review A 97.5 (2018): 053843.
- 28. Z. Zhang, J. Pu, and X. Wang, Opt. Lett. 33, 49 (2008).
- 29. M. Friese, T. Nieminen, N. Heckenberg, and H. Rubinsztein-Dunlop, Nature 394, 348 (1998).
- 30. L. Paterson, M. MacDonald, J. Arlt, W. Sibbett, P. Bryant, and K. Dholakia, Science 292, 912 (2001).
- 31. C. Hnatovsky, V. G. Shvedov, W. Krolikowski, and A. V. Rode, Opt. Lett. 35, 3417 (2010).
- 32. Li, Manman, et al. "Orbit-induced localized spin angular momentum in strong focusing of optical vectorial vortex beams." Physical Review A 97.5 (2018): 053842.
- 33. Yu, Panpan, et al. "Orbit-induced localized spin angular momentum in the tight focusing of linearly polarized vortex beams." Optics letters 43.22 (2018): 5677-5680.
- 34. Nechayev, Sergey, et al. "Orbital-to-spin angular momentum conversion employing local helicity." Physical Review B 99.7 (2019): 075155.

6

Orbit-orbit interaction of light in two-mode optical fiber

This chapter discusses orbit-orbit interaction of light in two-mode optical fiber. The on-axis and off-axis propagation of linearly-polarized Gaussian beam is investigated with reference to spatial mode changes and the corresponding phase variations. An intuitive model for a fixed radial position with varying azimuthal off-axis launch positions for different and same polarization is provided to understand the output spatial mode behaviour. Off-axis launch of vertical linearly-polarized Gaussian beam results in HG-like output LP_{11} mode, which rotates as a function of azimuthal launch position. This rotation is understood as effected due to the OOI of light, resulting from the accumulation of orbital-Berry phase of constituent optical vortex modes of the two-mode optical fiber. Apart from rotation, the diametrically opposite launch positions result in a π phase shift between the output LP_{11} modes. A Mach-Zehnder interferometer is built to superpose the output LP_{11} with the reference Gaussian beam, for extracting the phase information. Fourier fringe analysis method is employed to extract the phase, and an autocorrelation technique is applied for finding the rotation angle of the output LP_{11} modes.

6.1 Introduction

Broadly, the angular momentum of light is categorized into two parts: a) Intrinsic – independent of the axis and b) Extrinsic – dependent on the axis. The spin angular momentum (SAM) of light does not depend on the axis (Intrinsic). It is associated with the state of polarization having the values \hbar and $-\hbar$ for RCP and LCP, respectively. The angular momentum arising from the spiral phase front of a phase singular optical vortex (OV) beam is either intrinsic or extrinsic, depending on the position of reference axis used for measurement [1]. It is generally referred to as IOAM of light with OAM value defined as $\pm l\hbar$ [2]. The extrinsic orbital angular momentum of light (EOAM) is axis dependent and related to the motion of the center of the light beam's intensity [3].

The propagation of polarized light through inhomogeneous or anisotropic or biaxial media or tight focusing in free space, couples the spin and orbit AM of light due to transversality condition [3]. The spin-orbit coupling of light leads to two mutual effects: a) the effect of trajectory (EOAM) of a light beam on the state of polarization (SAM) leads to accumulation of geometric Berry phase due to parallel transport law [4,5] b) And the influence of polarization (SAM) on the path (EOAM) of beam leads to spin-dependent transverse splitting of optical beam for RCP and LCP, resulting in SHE [3]. The spin-Hall shifts are typically of the order of wavelength, making it challenging to measure and requiring weak measurement technique to amplify the shift for measurement and subsequent analysis. The spin-redirection geometric Berry (RVB) phase was first experimentally measured for the propagation of polarized light through helically wound optical fiber around a cylinder in 1986 by Chiao and Wu [4,5]. Later, in 1992 Zel'Dovich et al. measured the optical Magnus effect (SHE) in an optical fiber (inhomogeneous media) [6].

Following the SOI terminology of light, the interaction between IOAM and EOAM of light is termed as orbit-orbit interaction (OOI) of light. The OOI of light results in the orbital-Berry phase and orbital-Hall effect of light analogous to geometric Berry phase and spin-Hall effect of light but in the modal domain [7]. The effects associated with the interaction of IOAM and EOAM have gained attention due to the fundamental nature of interaction and possible applications in optical communications, nano-photonics, imaging,etc [3]. Due to similarities between SAM and IOAM, it was predicted that the propagation of polarization independent OV beams through a helical trajectory would result in *l* dependent a) transverse rotation of optical beam due to orbital Berry phase (OBP) and b) transverse topological charge-dependent shift of OV beam, or orbital-Hall effect

of light [7]. Here, we describe the off-axis propagation of gaussian beam in a straight, torsion-free two-mode optical fiber, leading to the observation of the transverse rotation of optical output field due to the orbital-Berry phase of light.

Previously, chapters (3, 4, and 5) have focused on the on-axis and off-axis propagation of polarized Gaussian and OV beams through the GRIN rod. The off-axis launching positions were restricted to the X direction. This chapter deals with the general off-axis propagation of linearly polarized Gaussian beam in a two-mode optical fiber. The off-axis launching positions were varied azimuthally for different radial positions resulting in a mesh-like input position pattern. Here, the off-axis propagation and its associated changes in the output beams spatial structure and phase are discussed. Due to off-axis launching and propagation, the cylindrical symmetry transforms into a mix of cylindrical and rectangular symmetry. We anticipate that this breaking of rotational symmetry would impact the beams modal characteristics corresponding to the input beam position.

6.2 Theoretical formalism

Light propagation through an optical fiber can be divided into two categories, a) on-axis and b) off-axis (skewed) propagation. The propagation of light through the axis of optical fiber excites the fundamental mode. Generally, the fundamental mode is a circular symmetric Gaussian beam mode with uniform phase, symbolically depicted as LP_{01} . The amplitude and weightage of the fundamental mode in an optical fiber is determined by the input light mode, lens position, and numerical aperture (N.A). The excitation of the fundamental mode is subject to the type of input light mode illuminating the optical fiber. If the input mode is Gaussian, the fundamental mode is Gaussian, but if the optical fiber is illuminated by LG mode, the fundamental mode is LG beam as LG beams also are eigenmodes of the optical fiber.

Additionally, the position of launching plays a role in determining the fundamental mode dynamics. Here, we have shown that the weighted contribution of fundamental mode varies as a function of input launch position into the optical fiber [8]. The input spatial mode used to excite the optical fiber modes is restricted to Gaussian mode throughout the analysis and experiment.

The optical fiber exhibits cylindrical symmetry, otherwise known as translational invariance [9]. The propagation of the Gaussian beam through the optical fiber axis excites the symmetric fundamental gaussian mode. The cylindrical symmetry of the optical fiber can be broken by either oblique angle

or off-axis launching of the incident light field. This breaking of cylindrical symmetry of the system leads to asymmetric propagation of light field. The modes of an optical fiber are the resonance of the all the transverse fields determined by the boundary conditions [9]. Thus, the spatial intensity profile of the excited mode is governed by the boundary conditions. The off-axis (asymmetric) launching of light modifies the boundary conditions leading to a combination of cylindrical and cartesian symmetry, resulting in an asymmetric beam mode profile at the output due to asymmetry experienced by propagation vectors. The asymmetry in the optical fiber system excites the higher-order linearly polarized (LP_{11}) modes, LP_{11}^{ey} , LP_{11}^{ey} , LP_{11}^{ex} and LP_{11}^{ox} . The LP_{11} modes are solutions of the wave equation for the optical fiber under Cartesian symmetry [8,9]. And the output is composed of the four eigenvector modes [8,9]. The polarization variations in the LP_{11} modes are limited to X and Y polarizations due to weakly-guiding approximation [8,9]. Hereafter, the higher-order LP_{11} modes will be referred to as LP modes.

The propagation of light through the optical fiber is modelled under weakly guiding approximation. The propagation model is shown in Fig. 1 for different input conditions. The blue coloured disc represents the optical fiber core, while the incident beam's launch position and state of polarization are represented by red dots and blue arrows respectively. The input launch position is determined by the shift from on-axis (ρ') and azimuthal angle (φ') . The input launching parameter $\rho' = \rho'_0$ is fixed while φ' is varied for modelling the optical output fields. The orientation of the arrow represents the state of polarization (SoP) of the incident light beam. The critical difference between Fig. 1 (a) and (b) is that the SoP of the incident light beam varies along with the input launch position for Fig. 1 (a) while SoP remains fixed for Fig. 1(b). The resulting optical output fields are depicted adjacent to the input position, with polarization represented byarrows. The resulting optical output field in Fig. 1 (a) can be understood as though the entire system (optical fiber, SoP) is under coordinate rotation. The input conditions under this coordinate rotation remain the same, resulting in rotated output with no notable changes. The phase changes associated with the coordinate rotation is compensated by the SoP change, resulting in an identical output for diametrically opposite input launch positions. The asymmetry in the launching position is determined by both position (ρ') and azimuthal angle (φ'). The input launching position (ρ') and azimuth angle (φ') determine excitation and orientation of the output LP modes (due to the asymmetry experienced by propagation vectors) under weakly-guiding approximation as depicted in Fig. 1.

It is important to note that the orientations of the excited LP modes are equal to the input azimuth angle due to asymmetry in the propagation vectors.

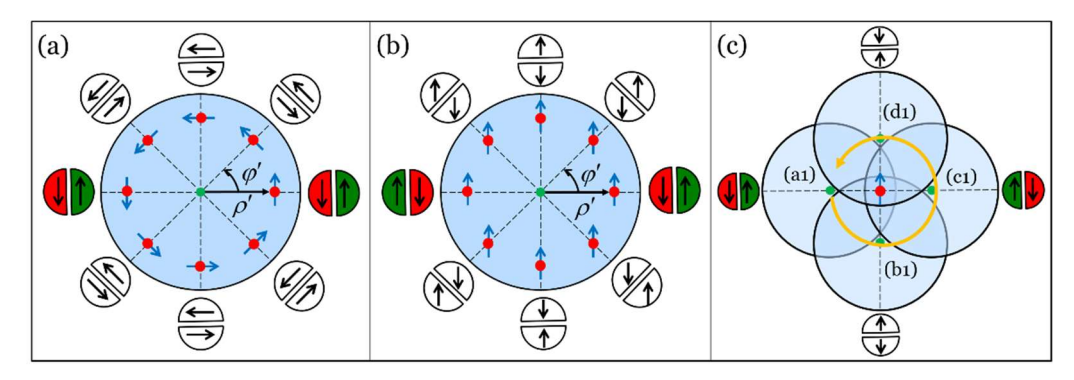


Figure 1. Intuitive figurative models for the off-axis propagation of Gaussian beam for different azimuthal positions with (a) varying and (b) fixed input linear polarization. The outputs are depicted adjacent to the input position outside the disc (optical fiber core) (c). The propagation model shown in figure (b) is visualized as fiber alone rotation with a path (a1-b1-c1-d1-a1) leading to π phase shift for 0° and 180° input azimuthal angles. The red dots and blue arrows are input position and linear polarization of the Gaussian beam respectively.

The optical output fields in Fig. 1 (b) reveal a π phase shift for the LP modes for diametrically opposite launch positions. This phase shift for the output LP_{11} mode is noticeable from the colour changes for input azimuthal angles $\varphi' = 0^{\circ}$ and $\varphi' = 180^{\circ}$. The results can be understood as the rotation of the optical fiber alone with input polarization fixed. This rotation of optical fiber alone is depicted in Fig. 1 (c). The launch position is the axis for the rotation with the trajectory a1-b1-c1-d1-a1 resulting in a π phase shift for the output LP modes.

The Geometric Berry phase is the influence of geometry on the polarization vector of a propagating light field in momentum space. It was experimentally demonstrated for the propagation of polarized light field in helicoid optical fiber, resulting in the change of orientation of the polarization vector due to the geometric Berry phase [4,5]. Analogously, Bliokh predicted that the propagation of HG beam mode through a helical trajectory results in a transverse rotation of HG beam mode due to orbital Berry phase (OBP) in the modal domain [7]. The OBP corresponding to the transverse rotation of the HG beam is $-\Theta_{BO}$ [7].

Hence, the rotation of output LP modes for the off-axis propagation of the Gaussian beam can be understood as due to φ' dependent OBP for the constituent LG beams of topological charges ± 1 . The off-axis propagation of light field in the optical fibers results in the helical trajectory of k-vectors [9]. This leads to the accumulation of differential OBP for the constituent LG beam modes resulting in the transverse rotation of output LP modes. The output LP beam can be expressed as a superposition of LG beams with opposite topological charges ($l = \pm l$) [7].

$$E_o = \left\{ F^{p',|l|} \exp (il\phi) + F^{p,|l'|} \exp (il'\phi) \right\}$$
 (1)

With F being the radial function, p=1,2,3 ..., l is topological charge and ϕ is azimuthal phase profile of the LG beam. The constituent LG beams propagate with slightly shifted trajectories in the fiber due to opposite helical phase fronts [7]. The shifted trajectories are a manifestation of differential OBP accumulation for +1 and -1 LG beams resulting in the transverse rotation of the output HG beam. With the inclusion of OBP (ϕ) and dynamic phase parameters, the optical output field from the optical fiber can be expressed as,

$$E_{o}(\varphi) = F^{p',|l'|} \exp\left[\left(i(\varphi - \varphi') + i\int kds\right)\right] + F^{p,|l|} \exp\left[\left(i(-\varphi + \varphi') + i\int kds\right)\right]$$

$$= \left\{F^{p',|l'|} \left[\exp(i\varphi) \times \exp(-i\varphi') + \exp(-i\varphi) \times \exp(i\varphi')\right]\right\} \exp\left(i\int kds\right)$$
(2)

The parameter ϕ' represents not only the input azimuthal coordinate but also the position-dependent accumulation of OBP. The integrand indicates the dynamic phase factor along the propagation direction. The changes in phase structure of the optical output field can be understood by varying the parameter ϕ' . Let us examine the output for $\phi'_1 = 0$, $\phi'_2 = \pi/2$, $\phi'_3 = \pi$ and $\phi'_4 = 2\pi$ values at a fixed radial position as considered in Fig. 1 (b), with polarization unchanged for all input positions. Eq.2 describing the optical output field transforms into the following.

$$E_{o}(\varphi'_{1}) = \left\{ F^{p',|l'|}(\exp(i\phi) + \exp(-i\phi)) \right\} pd$$

$$E_{o}(\varphi'_{2}) = \exp(-i\pi/2) \left[F^{p',|l'|}(\exp(i\phi) - \exp(-i\phi)) \right] pd$$

$$E_{o}(\varphi'_{3}) = \exp(-i\pi) \left[F^{p',|l'|}((\exp(i\phi) + \exp(-i\phi)\exp(i2\pi))) \right] pd$$

$$= \exp(i\pi) E_{o}(\varphi'_{1})$$

$$E_{o}(\varphi'_{4}) = \exp(-i2\pi) \left[F^{p',|l'|}((\exp(i\phi) + \exp(-i\phi)\exp(i4\pi))) \right] pd$$

$$= \exp(-i2\pi) E_{o}(\varphi'_{1})$$

$$= \exp(-i2\pi) E_{o}(\varphi'_{1})$$
(3)

here $pd = \exp(i\int kds)$ represents the dynamic phase factor. The phase changes in the optical output field are linearly dependent on input azimuthal position, as shown in Eq. 3. As anticipated, the optical output field undergoes a π phase shift for the diametrically opposite launch positions $\varphi_1' = 0 \& \varphi_3' = \pi$. Further, an adiabatic change in the input azimuthal launch position results in the evolution of optical output field phase from 0 to 2π . The orientation of output HG mode is directly correlated to the phase changes associated with input azimuthal launch position. The calculated optical output field for different input azimuthal launch positions is shown in Fig. 2.

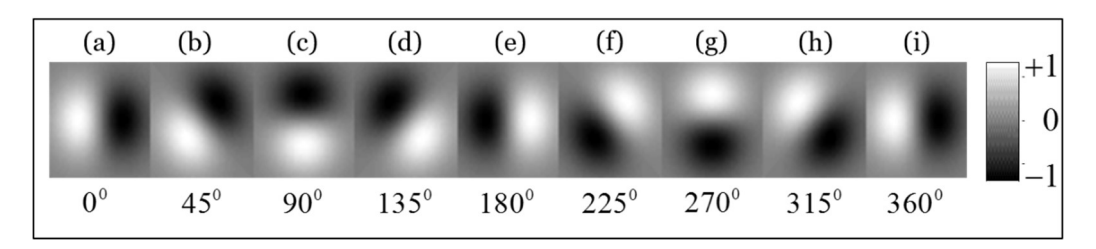


Figure 2. The rotation of HG-like output LP modes is due to the accumulation of OBP for different input azimuthal angles. The variation in the input azimuthal angles is mentioned below each image from (a) 0° to (i) 360°.

The images in Fig. 2 represent optical output field for a fixed input radial position with varying φ' . The off-axis propagation of the Gaussian beam excites not only first-order LP modes but also position-dependent weak fundamental Gaussian mode as well. The contribution of fundamental Gaussian mode in the optical output field tapers off as the input launching varies from on-axis to extreme off-axis position. The contributions of fundamental Gaussian beam and first-order LP modes are modelled by input position-dependent Gaussian and

LG functions. The optical output field encompassing all input launching positions is expressed as

$$E_{f}(\rho', \varphi') = G(\rho', \varphi', \omega_{0}) L P_{01}$$

$$+ \rho' G(\rho', \varphi', \omega_{1}) E_{\rho}(\varphi')$$

$$(4)$$

Here $G(\rho', \varphi', \omega_0) = \exp(-{\rho'}^2/2(\omega_0^2))$ represents the Gaussian function. The beam waists ω_0 and ω_1 in the Gaussian function describe the input position-dependent excitation of LP_{11} and fundamental Gaussian mode in the optical fiber. Using Eq. 4, the optical output field is computed for a step-index fiber with refractive indices $n_{co} = 1.4142$, $n_{cl} = 1.3999$ and a core radius of $4\mu m$. The input position for the calculations is varied in steps of $1\mu m$. The beam waist values $\omega_0 = 0.35$ and $\omega_1 = 0.70$ are used to obtain the amplitude and phase distribution of the optical output field, as shown in Fig. 3. The π phase change for the diametrical launch positions can be seen in Fig. 3 (b).

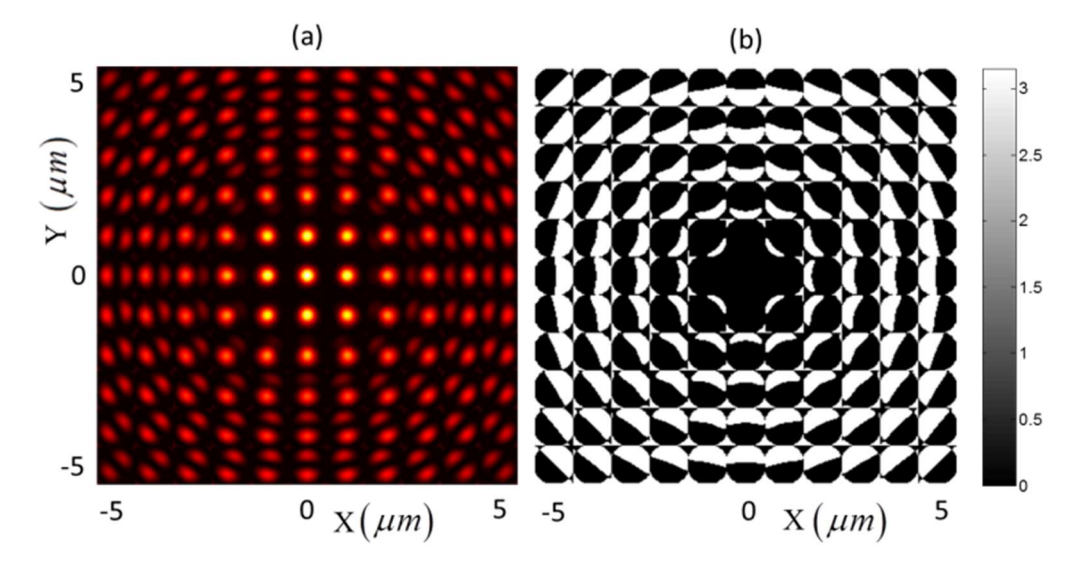


Figure 3. (a) The optical output field mapped as a grid corresponding to the input (radial and azimuthal) positions varied with a step size of $1\mu m$, and (b) the corresponding optical phases.

6.3 Experimental details

A step-index two-mode optical fiber with a diameter of $8\mu m$ and V number \sim 3.805 is chosen for the experiment. The wavelength 632.8 nm, V value 3.805 ensures a two-mode excitation in the optical fiber. Our initial analysis showed that an optical fiber of length 24.7 cm resulted in the excitation of near LP modes for off-axis light propagation through the optical fiber. The polarization and birefringent effects are minimized by keeping the optical fiber horizontal without torsion.

After passing through the Glan-Thompson polarizer, the vertically polarized light is split into two beams, one for position-dependent excitation of optical modes in the optical fiber and the other as reference beam for extraction of phase through the interference of both beams. A 4-f lens system is constructed as shown in Fig. 4. The glass plate is mounted on the goniometer, which is positioned on the LabView controlled rotation motor. A glass plate is located at the focal plane of a 4-f lens system and it is tilted and rotated by goniometer and rotation motor to vary the input optical beam position along Y and X directions respectively. The shifted optical beam due to the tilt and rotation of the glass plate is further passed through the 0.2 NA 20X microscopic objective lens O1 to launch the light into the optical fiber. Before launching light into the optical fiber, the changes in the optical beam position due to the rotation/tilt of the glass plate are recorded at the focal plane of O1. The positional shifts of the optical beam at the focal plane (O1) are used to calibrate the rotation angle of the glass plate. The output from the optical fiber is passed through a 0.2 NA 20X microscopic objective lens O2 whose position is adjusted to collimate the output. A Mach-Zehnder interferometer is constructed for obtaining the optical output beam phase by interfering with a reference beam of same polarization. The interferometer is composed of beam-splitters BS1, BS2 and mirrors M1 and M2. The interference between the optical output field and the reference beam is captured using CCD. The position of the glass plate along Y-axis direction is manually controlled while the rest of the process is automated using LabVIEW. For a particular position of the goniometer, the glass plate is rotated to shift the input beam position along X-axis direction using the rotation motor. Subsequently, the interferograms are captured through the CCD synchronously for all rotation values through LabVIEW automation to minimize error. This process is repeated for different goniometer position (Y) values, and the optical output field is mapped as a grid in correlation with the input position.

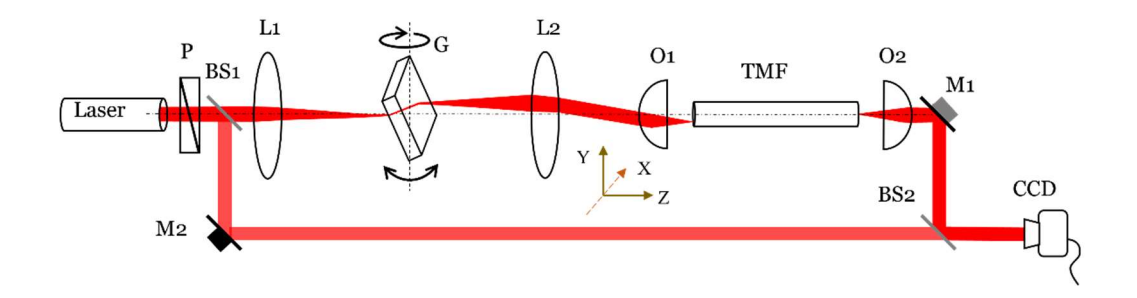


Figure 4. Experimental setup used to investigate the parallel transport of output LP modes due to off-axis propagation of linearly polarized Gaussian beam through the two-mode optical fiber with a Mach-Zehnder interferometer.

6.4 Results and discussion

Let us now examine the optical output fields for the opposite launch positions and the corresponding phase changes mentioned in Section 6.3. As anticipated, the off-axis launch resulted in the excitation of LP modes, as shown in Fig. 5. The images Fig. 5 (a) and (e) correspond to opposite input launch positions. The lopsided intensity distribution signifies the contribution of fundamental Gaussian beam in the optical output field. The interferogram due to interference with the reference beam is shown in Fig.5 (b) and (f) corresponding to images Fig. 5 (a) and (e) respectively. The highlighted sections in Fig. 5 (a,b) and (e,f) are considered for obtaining the phase information. The interferograms were analysed using Fourier transform method [10] and extracted phase information is shown in Fig. 5 (c) and (g). The opposite gradients in Fig.5 (c) and (g) imply the π phase change in the corresponding outputs. Further, the line profile of the extracted phase confirms the π phase change for optical output fields due to opposite launch positions.

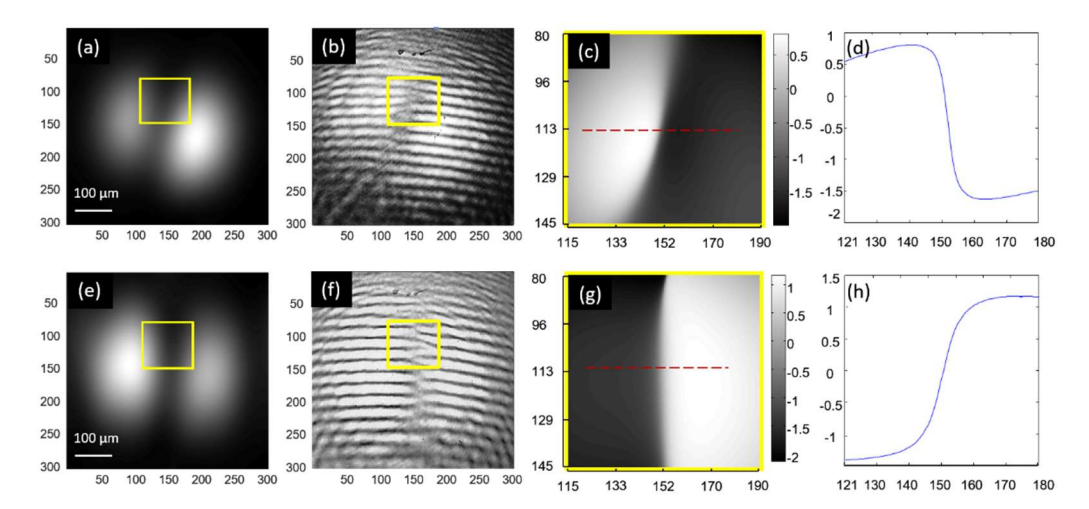


Figure 5. The selected optical phases are depicted inside yellow square boxes. The optical output field for the input azimuthal angles are (a) $\varphi'=0$ (e) $\varphi'=\pi$ and their corresponding interferograms are (b) and (f). The optical phase extracted using Fourier fringe analysis of the interferograms (b) and(f) are (c) and (g), respectively. The line profiles reveal the π phase shift between the optical output fields for the input positions (d) $\varphi'=0$ and (h) $\varphi'=\pi$ with a fixed radius $\rho'=\rho'_0$.

Along with the phase changes for the opposite launch input positions, the phase change dynamics for all the input positions is studied. It is mentioned in Section 6.3 (Eq.3) that the phase of the optical output field is correlated to the azimuthal input angle and orientation of the output LP modes. To extract phase changes for all the input positions, it is essential to obtain the orientation of optical output fields for input positions. The asymmetry in the optical output field's spatial amplitude makes it challenging to obtain orientation values. We have developed an auto-correlation technique to extract the orientation values of asymmetric modes. The auto-correlation of an asymmetric spatial mode results in a symmetric two-lobed spatial mode with the same orientation making it easier to obtain the orientation and thus phase values.

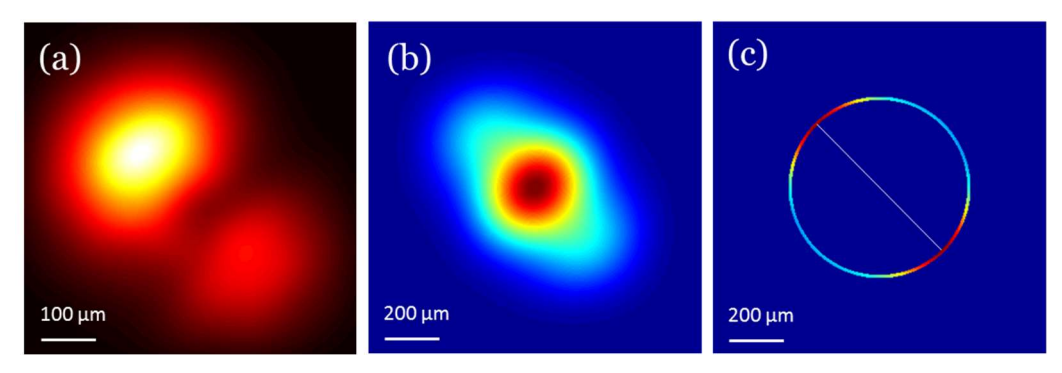


Figure 6. (a) the optical output field for a general off-axis position and corresponding (b) auto-correlated image and (c) the application of the ring mask to obtain the orientation value of output LP mode.

The asymmetric output spatial mode for a given input launch position is shown in Fig. 6 (a), and the corresponding auto-correlated image is shown in Fig. 6 (b). To extract the orientation of the symmetric auto-correlated image, we have used the ring filter method. The auto-correlated image is multiplied with a ring filter to obtain the orientation values, as shown in Fig. 6 (c). The image in Fig.6 (c) has two maxima values (red arcs) which are combined to obtain the orientation values, and the process is repeated for all the optical output fields.

As discussed, the input launching position is varied by tilting (Y goniometer) and rotating (X – rotation motor) the glass plate. The focal spot radius due to MO (O1) is $20\,\mu m$, and a 1° rotation of glass plate shifts the focal spot by $1\mu m$. A grid area of $11\mu m\times 11\mu m$ is raster scanned through the rotation of glass plate with a step size of $1\mu m$. The optical output field is mapped into a grid as a function of input position as shown in Fig. 7 (a). The corresponding LP modes rotation angle obtained through the auto-correlation technique is shown in Fig. 7 (b). The rotation angles in the image Fig. 7 (b) represent the OBP acquired by the constituent LG modes of the LP modes. The rotation angle forms a topological structure akin to LG beam's phase profile with phase singularity.

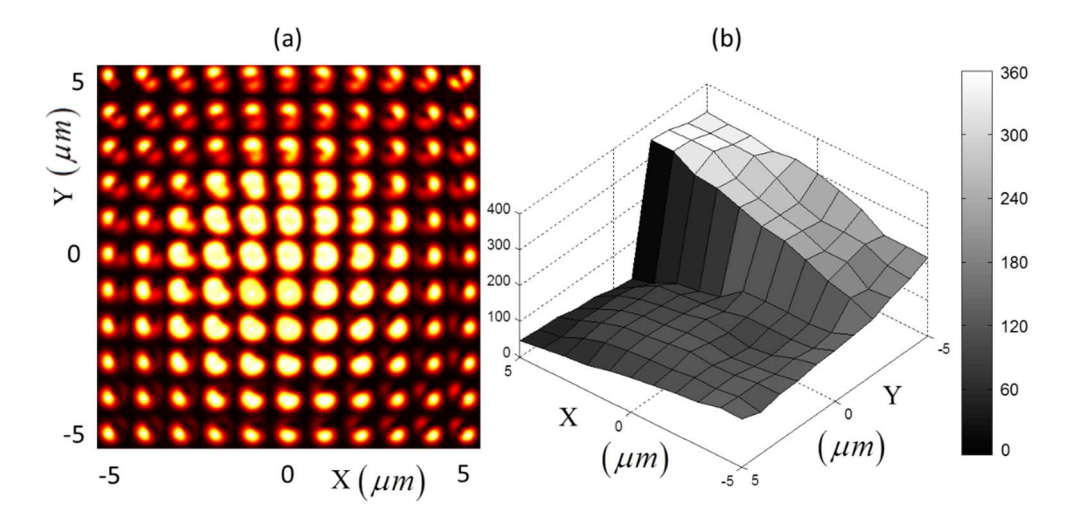


Figure 7. The experimental equivalence of the simulated figure 3, (a) The optical output fields arranged in correlation to the input position of the linearly polarized Gaussian beam varied by $1 \, \mu m$ step size forming a $11 \times 11 \mu m$ grid. b) the corresponding OBPs extracted through the auto-correlation technique revealing the topological character of OBP for all the positions.

From the above analysis, the orientation and asymmetry of the output *LP* spatial modes may provide new degrees of freedom in optical communications and signal analysis. Incorporating the SOI and OOI-related effects for the propagation of light can lead to the controllable excitation and filtering of different optical modes. Often the cross-talk is viewed as noise in optical fiber propagation models. Still, when used in the context of SOI and OOI of light, they would provide the flexibility to tailor the output according to the need in the light propagation.

6.5 Summary

In this chapter, we have investigated the input azimuthal angle-dependent excitation of higher-order LP modes. The LP modes have two characteristics a) Asymmetric spatial mode b) input azimuthal angle-dependent Orientation values. Both features of output LP modes are due to the accumulation of OBP by constituent LG beams and the contribution of the fundamental Gaussian beam. The OBP accumulation is demonstrated for a horizontally held torsion-free two-mode optical fiber by carefully selecting optical parameters such as fiber type (V-number), length, and input polarization.

References:

- 1. Vasnetsov, M. V., V. A. Pas' Ko, and M. S. Soskin. "Analysis of orbital angular momentum of a misaligned optical beam." *New Journal of Physics* 7.1 (2005): 46.
- 2. O'neil, A. T., et al. "Intrinsic and extrinsic nature of the orbital angular momentum of a light beam." *Physical review letters* 88.5 (2002): 053601.
- 3. Bliokh, Konstantin Yu, et al. "Spin-orbit interactions of light." *Nature Photonics* 9.12 (2015): 796-808.
- 4. Chiao, Raymond Y., and Yong-Shi Wu. "Manifestations of Berry's topological phase for the photon." *Physical review letters* 57.8 (1986): 933.
- 5. Tomita, Akira, and Raymond Y. Chiao. "Observation of Berry's topological phase by use of an optical fiber." *Physical review letters* 57.8 (1986): 937.
- 6. Liberman, V. S., and B. Ya Zel'dovich. "Spin-orbit interaction of a photon in an inhomogeneous medium." *Physical Review A* 46.8 (1992): 5199.
- 7. Bliokh, Konstantin Yu. "Geometrical optics of beams with vortices: Berry phase and orbital angular momentum Hall effect." *Physical Review Letters* 97.4 (2006): 043901.
- 8. Chakravarthy, T. Pradeep, Dinesh N. Naik, and Nirmal K. Viswanathan. "Geometric phase due to orbit—orbit interaction: rotating LP11 modes in a two-mode fiber." *Journal of Optics* 19.10 (2017): 105607.
- 9. A. W. Snyder and J. D. Love, Optical Waveguide Theory (Chapman and Hall, 1983).
- 10. Takeda, Mitsuo, Hideki Ina, and Seiji Kobayashi. "Fourier-transform method of fringe-pattern analysis for computer-based topography and interferometry." *JosA* 72.1 (1982): 156-160.

Summary and Concluding remarks.

7.1 Summary

The scientific journey of the study of light is nothing short of spectacular, riddled with many mysteries and it is an ongoing journey towards understanding the fundamental nature of light. Socrates, Aristotle, Plato, Euclid & Ibn al-Haytham were the early contributors who helped us understand the reflection, refraction, and diffusion of light. Corpuscular theory by newton, Wave theory by Huygens, and Electromagnetic theory by Maxwell further improved our understanding of the nature of light. Max plank, and Einstein have put forward the quantum aspects of light in black body radiation and the photoelectric effect respectively.

The motion of a particle or wave is central to all the observable phenomena, and it is associated with linear/angular momentum and energy exchange dynamics. The oscillations of electric field of light is polarization and is quantified through stokes parameters [1]. The phase changes due to polarization lead to the accumulation of the Pancharatnam Berry (PB) phase [2]. Similarly, the phase changes associated with the wave-vector variations results in Rytov-Vladimirskii-Berry (RVB) phase [3]. Geometry traced by the motion of electric fields and wave-vectors of light determines the PB and RVB phase structures respectively and the corresponding outcomes. Geometric Berry phase underpins all the effects associated with the polarization and wave-vector of light. While the angular momentum associated with circular polarization is termed as spin angular momentum (SAM), the angular momentum due to helical wavefront is christened as orbital angular momentum (OAM) of light. And the motion of light with a shifted axis results in extrinsic(E) OAM.

Under paraxial approximation, the propagation of light in free-space does not change its direction and polarization content. But, the propagation of light in inhomogeneous or anisotropic or biaxial media couples the spin and orbit angular momentum of light due to transversality condition. This causes the spin-orbit interaction of light (SOI) [4]. The SOI phenomena occurs due to the changes in wave-vector direction or polarization vector of light in the respective media. The symmetry of the system plays a crucial role in determining the effects associated with SOI of light. We have considered cylindrical symmetric GRIN rod [Chapter 2-5] and two-mode optical fiber [Chapter 6] to investigate the SOI and OOIs' of light for both on and off-axis input launch conditions. The symmetry preserving on-axis propagation of circularly polarized (CP) Gaussian beam through GRIN rod generates an optical vortex ($l = \pm 2$) in orthogonal circular polarization conserving the total angular momentum of the light. Interference of the generated OV with a reference Gaussian beam with same polarization handedness.

Subsequent phase extraction through Fourier transform fringe analysis reveals the opposite helical phase structures for the input RCP and LCP gaussian beams confirming the spin to orbit conversion (SOC) of light. A reciprocal SOC (conversion of IOAM into spin content) is anticipated and observed through onaxis propagation of linearly polarized OV beam with different topological charges through the GRIN rod. The reciprocal SOC is experimentally measured through measurement of weak (S3) Stokes parameters, revealing topological charge-dependent orientation of the weak S3 (spin) content. The weak (S3) Stokes parameter contains equal RCP and LCP components with zero SAM conserving the total angular momentum of light [Chapter 2]. The off-axis propagation of linearly polarized Gaussian beam breaks the symmetry of system (GRIN rod and optical beam) and results in the SHE of light. The spin-Hall shifts are amplified through weak measurement technique for quantification. The SHE when plotted as a function of input position, exhibits a non-linear behaviour confirming the weak anisotropy of GRIN rod. The reciprocal SHE, influence of trajectory on polarization is measured for different off-axis positions through weak (S3) Stokes parameter. The plot of reciprocal SHE and position also is a non-linear curve validating the effect of weak anisotropy [Chapter 3].

The off-axis propagation of OV beam results in effects similar to SOI phenomena: orbital-Hall effect (OHE – transverse topological charge dependent shift of an OV beam) and reciprocal OHE (rotation of transverse intensity structure of an OV beam) of light. The OHE of light is experimentally observed for off-axis propagation of OV beam with varying topological charges. The OHE is scales linearly with the incrementaal change of topological charge of the OV beam. The off-axis propagation of HG beams (zero OAM) with different orientations for different input positions resulted in the rotation of output HG beams. Opposite rotations were observed for the input HG beams with ±45° orientations. The HG beams with orientations ±45° provide the spatial asymmetry, leading to the reciprocal OHE. The rotation can be used to sort-out HG beams with different orientations using the GRIN rod. The observed effects due to OOI of light are polarization-independent, requiring no polarization components in the measurement process. GRIN rod can also be used for filtering and sorting of the LG beams based on the OHE and OBP for the OV beams [Chapter 4]. The SOI and OOI effects were limited to first-order paired interaction, as discussed in Chapters 2-4. The propagation of circularly polarized (CP) optical vortex (OV) beam would bring in second-order effects (SOE) due to both SOI and OOI of light. The on-axis propagation of CP OV beam results in the creation and annihilation of topological charges in the orthogonal CP and may

be used for sorting of OAM beams. Extending it to the off-axis propagation leads to the observation of the spin-induced orbital-Hall effect of light.

The product σl acts as a control parameter in the second-order effects determining the net topological charge of orthogonal CP output and subsequently the spin and orbital Hall shift values. The rotational aspect of the OV beam significantly impacts the SHE of light. The SHE of light is transformed from the transverse (Y) shift to the general (X&Y) shift owing to the rotation of transverse intensity structure due to the orbital Berry phase. The shifts are asymmetric due to the contribution of OHE to the SHE. The asymmetries observed are 1) Rotational angle values of output optical beam projected using QWP and GT polarizer 2) Unequal RCP and LCP spin-Hall shifts due to OAM and 3) Unequal total spin-Hall shift value at an input position for +l and -l values. The asymmetries can be attributed to the orbital-Berry phase and curvature of the trajectory taken by the light beam. Apart from the second-order effects, the polarization changes associated with the propagation of LP OV beams also were studied using weak (S3) Stokes parameters. The weak (S3) Stokes parameter increases as a function of a) input position for a fixed topological charge value and b) topological charge for an input position. The cumulative weak S3 content plotted as a function of topological charge for different input positions also exhibits the asymmetry due to curvature of the trajectory of the light beam in the GRIN rod [Chapter 5].

The propagation dynamics of LP Gaussian beam in the two-mode optical fiber is studied for input positions comprising both on and off-axis positions. The horizontally held TMF (24.7 cm) without torsion and twist behaved as an HWP counterpart in the modal domain. The rotational dynamics of HG-like output LP modes is understood as due to the accumulation of orbital Berry phase for the constituent LG (± 1) modes of the optical fiber. The output LP modes and obtained phase structure through auto-correlation technique revealed a topological character dependent on the input azimuthal angle. The output LP modes for opposite launch positions exhibited π phase change. The propagation model is based on the weak-guiding approximation with no significant polarization effects. The asymmetrical spatial amplitude and orientation of the output HG like LP modes may aid in controllable excitation of optical modes and in filtering the cross-talk efficiently [Chapter 6].

7.2 Concluding remarks.

The thesis attempts to explore the spin-orbit and orbit-orbit interactions of light due to symmetry and asymmetry conditions in an inhomogeneous and weak anisotropic media such as GRIN rod and two-mode optical fiber. Previously, the studies about SOI and OOI effects of light were primarily centered around the first-order effects. The first-order effects certainly improved the scope and experimental verifications of these fundamental interactions in various media and conditions. Still, without the inclusion of the third AM, the spin-orbit-orbit dynamics of light are incomplete. Generally, the first-order effects are equal in magnitude but opposite in direction for RCP/LCP, $\pm l$ optical beams. On the other hand, the shifts and rotation dynamics due to second-order effects are unequal in magnitude and direction as well. The asymmetry in the SOE can be attributed to the OBP and curvature of light's trajectory in the GRIN rod.

The understanding of such effects would lead to applications in a large variety of areas. The precise measurement and control at the nanoscale using nano-photonic devices [5,6], optical signal processing, information encoding-decoding, information processing for optical communications using OAM beams [7,8], etc. The higher-order Poincaré beams can be used for optical image processing and optical interconnections using PB metalens for efficient optical communications [9].

In conclusion, we have experimentally measured the SOI and OOI effects of light due to weak anisotropy of the GRIN rod corresponding to local wave-vector directions through SHE, reciprocal SHE, OHE and reciprocal OHE effects. The SOE of light showed that the LP OV beams could differentiate the curvature changes due to the combined effect of OBP, RVB phases. The SOE's may become the standard to investigate the propagation of vector-vortex or higher-order Poincaré beams in various media. GRIN rod can be used to distinguish the OV beams with opposite topological charges and also can discriminate the HG beams with orientations other than $0^{\circ}/180^{\circ},90^{\circ}/270^{\circ}$. For the first time, all the reciprocal spin-orbit and orbit-orbit interactions of light are experimentally investigated in a single media (GRIN rod). Apart from SOE of light, First-order effects concerning the output LP modes behaviour for all the input positions in a TMF may provide a new way of filtering cross-talks and new degrees of freedom (asymmetrical spatial profile and orientation of LP modes) which may possibly find applications in OAM based optical communications.

7.3 Future prospects

Polarization singularities are inherent in the nature and are of fundamental importance to understand the various media and its interaction with light. GRIN rod with its inhomogeneity and weak anisotropy is suitable to investigate the polarization singularities at different off-axis positions. The off-axis position may possibly reveal the rotational aspect of polarization singularities.

Airy beams are intriguing due to their cubic phase function leading to a curved trajectory. As discussed in the Chapter 5, GRIN rod can distinguish and discriminate the curvature of the optical beam's trajectory by exhibiting the asymmetry in SHE and polarization content when illuminated with linearly polarized optical vortex beam at different positions. It would be interesting to investigate the Airy-beam properties in GRIN rod such as polarization structure of the output, effect of Airy-beam's trajectory on SHE and mutual interaction of Airy-beam's and GRIN rod's phase structures. Additionally, embedding vortex inside the Airy-beam would be fascinating owing to the presence of both helical phase and cubic phase structures coupled with graded-refractive index of GRIN rod.

Elliptical optical vortices (EOV's) are gaining traction due to added functionality in the form of radial intensity lines and different orientations. They have also been incorporated in generation of perfect optical vortices with different radial numbers. Considering the EOV's as general OV's akin to elliptical polarization for polarization, studying the evolution of EOV's in the GRIN rod may prove to provide information regarding the rotational aspects of EOV's.

References:

- 1. Stokes, George Gabriel. "On the composition and resolution of streams of polarized light from different sources." *Transactions of the Cambridge Philosophical Society* 9 (1851): 399.
- 2. Pancharatnam, Shivaramakrishnan. "Generalized theory of interference and its applications." *Proceedings of the Indian Academy of Sciences-Section A*. Vol. 44. No. 6. Springer India, 1956.
- 3. Berry, Michael Victor. "Quantal phase factors accompanying adiabatic changes." *Proceedings of the Royal Society of London. A. Mathematical and Physical Sciences* 392.1802 (1984): 45-57.
- 4. Bliokh, Konstantin Yu, et al. "Spin-orbit interactions of light." *Nature Photonics* 9.12 (2015): 796-808.
- 5. Rotenberg N and Kuipers L 2014 Mapping nanoscale light fields Nature Photon. 8 919
- 6. Bauer, Thomas, et al. "Nanointerferometric amplitude and phase reconstruction of tightly focused vector beams." *Nature Photonics* 8.1 (2014): 23-27.
- 7. Willner, Alan E., et al. "Optical communications using orbital angular momentum beams." *Advances in optics and photonics* 7.1 (2015): 66-106.
- 8. Huang, Zebin, et al. "All-Optical Signal Processing of Vortex Beams with Diffractive Deep Neural Networks." *Physical Review Applied* 15.1 (2021): 014037.
- 9. He, Yanliang, et al. "All-optical signal processing in structured light multiplexing with dielectric meta-optics." *ACS Photonics* 7.1 (2019): 135-146.

List of publications

Journal articles

- 1. T. Pradeep Chakravarthy, and Nirmal K. Viswanathan. "Direct and reciprocal spin-orbit interaction effects in a graded-index medium." *OSA Continuum* 2.5 (2019): 1576-1589.
- 2. T. Pradeep Chakravarthy, Dinesh N. Naik, and Nirmal K. Viswanathan. "Geometric phase due to orbit—orbit interaction: rotating LP11 modes in a two-mode fiber." *Journal of Optics* 19.10 (2017): 105607.
- 3. T. Pradeep Chakravarthy, and Nirmal K. Viswanathan. "Spin-orbit interactions of light in inhomogeneous-anisotropic medium -Higher order effects." (Manuscript under preparation)

Conference and workshop proceedings

Oral presentation

- 1. T. Pradeep Chakravarthy, Dinesh N. Naik, and Nirmal K. Viswanathan. "Parallel transport of fiber mode structure: orbit-orbit interaction." *Complex Light and Optical Forces XI*. Vol. 10120. International Society for Optics and Photonics, 2017.
- 2. T. Pradeep Chakravarthy, Dinesh N. Naik, and Nirmal K. Viswanathan. "Topology of the mode rotation in two-mode optical fiber." *International Conference on Fibre Optics and Photonics*. Optical Society of America, 2016.
- 3. T. Pradeep Chakravarthy, Dinesh N. Naik, and Nirmal K. Viswanathan. "Topology of the mode rotation in two-mode optical fiber." Student Conference on Optics and Photonics (SCOP Sept 2,3, 2016) at Physical Research Laboratory, Ahmedabad, INDIA.

Poster presentation

- 1. T. Pradeep Chakravarthy, Nirmal K. Viswanathan. "Spin-Hall effect of light in inhomogeneous medium." The International Conference on Fiber optics and Photonics (PHOTONICS 2018), Indian Institute of Technology Delhi.
- 2. T. Pradeep Chakravarthy, Nirmal K. Viswanathan. "Spin -induced orbital Hall effect of light in inhomogeneous medium." OSI International Symposium on optics (OSI-ISO 2018), Indian Institute of Technology Kanpur.
- 3. T. Pradeep Chakravarthy, Nirmal K. Viswanathan. "Spin -orbit interaction of light in GRIN rod A Mueller matrix analysis." International Topical Meeting on Applied and Adaptive Optics (INTOPMAA-2017), Indian Institute of Space Science and Technology (IIST).

Spin-orbit Interaction of Light in Graded-index Medium

by Pradeep Chakravarthy T

Gandhi Memorial Library

Central University P.O. HYDERABAD-500 045.

Submission date: 03-Nov-2021 03:38PM (UTC+0530)

Submission ID: 1691873843

File name: Thesis_Pradeep_final.pdf (5.3M)

Word count: 30167

Character count: 156065

Spin-orbit Interaction of Light in Graded-index Medium

ORIGINALITY REPORT			
10% SIMILARITY INDE	4% x INTERNET SOURCES	9% PUBLICATIONS	0% STUDENT PAPERS
PRIMARY SOURCES			
1 proxy	y.osapublishing.org	g	2%
Viswa inter	adeep Chakravarth anathan. "Direct ar action effects in a g ium", OSA Continu	nd reciprocal s graded-index	pin-orbit 2%
Naik, phas LP11	eep Chakravarthy, Nirmal K Viswana e due to orbit-orbi modes in a two-m cs, 2017	than. "Geomet t interaction: R	ric Rotating
Xinzh	e Li, Jingge Wang, Nong Li, Jie Tang. "Cature of a paraxial koling", Physical Revi	Changes of pha	ase \\\
	ey Nechayev, Jörg : hs_Peter Banzer_"		0/6

Leuchs, Peter Banzer. "Orbital-to-spin angular

momentum conversion employing local helicity", Physical Review B, 2019

Publication

Gupta, Subhasish, Nirmalya Ghosh, and Ayan <1% 6 Banerjee. "Spin-Orbit Interaction of Light", Wave Optics, 2015. Publication Hehe Li, Miaomiao Tang, Jingge Wang, <1% Jingxiao Cao, Xinzhong Li. "Spin Hall effect of Airy beam in inhomogeneous medium", Applied Physics B, 2019 Publication spie.org <1% Internet Source Krishna Rani Sahoo, T. Pradeep Chakravarthy, Rahul Sharma, Sumit Bawari et al. "Probing Proximity - Tailored High Spin-Orbit Coupling in 2D Materials", Advanced Quantum Technologies, 2020 **Publication** www.osapublishing.org 10 Internet Source Eliahu Cohen, Hugo Larocque, Frédéric 11 Bouchard, Farshad Nejadsattari, Yuval Gefen, Ebrahim Karimi. "Geometric phase from

Aharonov–Bohm to Pancharatnam–Berry

and beyond", Nature Reviews Physics, 2019

Publication

12	C. T. Samlan, Nirmal K. Viswanathan. "Field-controllable Spin-Hall Effect of Light in Optical Crystals: A Conoscopic Mueller Matrix Analysis", Scientific Reports, 2018 Publication	<1%
13	www.rsphysse.anu.edu.au Internet Source	<1%
14	Athira B S, Sounak Mukherjee, Anuraj Laha, Koushik Bar, Dibyendu Nandy, Nirmalya Ghosh. "Experimental observation of the orbital Hall effect of light through pure orbitorbit interaction for randomly and radially polarized vortex beams", Journal of the Optical Society of America B, 2021	<1%
15	Paramasivam Senthilkumaran. "Berry's phase fiber loop mirror characteristics", Journal of the Optical Society of America B, 2005	<1%
16	Jin Zhang, Xin-Xing Zhou, Xiao-Hui Ling, Shi-Zhen Chen, Hai-Lu Luo, Shuang-Chun Wen. "Orbit-orbit interaction and photonic orbital Hall effect in reflection of a light beam", Chinese Physics B, 2014 Publication	<1%
17	Wenguo Zhu, Weilong She. "Electrically	<1%

controlling spin and orbital angular

momentum of a focused light beam in a uniaxial crystal", Optics Express, 2012

Publication

18	academicworks.cuny.edu Internet Source	<1%
19	Hailu Luo, Shuangchun Wen, Weixing Shu, Dianyuan Fan. "Spin Hall effect of light in photon tunneling", Physical Review A, 2010 Publication	<1%
20	authors.library.caltech.edu Internet Source	<1%
21	Xiaohui Ling, Xinxing Zhou, Kun Huang, Yachao Liu, Cheng-Wei Qiu, Hailu Luo, Shuangchun Wen. "Recent advances in the spin Hall effect of light", Reports on Progress in Physics, 2017	<1%
22	Bliokh, KY, and A Aiello. "Goos-Hänchen and Imbert-Fedorov beam shifts: an overview", Journal of Optics, 2013. Publication	<1%
23	Pericles S. Theocaris, Emmanuel E. Gdoutos. "Matrix Theory of Photoelasticity", Springer Science and Business Media LLC, 1979 Publication	<1%
24	Tentori, D., C. Ayala-Díaz, and E. Ledezma- Sillas. "", Liquid Crystals XII, 2008.	<1%

25	repositorio.uniandes.edu.co Internet Source	<1%
26	Padgett, . "Optical Spanners", Series in Optics and Optoelectronics, 2010. Publication	<1%
27	Xu-Zhen Gao, Jia-Hao Zhao, Meng-Shuai Wang, Jin-Jin Liu, Guang-Bo Zhang, Yue Pan. "Bipolar-variant spin angular momentum and its evolution in a tight focusing process", Physical Review A, 2020 Publication	<1%
28	Yongzhou Ni, Guoquan Zhou. "Nonparaxial propagation of an elegant Laguerre-Gaussian beam orthogonal to the optical axis of a uniaxial crystal", Optics Express, 2012 Publication	<1 %
29	Hehe Li, Peiyong Ji. "The propagation of a polarized gaussian beam in a smoothly inhomogeneous isotropic medium", Optics Communications, 2012	<1%
30	L. Susskind. "Дуальная симметричная теория адронов.—I", Il Nuovo Cimento A Series 10, 1970	<1%
	onlinelihrary wiley com	

Krishna Inavalli, V.V.G.. "Switchable vector 32 vortex beam generation using an optical fiber", Optics Communications, 20100315

Publication

Kumar, Vijay, V.V.G. Krishna Inavalli, and 33 Nirmal K. Viswanathan. "Dynamic evolution of transverse energy flow in focused asymmetric optical vector-vortex beams", Optics Communications, 2012.

<1%

Publication

T Pradeep Chakravarthy, Dinesh N Naik, 34 Nirmal K Viswanathan. " Geometric phase due to orbit-orbit interaction: rotating LP modes in a two-mode fiber ", Journal of Optics, 2017 Publication

<1%

arxiv.org 35 Internet Source <1%

HEHE LI, ZHIGANG BU, YUEE LUO, WENBO 36 CHEN, PEIYONG JI. "THE SPIN-ORBIT INTERACTION AND THE SPIN-SPIN INTERACTION OF PHOTONS IN AN INHOMOGENEOUS MEDIUM", Modern Physics Letters B, 2013

Publication

37	Weixing Shu, Yachao Liu, Shizhen Chen, Hailu Luo, Shuangchun Wen, and Dianyuan Fan. "Giant photonic spin Hall effect in momentum space in a structured metamaterial with spatially varying birefringence", Light Science & Applications, 2015. Publication	<1%
38	Lorenzo Marrucci. "Spin and orbital angular momentum coupling", Elsevier BV, 2021	<1%
39	Dashiell L. P. Vitullo, Cody C. Leary, Patrick Gregg, Roger A. Smith et al. "Observation of Intrinsic Spin-Orbit Interaction of Light in Few- Mode Optical Fiber", Frontiers in Optics 2016, 2016 Publication	<1%
40	J. Bass. "Chapter 3 Positive Definite Functions in Quantum Mechanics and in Turbulence", Springer Science and Business Media LLC, 1991 Publication	<1%
41	Vijay Kumar, Nirmal K Viswanathan. "The Pancharatnam-Berry phase in polarization singular beams", Journal of Optics, 2013	<1%



P U Lamalle. Plasma Physics and Controlled Fusion, 09/1997

<1%

Publication



Bulut, K.. "Three-dimensional optical profilometry using a four-core optical fibre", Optics and Laser Technology, 200509

<1%

Publication

Publication



Fuyong Yue, A. Aadhi, Riccardo Piccoli, Vincenzo Aglieri, Roberto Macaluso, Andrea Toma, Roberto Morandotti, Luca Razzari. "Rotational Doppler Frequency Shift from Time - Evolving High - Order Pancharatnam-Berry Phase: A Metasurface Approach", Laser & Photonics Reviews, 2021

<1%

Exclude quotes

Exclude bibliography

On

Exclude matches

< 14 words

Ph.D. Thesis

School of Physics
University of Hyderabad